FINAL TECHNICAL REPORT

Ambient Vibration Measurements for Estimation of Site Fundamental Periods at the City of Mayagüez, Puerto Rico

USGS Grant Number: 10HQPAQ0001

Prepared by:

Luis E. Suárez, Ph.D.

Miguel A. Pando, Ph.D., P.Eng.

Raúl Ritta, M.Sc.

Department of Civil Engineering and Surveying
University of Puerto Rico at Mayaguez
PO Box 9000
Mayagüez, PR 00681-9000

NEHRP Element: CE

Research supported by the U.S. Geological Survey (USGS), Department of Interior, under USGS award number 10HQPAQ0001. The views and conclusions contained in this document are those of the authors and should not be interpreted as necessarily representing the official policies, either expressed or implied, of the U.S. Government.

May 2, 2012

ABSTRACT

The work presented herein involved ambient vibration measurements at 134 field monitoring sites within the city of Mayagüez, Puerto Rico with the main objective to generate a map of predominant site period to be used as a tool in ongoing seismic reduction hazard efforts. The study is motivated due to most of earthquake damage is associated with local site effects that consist of amplification of the seismic waves propagating from the bedrock due to local geological conditions. A simple and efficient to identify regions where local site effects could be important is through maps of the fundamental natural period of the soil deposit. To that effect, measurement and adequate processing of microtremors using triaxial sensors to allow recording both vertical and horizontal components is a convenient tool to estimate this period. The term microtemor is used to describe any environmentally-induced soil vibrations due to human activities, industries, traffic and noise produced by tides, wind and teleseisms.

As part of the effort of creating this map of soil periods, the study first involved a detailed comparison of different experimental techniques to determine the fundamental period of soil deposits. This report describes the final selected measuring protocol, post-processing technique, and the final map generated. The final map was based on ambient vibration measurements taken at 134 sites within the city of Mayagüez, Puerto Rico. The predominant site periods were determined using an approach based on the Nakamura (H/V ratio) technique. A discussion of the different factors that were found could affect the results is presented.

ACKNOWLEDGEMENTS

The authors would like to thank all the graduate students involved in the project, as well as their colleagues from the Civil Engineering Department of the University of Puerto Rico at Mayaguez (UPRM), whose comments and suggestions contributed to improve the project. In particular, we would like to acknolwledge the contributions of Dr. Carlos Huerta, Strong Motion Seismologist of the Puerto Rico Strong Motion Program (PRSMP). The help provided by the PRSMP and his Director, Dr. José Martínez-Cruzado, is also acknowledged.

TABLE OF CONTENTS

ABSTRACT ..... **ii**

ACKNOWLEDGEMENTS ..... **iii**

TABLE OF CONTENTS ..... **iv**

LIST OF FIGURES ..... **vi**

LIST OF TABLES ..... **viii**

CHAPTER 1 INTRODUCTION **1**

1.1 General introduction *1*

1.2 Justification *2*

1.3 Objectives *6*

1.4 Report organization *6*

1.5 Dissimination of results *7*

CHAPTER 2 BACKGROUND AND LITERATURE REVIEW **8**

2.1 Introduction *8*

2.2 H/V spectral ratio technique or Nakamura method *8*

CHAPTER 3 PILOT STUDY TO COMPARE SELECT TECHNIQUES USED TO ESTIMATE SITE FUNDAMENTAL PERIODS **15**

3.1 Introduction *15*

3.2 Techniques used to estimate fundamental site periods *15*

3.2.1 Fourier transform spectrum *15*

3.2.2 Spectral ratios with respect to a reference site *16*

3.2.3 Horizontal/Vertical spectral ratio (HVSR) *16*

3.3 Pilot study on ambient vibration measurements in Mayagüez, Puerto Rico *17*

3.3.1 Ground motion records *18*

3.4 Results *20*

CHAPTER 4 APPLICATION OF THE METHODOLOGY TO MAYAGÜEZ, PUERTO RICO **27**

4.1 Introduction *27*

4.2 General description of the city of Mayagüez *27*

4.2.1 Location and city division *27*

4.2.2 Seismic characteristics *27*

4.2.3 Geology *30*

4.2.4 Topography *32*

4.3 Ambient vibration measurements within study area *34*

4.3.1 Instrumentation *35*

4.3.2 Protocol followed for taking measurements *38*

4.3.3 Measurements in the area of Mayagüez *38*

4.4 Ambient vibration measurement analysis *41*

4.4.1 Hanning window *42*

4.4.2 Automatic window selector module *44*

4.5 Window Length (WL) Variation *48*

4.6 Percentage of overlap between windows (OW) variation *50*
4.7 Modification of time for the average short-period (tsta) *52*
4.8 Modification of time for the average long-period (tlta) *53*
4.9 Minimum sta/lta ratio variation *55*
4.10 Maximum sta/lta ratio variation *56*
4.11 Stability analysis of spectral ratio method H / V *58*
4.12 Ground modeling and spectral ratio comparison *59*

CHAPTER 5 ISOPERIOD MAP FOR THE CITY OF MAYAGÜEZ 61
5.1 Introduction *61*
5.2 Results obtained from the first measurements *61*
5.3 Second set of ambient vibration measurements *68*
5.4 Second measurement analysis *69*
5.5 Soil isoperiod maps for the city of Mayagüez *77*

CHAPTER 6 CONCLUSIONS AND RECOMMENDATIONS FOR FUTURE WORK 81

REFERENCES 83

APPENDIX A 87

Protocol followed for taking measurements 87
Required Equipment: *87*
Steel plate to improve soil-instrument contact: *88*
Procedure: *89*

APPENDIX B 91

Matlab programs 91
Program for ambient vibration data analysis *91*
Program for processing seismic accelerograms *98*
Program to determine the spectral ratio with respect to a reference site *100*
Program for determination of the theoretical transfer functions of a soil deposit *102*

LIST OF FIGURES

Figure 1.1: Damage distribution in Shimizu city, 1944 Tonankai earthquake (from Ohsaki, 1972) 2
Figure 1.2: Damage distribution in Nagoya city, 1944 Tonankai earthquake (from Yakoi, 1965) 3
Figure 1.3: Damage distribution in Nakamura town city, 1946 Nankaido earthquake (from Yakoi, 1965). 3
Figure 1.4: Puerto Rico seismic settings and major faults (from Clinton et al., 2006) 4
Figure 1.5: Study area location (from Pando et al., 2006) 5
Figure 2.1: Mayagüez map 28
Figure 2.2: Seismic and plate tectonics for the Caribbean region (from Tuttle et al., 2003). 29
Figure 2.3: Seismic activity and major faults of Puerto Rico (from Clinton et al., 2006). 29
Figure 2.4: Geological map of Mayagüez (from Curet, 1986) 31
Figure 2.5: Location of N-S topographic profile (from Lugo, 2004) 33
Figure 2.6: Topographic profile and associated population data for N-S section 34
Figure 2.7: Typical geological structure of a sedimentary basin (from Nakamura, 2000) 11
Figure 2.8: Transfer function for horizontal and vertical motion 14
Figure 3.1: Strong motion stations in the city of Mayagüez, Puerto Rico 18
Figure 3.2: (a) soil type, (b) shear wave velocities, and (c) N values for "el Viaducto" (from Pérez, 2005) 23
Figure 3.3: Surface response spectrum from the linear analysis and design spectrum according to UBC 97 for artificial earthquakes at "el Viaducto" (from Pérez, 2005) 24
Figure 3.4: Surface response spectrum from the linear analysis and design spectrum according to UBC 97 (El Salvador earthquake)at "el Viaducto" (from Pérez, 2005) 24
Figure 3.5: Surface response spectrum from the non linear analysis and design spectrum according to UBC 97 for artificial earthquakes at "el Viaducto" (from Pérez, 2005) 25
Figure 3.6: Surface response spectrum from the non linear analysis and design spectrum according to UBC 97 (El Salvador earthquake)at "el Viaducto" (from Pérez, 2005) 25
Figure 4.1: ETNA accelerograph used for ambient vibrations 35
Figure 4.2: Biology parking lot (P#1) and Civil Engineering courtyard (P#2) 36
Figure 4.3: Spectral ratio H/V for P#1 using both instruments 37
Figure 4.4: Spectral ratio H/V for P#2 using both instruments 37
Figure 4.5: Location of measurement sites at Mayagüez city 39
Figure 4.6: Location of measurement sites at Mayagüez city with topography 40
Figure 4.7: ETNA accelerometer setting 41
Figure 4.8: Frequency response of a typical window function (from http://en.wikipedia.org/wiki/Window_function). 43
Figure 4.9: Hanning window function (left) and its response in frequency (right) 44

Figure 4.10: JSesame graphical interface. Selected windows are shown in green. 45
Figure 4.11: Ambient vibration records without correcting for site P#3 47
Figure 4.12: Corrected ambient vibration for site P#3 47
Figure 4.13: Spectral ratio H/V for site P#3 48
Figure 4.14: Spectral ratio H/V for site P#3 with WL = 10 seconds 49
Figure 4.15: Spectral ratio H/V for site P#3 with WL = 30 seconds 49
Figure 4.16: Overlapping between adjacent windows 50
Figure 4.17: Spectral ratio H/V for site P#3 with OW = 5% 51
Figure 4.18: Spectral ratio H/V for site P#3 with OW = 50% 51
Figure 4.19: Spectral ratio H/V for site P#3 with tsta = 0.5 seconds 52
Figure 4.20: Spectral ratio H/V for site P#3 with tsta = 2 seconds 53
Figure 4.21: Spectral ratio H/V for site P#3 with tlta = 20 seconds 54
Figure 4.22: Spectral ratio H/V for site P#3 with tlta = 40 seconds 54
Figure 4.23: Spectral ratio H/V for site P#3 with sta/lta = 0.1 55
Figure 4.24: Spectral ratio H/V for site P#3 with sta/lta = 0.8 56
Figure 4.25: Spectral ratio H/V for site P#3 with sta/lta = 1.5 57
Figure 4.26: Spectral ratio H/V for site P#3 with sta/lta = 10 57
Figure 4.27: Spectral ratio H/V for different times during a day for site P#79 58
Figure 4.28: Spectral ratio H/V for site P#17 59
Figure 4.29: Transfer function between surface and basal rock for site P#17 60
Figure 5.1 Preliminary map of fundamental periods for the city of Mayagüez 66
Figure 5.2: Sites where new ambient vibration measurements were taken 67
Figure 5.3: New ambient vibration measurement located at the east area of Mayagüez 69
Figure 5.4: Location of all ambient vibration measurements sites 75
Figure 5.5: Sites where a reliable fundamental period was obtained 76
Figure 5.6: Location of sites where fundamental periods were not obtained 77
Figure 5.7: Site fundamental period map for the city of Mayagüez 78
Figure 5.8: Interpolation types (Adapted from Colin Childs, 2004) 79
Figure 5.9: Isoperiod map for the city of Mayagüez 80

LIST OF TABLES

Table 2.1: Geological stratigraphy table for Mayagüez area (from Curet, 1986) 32
Table 2.2: Population data for areas along the N-S topographic profile (from US Census Bureau, 2000) 34
Table 3.1: Seismic stations information 17
Table 3.2: Recorded earthquake characteristics 19
Table 3.3: Epicentral distances (km) for each seismic station with respect to each earthquake 19
Table 3.4: PGA for each seismic station 19
Table 3.5: PGA for each Seismic Station (May1) 20
Table 3.6: Summary of predominant site periods and frequencies for Dic11 and Oct 17 earthquake 21
Table 3.7: Summary of predominant site periods and frequencies for May 1 earthquake 21
Table 3.8: NEHRP soil profile classification (from UBC 1997) 22
Table 4.1: Parameters used in data processing 46
Table 4.2: Soil properties for site P#17 60
Table 5.1: First set of ambient vibration measurement results 62
Table 5.2 Repetition of ambient vibration measurement at selected sites results 68
Table 5.3: Repetition of ambient vibration measurement at selected sites results 70
Table 5.4: Summary of all ambient vibration measurements 71

CHAPTER 1 INTRODUCTION

1.1 *General introduction*

During an earthquake, the intensity of ground motions at a particular site are a function of several factors such as characteristics of the particular earthquake (e.g., magnitude, duration, frequency content), the epicentral distance, the characteristics of the seismic source, and to a great extent the local geotechnical conditions of the site. The local site conditions (geotechnical conditions and geology) are considered one of the most important factors since they greatly influence the shaking levels experienced at this site. The local site conditions can be cassessed using various techniques including profiles of the shear wave velocity (or average value for the the upper 30 meters in the form of Vs_{30}) or the predominant period of the site (Ts). In this study the focus was to obtain the predominant period (Ts) at each test site as a way of assessing local site conditions and to generate a map of isoperiods for the city Mayagüez, Puerto Rico (PR).

Surveys of distribution of post-earthquake damage over the years has confimed a severe damage is often located in areas with local site effects such as soft soils and high predominant period, thus highlighting the importance of local site effects. Since the severity of the damage is usually related to local amplifications, that in turn are due to geological and geotechnical conditions at any particular site, it is important to develop tools for seismic microzonation of local site effects. The classical method to evaluate local site effects is to use historical earthquake records obtained at several sites within a city or region and compare ground motion levels as a function of soil site conditions and if possible compare record with respect to a reference rock site. This method although useful may not be practical if the city or region does not have a dense network of strong motion instruments or if it has a low recurrence period of earthquakes. In the study city focus of this study the strong motion instrument network is reasonably dense, but the recurrence period of large earthquakes is too large to make this traditional approach practical. Thus the approach deselected consisted in using ambient vibration monitoring using portable instrumentation and carry out the measurements within a dense array of test sites to allow generation of a map of predominant site periods and with this map outline areas within the city of Mayagüez, PR where local site effects may increase the seismic hazard.

1.2 *Justification*

The importance of local site effects and geology on the seismic ground shaking has been recognized since the beginning of modern seismology. For example, the phenomenon of site effects was documented in the early eighteenth century in Japan (Ohsaki, 1972). More recent examples include surveys of post-earthquake damage such as the one shown in Figure 1.1. This figure shows the damage distribution in wood buildings in the city of Shimizu, Japan after the Tonankai earthquake in 1944. About 80% of the buildings in this city that presented damage were concentrated around the estuary of a river which were sites characterized by presence of deep and soft soil deposits (Ohsaki, 1972).

Yakoi et al. (1965) reported similar damage distribution for the same earthquake in Nogoya city (Figure 1.2). It was found that the values of the number of blows (N) from the standard penetration test were very low in the first 10 meters from the surface.

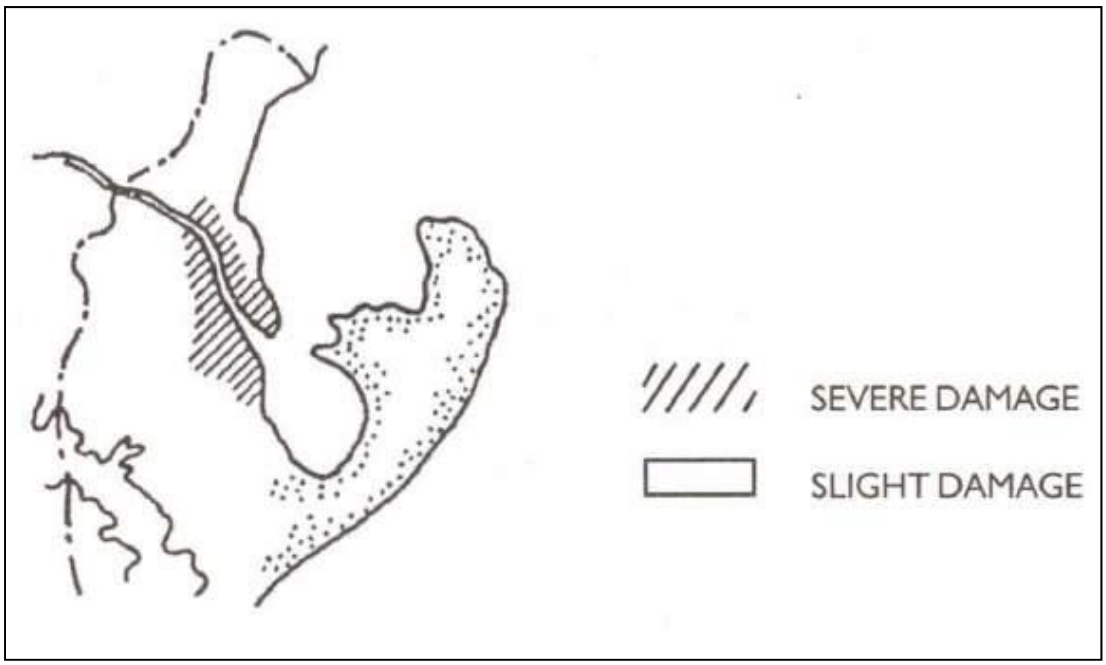

Figure CHAPTER 1.1: Damage distribution in the City of Shimizu, Japan after the 1944 Tonankai earthquake
(adapted from Ohsaki, 1972)

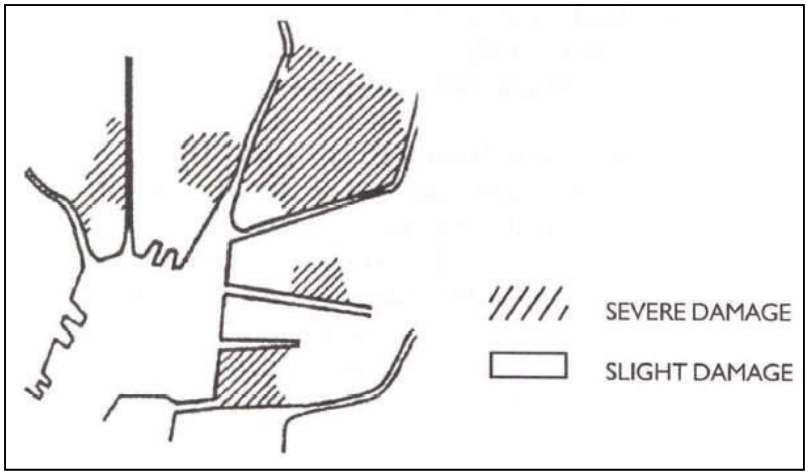

Figure CHAPTER 1.2: Damage distribution in Nagoya city, Japan after the 1944 Tonankai earthquake (adapted from Yakoi, 1965)

Similarly, Figure 1.3 shows damage distribution to wooden buildings in the town of Nakamura, after the Nankaido earthquake in 1946, which again clearly highlighted strong correlation between areas of severe damage and presence of soft soils deposits (Shimizu and Suehiro, 1947). These few examples show how the phenomenon of amplification of the seismic ground motions at sites with soft sediments has been recognized and extensively studied for several decades. Therefore, mapping efforts of soft soil sites (i.e., with long predominant period) is important for seismic hazard reduction efforts for urban centers located in regions of high seismic activity as it can help identify areas with high potential for seismic amplification as well as help identify possible resonance conditions with surrounding buildings.

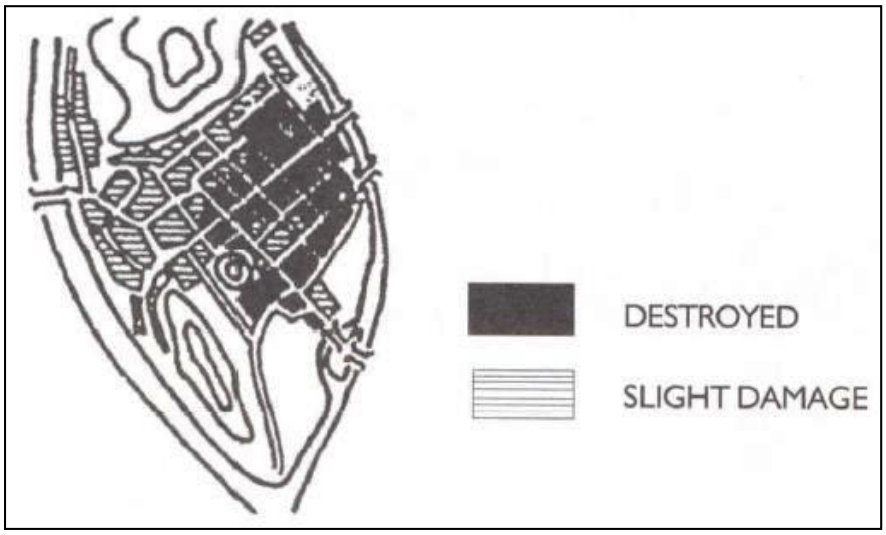

Figure CHAPTER 1.3: Damage distribution in Nakamura town city, 1946 Nankaido earthquake (from Yakoi, 1965)

This NEHRP funded project is for the city of Mayagüez located in the U.S Commonwealth of Puerto Rico (PR). PR has a population of approximately 3.7 million (2010 census) and a territorial extension of about 178 km from west to east, and 65 km from north to south with an average population density of about 400 inhabitants/km^2 which is the second highest population density among U.S. State and territories. Beside a high population density, the island of Puerto Rico is located in a highly seismic region as shown in Figure 1.4. The main sources of seismic activity in Puerto Rico are: 1) The Puerto Rico Trench, a subduction zone to the north; 2) The Muertos Through, a subduction zone to the south; 3) the Anegada Through, an extension zone to the east; 4) the Mona Canyon, and extension zone to the west. All these regions have been deemed capable of producing seismic events greater than M 7.0, and historical records show that all these seismic sources have generated such magnitude events (Asencio, 1980; Moya y McCann, 1992; Clinton et al., 2006). The current standard building code in Puerto Rico, assigned Puerto Rico as seismic zone 3.

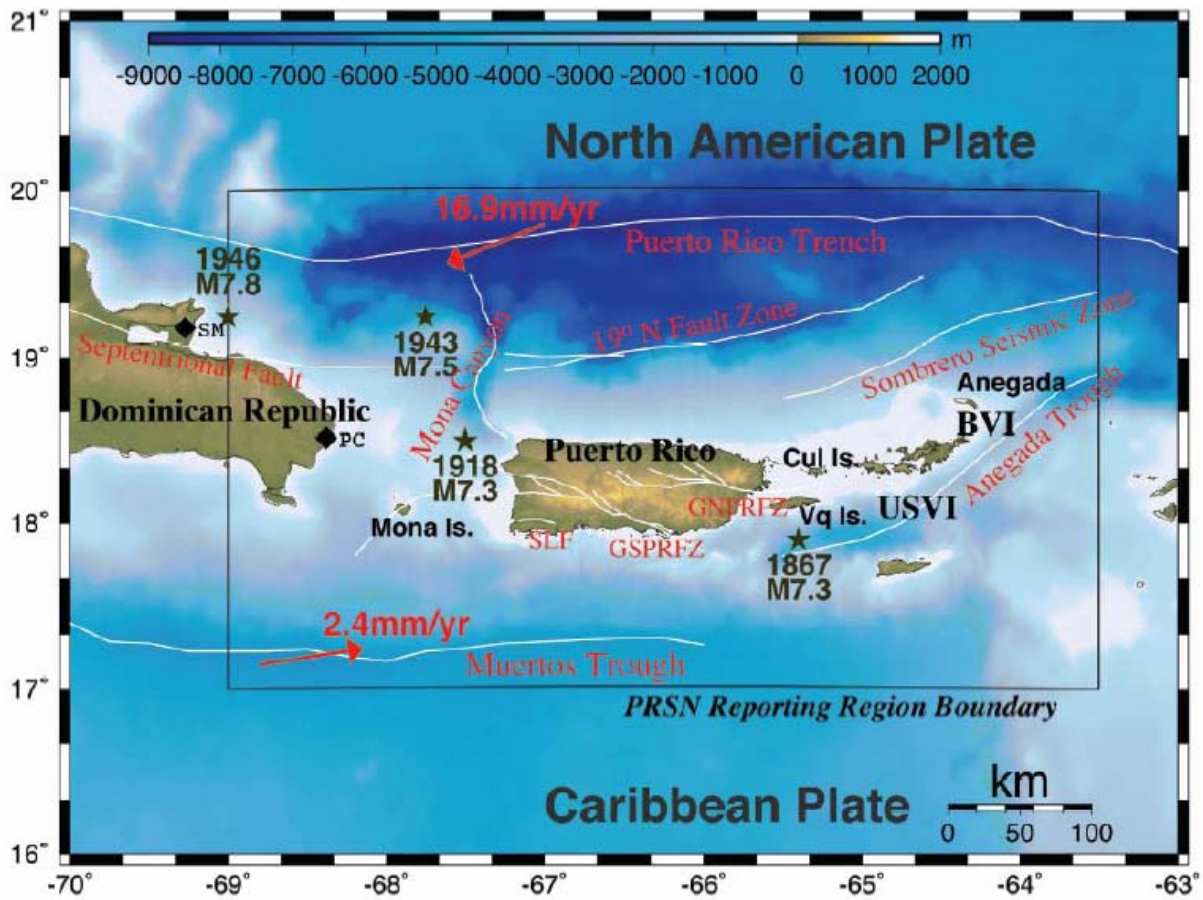

Figure CHAPTER 1.4: Puerto Rico seismic settings and major faults (from Clinton et al., 2006)

For the specific study area of this research, the city of Mayagüez, shown in Figure 1.5, was severly affected by the earthquake of 1918 (Reid and Taber, 1919). This event, which was generated by Mona Canyon, had a magnitude M7.3 (Pacheco and Sykes, 1992). The earthquake caused major structural damage, induced liquefaction in a region near Mayagüez, generated a tsunami, and caused damage of approximately $ 4 million, and 116 people lost their lives (Reid and Taber, 1919, Moya and McCann, 1992; Mercado and McCann, 1998). The modern Mayagüez metropolitan area has a far greater population density and larger presence of infrastructure (with most of its structures without having experienced a strong seismic event as they most have been built after the 1918 earthquake), a similar seismic event would likely lead to more severe damage as experienced in the 1918 earthquake (Clinton et al., 2006).

Figure CHAPTER 1.5: General location map shown study area

Despite the high seismicity of Mayagüez and its high population density, research to identify and properly mitigate the seismic risk lags behind with other active seismic regions of the United States.

1.3 *Objectives*

The main objective of this project was to develop a map of soil predominant periods for the city of Mayaguez, PR to be used for seismic risk reduction purposes. Additional specific objectives for this project were:

- Compare different commonly used techniques to estimate site effects from ambient vibration measurements and strong motion records.
- Obtain experimentally fundamental soil periods in different areas of Mayagüez using ambient vibration measurements in conjunction with the spectral ratio technique of Nakamura.
- Construct an isoperiod map for the city of Mayagüez.

1.4 *Report organization*

This repot consists of five chapters organized in the following manner:

- Chapter 1 describes the general motivation and objectives of this study, and describes the seismicity of the study area.
- Chapter 2 presents a summary of the theoretical background of the techniques commonly used to obtain predominant site periods using ambien vibrations. The main focus however was the H/V spectral ratio technique, also referred in the literature as the Nakamura methodology.
- Chapter 3 presents a comparison between select techniques commonly used to estimate the fundamental site period. This comparison was done based on an initial pilot project carried also in Mayagüez, Puerto Rico with the main objective to select the most adequate technique to be used for the main field campaing required for this project.
- Chapter 4 describes the geoleogy, geotechnical conditions, and topography of the city of Mayaguez. It also presents and discussed the field results obtained for the study area using the selected H/V spectra ratio technique.

- Chapter 5 presents the map of predominat site periods generated for the city of Mayagüez. This chapter also describes the methodology followed to construct the isoperiod map.

- Chapter 6 presents the principal conclusions drawn form this project and suggested recommendations for possible future work.

1.5 *Dissimination of results*

The work funded from this NEHRP grant (USGS Grant Number: 10HQPAQ0001) resulted in one mayor deliverable in the form of a isoperiod map which has been distributed through the Puerto Rico Strong Motion Program. Additional dissemination efforts have included the folloing peer-reviewed articles in progress or completed:

- Suarez-Colche, L.E., *Pando, M.A., and Ritta, R. (2012), "Ambient Vibration Measurements for Estimation of Site Fundamental Periods -Case History of the City of Mayaguez, Puerto Rico", Paper accepted for the 15th World Conference of Earthquake Engineering (15WCEE), Lisbon, Portugal, 24-28 September, 2012, 10 p.

- Ritta, R.J., Suarez, L.E., and Pando, M.A. (2012), "Determinación del Período Fundamental del Suelo usando Vibración Ambiental y el Cociente Espectral Horizontal/Vertical", (In Spanish), Submitted and accpeted to the Mecanica Computacional, Vol. XXXI, Eds. Cardona, Kohan, Quinteros, and Storti, Salta, Argentina, Nov. 13-16, 2012, 11 p.

- Huerta-Lopez, C.I., Pando, M.A., Suarez, L.E., Ritta, R., and Martinez-Cruzado, J.A. (2009), "Shallow Soil Layers Fundamental Vibration Mode: A Comparison of Estimations Obtained With the Random Decrement Method and H/V Spectral Ratios Using Weak and Moderate Seismic Ground Motions", American Geophysical Union, Spring Meeting 2009, Abstract #NS23B-01.

CHAPTER 2 BACKGROUND AND LITERATURE REVIEW

2.1 *Introduction*

This chapter presents a literature review regarding methodologies used to estimate the predominant site period using ambien vibrations. The main focus however was on the spectral ratio method developed by Nakamura (Nakamura, 1989).

2.2 *H/V spectral ratio technique or Nakamura method*

Since the late 50's in Japan and nowadays around the world several publications are available regarding the use of microtemblor measurements to evaluate certain site characteristics. The use of microtemblors also known as ambient vibration to evaluate local seismic effects provides several advantages as long as the results are reliable under a theoretical and practical point of view.

Japan started to take advantage of the microtemblors systematic records to infer soil properties in the 50's which produced a more accurate and reliable development in seismic design codes. Nakamura postulates that ambient vibrations recorded in the ground surface can be caused by two different of waves: surface waves (Rayleigh waves) and body waves (P and S waves). If any superficial source generates body waves through a medium formed by a elastic layer over a rock with a large difference in impedance, this waves propagates following a complex pattern which depends on the origin and localization of the source that originate them. Due to the reflections that occur in the soil-rock interface, part of the P and S waves that propagates from the base to the surface can be recorded by sensors. Based on the hypothesis that ambient vibrations result from two type of waves, it is possible to explain why the H/V spectral ratio technique can be used for vibrations produced by earthquakes.

Taking into account the previous assumptions, Nakamura (2000) formulated the soil movement on the surface as the sum of motion due to body waves traveling from the base plus

the contribution of surface waves. The superposition should be done it in the frequency domain. As demonstrated in soil dynamics, the contribution of the waves that propagate from the rock towards the surface can be expressed as the product of the transfer function between the rock and soil (this is known as Frequency Response Function in Structural Dynamics) by the Fourier transform of the motion in the rock. Thus, the surface Fourier spectrum of can be expressed as the sum of these contribution plus the Rayleigh waves Fourier spectrum . For example, for the horizontal component this can be expressed mathematically as:

$$H_f(\omega) = A_h(\omega)\, H_b(\omega) + H_s(\omega) \tag{2.1}$$

where:

- $A_h(\omega =$ Transfer function between the rock and surface of the horizontal motion (called amplification factor by Nakamura)
- $H_b(\omega)$ = Fourier transform of the horizontal motion in the basal rock
- $H_s(\omega)$ = Fourier transform of the horizontal motion in the surface due to Rayleigh waves
- $H_f(\omega)$ = Fourier transform of the surface motion taking into account both types of waves (body and surface)

For the vertical motion a similar expression can be formulated as:

$$V_f(\omega) = A_v(\omega)\, V_b(\omega) + V_s(\omega) \tag{2.2}$$

where the four functions have the same meaning as equation 2.1 but with the vertical motion components.

It is demonstrated in Soil Dynamics that the transfer function for horizontal movement of a soil deposit with depth h, a material density ρ, damping ratio ξ and shear wave propagation velocity is:

$$A_h(\omega) = \frac{1}{\cos\left(\omega h / v_s^*\right)} \tag{2.3}$$

where v_s^* is the complex shear wave velocity:

$$v_s^* = v_s\sqrt{1+i2\xi} \tag{2.4}$$

and $v_s = \sqrt{G/\rho}$ is the shear wave velocity, G being the shear modulus and ρ the material density from which the shear wave is propagated.

Transfer Function Av (ω) for the vertical motion has the same shape as that of equation (2.3), but the complex velocity vs* must be replaced by the complex velocity of P waves : $v_p^* = v_p\sqrt{1+i2\xi}$.

H_f (ω) and V_f (ω) spectra in equations (2.1) and (2.2) are not useful to identify the natural frequencies of the deposit because they also contain the dominant frequencies of the sources that generated the waves. To identify the natural frequencies, it is common to use ratios between the motion spectra of two points in the soil deposit (thus eliminating the so-called "fountain effect"). This ratio defines the transfer function between the two points. For example, Nakamura proposes two spectral ratios called T_h (ω) and T_v (ω):

$$T_h(\omega) = \frac{H_f(\omega)}{H_b(\omega)} \quad ; \quad T_v(\omega) = \frac{V_f(\omega)}{V_b(\omega)} \tag{2.5}$$

where T_h(ω) is the transfer function between the horizontal motion in the surface and the corresponding motion in the basal rock (see figure 2.7). In the same manner, T_v(ω) is the transfer function between the vertical motion in the surface and the basal rock.

Nakamura (2000) considers that H_b (ω) and V_b (ω) are equal to the spectra on a rocky outcrop, which are called H_r (ω) and V_r (ω) (see Figure 2.4). This could be considered as an approximation, but is not strictly true: the peaks of the spectra do agree but the magnitudes of H_r (ω) and V_r (ω) are lower than those of H_b (ω) and V_b (ω).

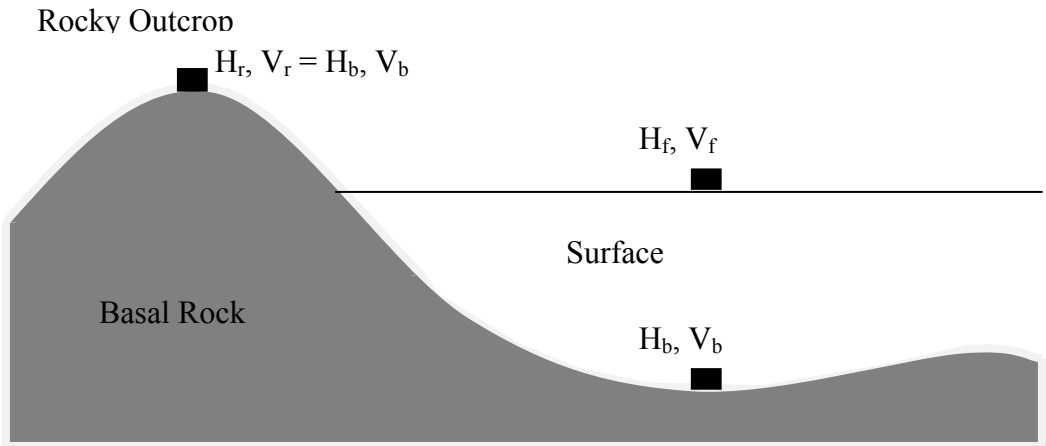

Figure CHAPTER 2.1: Typical geological structure of a sedimentary basin (from Nakamura, 2000)

If the function T_h (ω) were available, it would be possible to determine the natural frequencies of the deposit, but due to difficulty or inconvenience in obtaining Hb (ω), it is not usually possible to obtain T_h (ω) .Nakamura proposes to use a function of frequency which is defined as the ratio of transfer functions T_h (ω) and T_v (ω):

$$T_h^*(\omega) = \frac{T_h(\omega)}{T_v(\omega)} \tag{2.6}$$

Some authors (Lerman and Chavez-Garcia, 1993) indicated that the transfer function T_h (ω) is divided by T_v (ω) to compensate "the effect of the source." However, as discussed below, setting the ratio in equation (2.6), the measurements need to be made to identify the fundamental frequency of the site are simplified significantly.

Replacing T_h(ω) and T_v (ω) from equation (2.5) into (2.6):

$$T_h^*(\omega) = \frac{T_h(\omega)}{T_v(\omega)} = \frac{H_f(\omega)/H_b(\omega)}{V_f(\omega)/V_b(\omega)} = \frac{H_f(\omega)}{V_f(\omega)} \frac{1}{H_b(\omega)/V_b(\omega)} \tag{2.7}$$

Using results from experimental measurements, Nakamura considers that the ratio of H_b (ω) and V_b (ω) is approximately equal to 1, at least within the deposit fundamental frequency (ω_o)

range. This result was later verified by other researchers (Lerman and Chavez-Garcia, 1994; Huang and Chiu, 1998). the ratio T_b (ω) / T_v (ω) results being:

$$T_h^*(\omega) = \frac{T_h(\omega)}{T_v(\omega)} \approx \frac{H_f(\omega)}{V_f(\omega)} \tag{2.8}$$

Replacing $H_f(\omega)$ and $V_f(\omega)$ from. (2.1) and (2.2):

$$T_h^*(\omega) \approx \frac{H_f(\omega)}{V_f(\omega)} = \frac{A_h(\omega)H_b(\omega)+H_s(\omega)}{A_v(\omega)V_b(\omega)+V_s(\omega)} \tag{2.9}$$

The ratio H_f (ω) / V_f (ω) is called QTS by the acronym of "Quasi Transfer Spectrum" However, the engineering community calls it simply the ratio H / V. Using Nakamura notation and knowing that $H_b(\omega)/V_b(\omega) \approx 1$, T_h^* (or QTS) , the following expression is obtained:

$$QTS = \frac{H_b(\omega)}{V_b(\omega)} \times \frac{\left(A_h(\omega)+\frac{H_s(\omega)}{H_b(\omega)}\right)}{\left(A_v(\omega)+\frac{V_s(\omega)}{V_b(\omega)}\right)}$$

$$QTS \approx \frac{A_h(\omega)+\frac{H_s(\omega)}{H_b(\omega)}}{A_v(\omega)+\frac{V_s(\omega)}{V_b(\omega)}} \tag{2.10}$$

Note that if there were no Rayleigh waves or their effect is negligible, , $H_s(\omega) \approx 0$ and $V_s(\omega) \approx 0$, the Quasi Transfer Spectrum or ratio H/V becomes:

$$QTS \approx \frac{A_h(\omega)}{A_v(\omega)} \tag{2.11}$$

Nakamura argues that in the vicinity of the fundamental frequency ω_o for the corresponding deposit horizontal, the transfer function A_v (ω) for P waves is approximately equal to 1. Nakamura's argument is based on the fact that P-wave velocity is three to four times the S wave

and the vertical component is hardly amplified in natural frequency zone. In Fact, The relationship between P wave S wave velocities depends on Poisson's ratio ν according to the following expression:

$$v_p = \sqrt{\frac{2(1-\nu)}{1-2\nu}} v_s \tag{2.12}$$

Figure 2.8 shows the transfer functions for a soil composed of an uniform layer over a rigid rock. The deposit has a depth h = 540 feet, Poisson's ratio ν = 0.4 (thus v_p = 2.45 v_s), the S-wave velocity is v_s = 1500 ft / sec and the soil damping ratio is ξ = 0.08. It is shown that close to the first fundamental frequency (ω_o = 4.36 rad / s), | Av (ω) | is approximately 1, and is closer to 1 as ν increases. Considering this approach as valid, and if the effect of Rayleigh waves is negligible, the quasi-transfer function is QTS ≈ Ah (ω). In this case the ratio H / V can be used not only to identify the fundamental frequency of the deposit but also to estimate the S wave's amplification travelling through the soil deposit.

If the presence of Rayleigh waves is significant, the second terms in the numerator and denominator of equation (2.10) are dominant:

$$\frac{H_s(\omega)}{H_b(\omega)} \approx A_h(\omega) \quad ; \quad \frac{V_s(\omega)}{V_b(\omega)} \approx A_v(\omega) \tag{2.13}$$

Under this situation and using again the fact that $H_b(\omega) / V_b(\omega) \approx 1$, the Quasi Transfer Spectrum is reduced to:

$$QTS \approx \frac{H_s(\omega)}{H_b(\omega)} \frac{V_b(\omega)}{V_s(\omega)} = \frac{H_s(\omega)}{V_s(\omega)} \frac{1}{H_b(\omega) / V_b(\omega)} \approx \frac{H_s(\omega)}{V_s(\omega)}$$

$$QTS \approx \frac{H_s(\omega)}{V_s(\omega)} \tag{2.14}$$

Nakamura also argues that in this case (dominant Rayleigh waves), the term $V_s(\omega)$ near the frequency ω_o is small compared to $H_s(\omega)$, resulting in a peak ratio $H_s(\omega) / V_s(\omega)$. Besides, this

peak roughly coincides with the natural frequency for horizontal vibrations. This may be due to the fact that the horizontal components of the elliptical motion of Rayleigh waves excite the natural frequency ω_o of the deposit since as mentioned before, the vertical amplification is not significant close to ω_o.

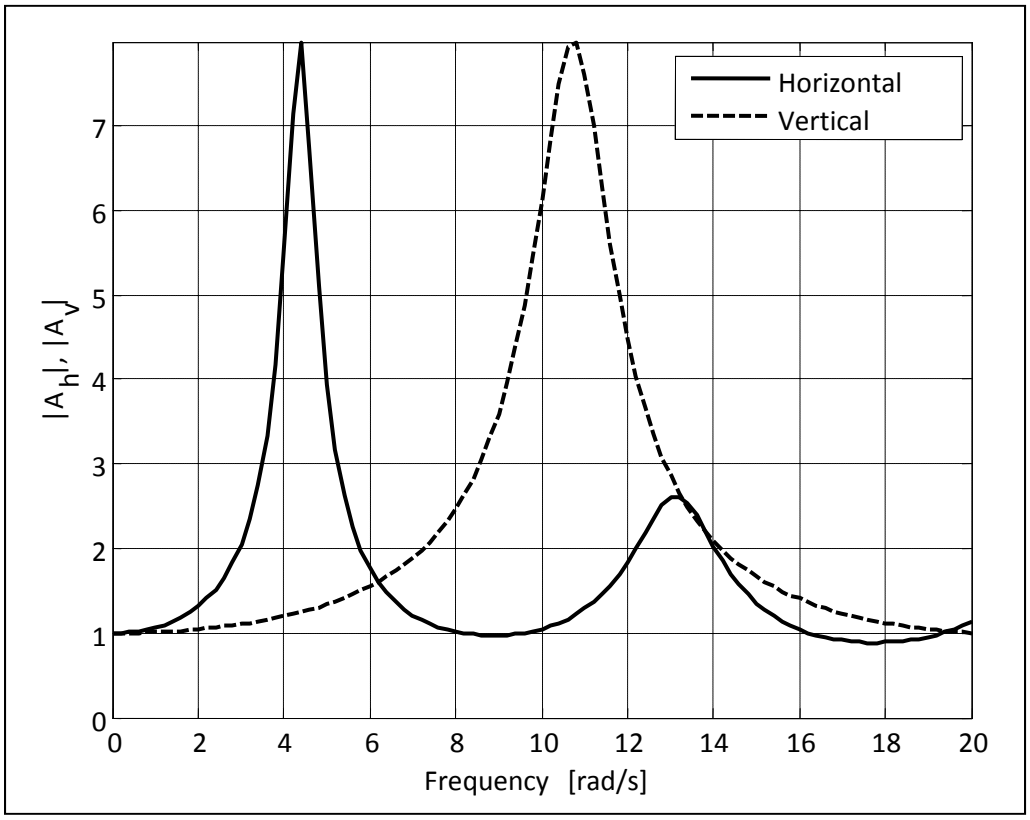

Figure CHAPTER 2.2: Transfer function for horizontal and vertical motion

In conclusion, regardless of the type of waves and their relative importance in the records of surface motions $H_f(\omega)$ and $V_f(\omega)$, the relationship between them (the quasi-spectrum or H / V ratio) has a peak that is consistent with the deposit fundamental frequency ω_o associated with horizontal vibration.

CHAPTER 3 PILOT STUDY TO COMPARE SELECT TECHNIQUES USED TO ESTIMATE SITE FUNDAMENTAL PERIODS

3.1 *Introduction*

This chapter presents the results of an initial pilot study carried out to compare and test the ease of implementation of different techniques commonly used to estimate site fundamental periods. Although the H/V spectral ratio or Nakamura technique has received a broad acceptance among the seismic community due to its simple and economic application, there are other techniques available to determine site predominant periods. This chapter describes select techniques commonly used to analyze different type of data to determine site effects. The results of this pilot study will compare the different techniques and compare them with the spectral ratio H/V. Preliminary results and observations from this pilot study were presented in Pando et al. (2008).

3.2 *Techniques used to estimate fundamental site periods*

3.2.1 *Fourier transform spectrum*

This technique consists in examining the horizontal component from the Fourier spectrum. The technique has been applied either to microtemblors or earthquakes. (e.g. Lermo and Chavez-Garcia, 1994; Ojeda and Escallon, 2000). Initially, the method examines Fourier Spectrum horizontal components obtained from ambient vibration records to determine the site fundamental period and the corresponding amplification factor. However, dominant period interpretation can be difficult for earthquake records where the dominant period of the ground motion is quite different from the site fundamental period. This technique is only recommended for a preliminary data analysis before performing a more intensive investigation to determine the results reliability.

3.2.2 *Spectral ratios with respect to a reference site*

This technique is also referred as Kagami spectral ratio or Borcherdt method. Kagami et. Al (1982) used this concept using microtemblors and Borcherdt (1970) applied the technique to ground motion generated by nuclear explosions in Nevada and recorded in several stations located at San Francisco Bay. Borcherdt also analyzed strong motion data caused by San Francisco earthquake on March 22, 1957.

The methodology consist in computing the ratio of Fourier spectral amplitudes between the motion horizontal components recorded on a site and other close but in rock, which is used as a reference site (With respect to a common source). The spectral ratio is calculated as follows:

$$K_{SB} = \frac{H_S}{H_B} \tag{3.1}$$

where HS and HB are the Fourier spectra amplitudes of the site horizontal components and reference site on rock, respectively.

3.2.3 *Horizontal/Vertical spectral ratio (HVSR)*

As explained in chapter 2, this method is attributed to Nakamura (1989) and essentially consists of calculating the spectral ratio between horizontal and vertical components of records obtained at the site of interest. The application of this technique does not require a reference site which is an advantage because this is not always one available. The literature shows that it has been mainly applied to microtemblor records, but has also been applied to earthquake records. The methodology applied to microtemblor was studied in considerable detail in the European research project SESAME (SESAME, 2004). The spectral ratio H / V is usually defined as:

$$\frac{H}{V} = \sqrt{\frac{H_{E-O}^2 + H_{N-S}^2}{2 \times V^2}} \tag{3.2}$$

where $H_{E\text{-}w}$, $H_{N\text{-}S}$ and V are the spectral Fourier amplitude in E-W, N-S and vertical direction respectively.

3.3 *Pilot study on ambient vibration measurements in Mayagüez, Puerto Rico*

The ground motion recorded and analyzed to compare the various techniques described above corresponded to five strong motion seismic stations located within the city of Mayagüez, which is located on the west coast of Puerto Rico. These stations are part of a relatively dense network of strong motion instrumentation of the city, which is administered by the Strong Motion Program of Puerto Rico (PRSMP by its initials in English). Figure 3.1 shows the location of seismic stations in Mayagüez, and the five stations analyzed. Table 3.1 summarizes relevant information from each of the stations used in this analysis while figure 3.1 shows the station location within the city. Additional details of the pilot study can be found in Pando et al. (2008).

Table CHAPTER 3.1: Seismic stations information

Station Name	Abrev.	Geographic Coordinates	Sensor Type	Activation Level [1] (%g)	Ground Conditions[2]
Parroquia de Fátima	MY02	N 18.167150 O 67.151370	Triaxial EpiSensor	H = 1.0 V = 0.2	Soil Type NEHRP: D Topography: Plain
Capilla Santo Niño	MY03	N 18.240750 O 67.172200	Triaxial EpiSensor	H = 1.0 V = 0.2	Soil Type NEHRP: F Topography: Plain
Monasterio Benedictino	MY05	N 18.185450 O 67.138030	Triaxial EpiSensor	H = 1.0 V = 0.2	Soil Type NEHRP: B/C Topography: Top of a Hill
Catedral de Mayagüez	MY08	N 18.200178 O 67.137512	Triaxial EpiSensor	H = 1.0 V = 0.2	Soil Type NEHRP: E Topography: Plain
Edificio Darlington	MY09	N 18.205160 O 67.147000	Triaxial EpiSensor	H = 1.0 V = 0.2	Soil Type NEHRP: D Topography: Plain

Notes: (1): The trigger levels reported are values used by PRSMP operation. For records of ambient vibration trigger levels were removed to ensure continuous records H = horizontal component, V = vertical component. (2): NEHRP soil classification (BSSC, 2001) based on Llavona (2004) and Pando et al. (2006).

From the five sites listed above, MY05 was selected as a reference site (rock site) for SRRS technique. This site is considered the most competent among all seismic stations located within the city. The soil profile for this site can be classified as B and C, according to NEHRP soil classification, and corresponds to a very dense soil or soft rock with an average shear wave velocity between 360 and 760 m / s (1200 to 2500 ft / s). This site was also selected as a reference because it is located on top of a mountain that falls within the geological stratigraphy of Maricao, which is composed of massive breccia, conglomerate sandstone and limestone

(Curet, 1986). Therefore, all fundamental period predictions that require ratios with respect to a reference rock site will be computed using the station MY05.

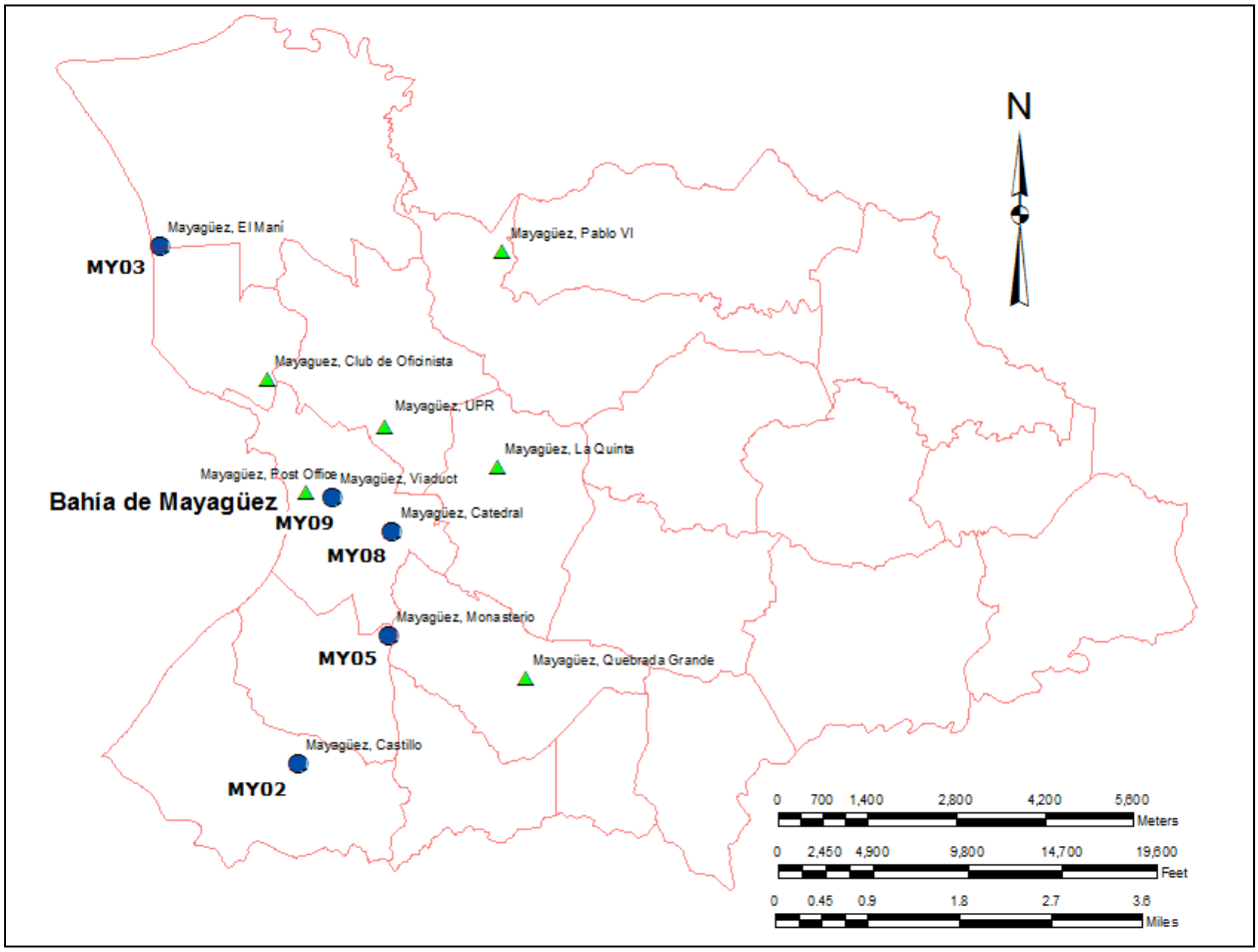

Figure CHAPTER 3.1: Strong motion stations in the city of Mayagüez, Puerto Rico

3.3.1 *Ground motion records*

The ground motion seismic events studied included three low environmental vibration intensity and recorded during a period of 24 hours at each seismic station. The three analyzed seismic events were recorded on December 11, 2000, October 17, 2001 and May 1, 2007. The December 2000 event had a magnitude of 5.4 MW and was generated by the Puerto Rico Trench (see Figure 1.1) to a estimated depth of 46.9 km (PRSMP, 2008). The October 2001 event had a local magnitude ML of 4.3 and was generated by Mona Cannon (see Figure 1.1) to an estimated depth of 25.1 km (PRSMP, 2008). The May 2007 event had a magnitude of 3.3 ML and an estimated depth of 5.9 km. Table 3.2 shows the geographical coordinates geographical coordinates of the

three earthquakes as well as their magnitudes, source and focal depths, while Table 3.3 shows the epicentral distances (in km) of each recording station for each earthquake. The analysis of these earthquakes will be divided into two parts because they have not been recorded in all seasons. The first two appointed earthquakes were recorded by stations MY02, MY03, MY05 and MY08, while the third earthquake was recorded by stations MY02, MY05 and MY09. The peak ground accelerations (PGA) for these three weak seismic events are summarized in Tables 3.4 and 3.5.

Table CHAPTER 3.2: Recorded earthquake characteristics

	December 11 / 2000	October 17 /2001	May 1 / 2007
Latitude (N)	19.070	18.366	18.124
Length(O)	67.058	67.617	67.060
Magnitude	5.4 (M_W)	4.3 (M_L)	3.3 (M_L)
Seismic Source	PR Trench	Mona Cannon	San German
Focal Depth (Km)	46.9	25.1	5.9

Table CHAPTER 3.3: Epicentral distances (km) for each seismic station with respect to each earthquake

	December 11 / 2000	October 17 /2001	May 1 / 2007
MY02	100.41	53.94	10.78
MY03	92.56	49.04	-
MY05	98.26	54.4	10.69
MY08	96.6	53.93	-
MY09	-	-	12.85

Table CHAPTER 3.4: PGA for each seismic station

Station	Estimated NEHRP classification	December 11 / 2000 (M_W = 5.4)		October 17 / 2001 (M_L = 4.3)		Ambient Vibration
		Horizontal PGA (cm/s^2)	Vertical PGA (cm/s^2)	Horizontal PGA (cm/s^2)	Vertical PGA (cm/s^2)	Horizontal PGA (cm/s^2)
MY02	D	5.59	1.88	6.09	2.82	0.016
MY03	F (E)[1]	5.83	2.81	11.27	9.19	0.011
MY05	B/C	2.23	1.21	5.72	2.27	0.006
MY08	E	7.95	1.92	12.53	3.47	0.014

Note: (1): The site is listed as a class MY03 NEHRP F because it is susceptible to liquefaction. In terms of the velocity profile of the shear wave, classified as E.

As expected, higher values of horizontal PGA were recorded in MY03 and MY08 stations for earthquakes on December 2000 and October 2001, while for the earthquake on May 2007, the highest values occurred at stations MY02 and MY09. This coincides with the NEHRP classification of the stations. PGA values for the October 2001 event were higher than those for the December 2000 event due to the greater proximity of this event, which was originated in the Mona Canyon.

Table CHAPTER 3.5: PGA for each Seismic Station (May1)

Station	Estimated NEHRP classification	May 1 / 2007 (M_L = 3.3)		Ambient Vibration
		Horizontal PGA (cm/s^2)	Vertical PGA (cm/s^2)	Horizontal PGA (cm/s^2)
MY02	D	16.801	8.898	0.016
MY05	B/C	6.908	4.688	0.006
MY09	D	8.362	4.839	0.437

3.4 *Results*

The processing of the measurements was conducted using three programs written in Matlab (HVSRAV.m, HVSREA.m and SRRS.m, which are presented in Appendix B) and a commercial program, JSesame, whose origin is the European SESAME project(SESAME , 2004). The objective of this analysis is to compare the fundamental period obtained for each of the sites, using different techniques described above, but mainly to check the validity of the technique H / V using microtemblor records.

The predominant site periods estimated for the five recording sites are summarized in Tables 3.6 and 3.7. The tables present the results divided into two groups: estimates based on seismic records and weak environmental vibration (microtemblor). Table 3.6 presents the results obtained using earthquakes on Dic11 Oct17, while Table 3.7 presents for the earthquake May1.

In general, the predictions obtained with different methods compare reasonably well, except for the MY05 reference site, as shown in Table 3.6. In terms of computational effort, the simplest method was HVSR-VA, which has the additional advantage that data can be obtained easily and quickly without having to wait for the occurrence of an earthquake.

Table CHAPTER 3.6: Summary of predominant site periods and frequencies for Dic11 and Oct 17 earthquake

Station	NEHRP Classification	Estimates based on weak earthquakes			Estimates based on microtemblors	
		FTS-MD	SRRS	HVSR-MD	FTS-VA	HVSR-VA
MY02	D	0.22 s (4.65 Hz)	0.21 s (4.78 Hz)	0.22 s (4.42 Hz)	0.21 s (4.87 Hz)	0.18 s (5.57 Hz)
MY03	F (E)	0.47 s (2.12 Hz)	0.56 s (1.77 Hz)	0.52 s (1.94 Hz)	0.37 s (2.70 Hz)	0.39 s (2.55 Hz)
MY05	B/C	0.27 s (3.71 Hz)	Ref.	0.19 s (5.32 Hz)	0.10 s (10.0 Hz)	0.10 s (9.7 Hz)
MY08	E	0.28 s (3.57 Hz)	0.28 s (3.60 Hz)	0.27 s (3.74 Hz)	0.27 s (3.73 Hz)	0.27 s (3.70 Hz)

Note: FTS = Direct interpretation of the Fourier spectrum; SRRS = spectral ratios with respect to a reference rock site (Kagami) HVSR Spectral Ratio = Horizontal / Vertical on a given site (Nakamura), MD = Weak Motion VA = Environmental Vibration Ref =reference site.

Table CHAPTER 3.7: Summary of predominant site periods and frequencies for May 1 earthquake

Station	NEHRP Classification	Estimates based on weak earthquakes			Estimates based on microtemblors	
		FTS-MD	SRRS	HVSR-MD	FTS-VA	HVSR-VA
MY02	D	0.21 s (4.70 Hz)	0.21 s (4.77 Hz)	0.20 s (4.90 Hz)	0.21 s (4.87 Hz)	0.18 s (5.57 Hz)
MY05	B/C	0.12 s (8.49 Hz)	Ref.	0.15 s (6.62 Hz)	0.10 s (10.0 Hz)	0.10 s (9.70 Hz)
MY09	D	0.70 s (1.42 Hz)	0.75 s (1.34 Hz)	0.77 s (1.30 Hz)	0.28 s (3.63 Hz)	0.67 s (1.50 Hz)

Note: FTS = Direct interpretation of the Fourier spectrum; SRRS = spectral ratios with respect to a reference rock site (Kagami) HVSR Spectral Ratio = Horizontal / Vertical on a given site (Nakamura), MD = Weak Motion VA = Environmental Vibration Ref =reference site.

The estimated site period increases as the NEHRP soil classification increases as expected (Table 3.8 shows the NEHRP soil classification). However, the estimate using the FTS-

MD technique for site MY05 does not meet this trend which is expected since as it was mentioned before, this technique does not always yield favorable results and should only be used for preliminary analysis of the data.

In order to validate the obtained results, another comparison is performed using the results presented by Perez (2005) in his master's thesis. Perez presented a linear and nonlinear analysis equivalent to the ground response, using data from SASW (Spectral Analysis of Surface Waves) and standard penetration for one dimensional case. This study also showed the surface ground spectra response for each of the studied sites. The calculation of the ground response was performed using the program SHAKE2000 along with several earthquake records. The required input data were a history of accelerations of an earthquake, the ground profile and the dynamic properties of the soil. Five earthquakes were used as acceleration records, four artificial and the El Salvador earthquake occurred on October 10, 1986.

Table CHAPTER 3.8: NEHRP soil profile classification (from UBC 1997)

Soil Type	Soil Profile Description
A	Hard rock with shear wave velocity Vs> 5000 ft / s (1500 m / s)
B	Rock with shear wave velocity of 2500 <Vs ≤ 5000 ft / s (760 <Vs ≤ 1500 m / s)
C	Very dense soil and soft rock with shear wave velocity of 1200 <Vs ≤ 2500 ft / s (360 <Vs ≤ 760 m / s) or standard penetration resistance N> 50 or shear strength of the moist specimen S_u ≥ 2000 psf (100 kPa)
D	Rigid Soil shear wave velocity of 600 <Vs ≤ 1200 ft / s (180 <Vs ≤ 360 m / s) or standard penetration resistance of 15 ≤ N ≤ 50 or shear strength of the wet specimen 1000 ≤ S_u < 2000 psf (50 ≤ S_u < 100 kPa)
E	Soil profile with shear wave velocity Vs <600 ft / s (180 m / s) or any profile with more than 10 ft (3 m) of soft clay defined as soil with plasticity index PI> 20, water content w ≥ 40% and shear strength of the wet specimen S_u < 500 psf (25 kPa)
F	Soils requiring site specific evaluation: Soils susceptible to failure or collapse under seismic loading, ie, sensitive liquefaction of sensitive clay soils or slightly cemented soils that can collapse under seismic loading. Layers of peat and / or highly organic clay with a thickness greater than 10 ft (3 m) Layers of clay with high plasticity (PI> 75) and a thickness greater than 25 ft (8 m) Layers of soft to medium clay with a thickness greater than 120 ft (36 m)

One of the analyzed sites analyzed was “el Viaducto” located on Highway # 2 at Mayagüez, which is close to the seismic station located in the Darlington building (MY09). Figure 3.2 shows the soil profile characteristics in the Viaduct (soil description, shear wave velocities and N values obtained from standard penetration test). The spectrum response obtained from the linear and nonlinear analysis for the artificial earthquakes (arithmetically averaged) and El Salvador earthquake can be seen in figures 3.3, 3.4, 3.5 and 3.6. From the results obtained by Perez (2005), the fundamental period obtained using linear analysis at “el Viaducto” was 0.5 seconds, while the non-linear analysis fundamental period was 0.74seconds. The fundamental periods at site MY09 are closer to the periods obtained from the nonlinear analysis, except for the FTS-VA method as per table 3.7. If the obtained fundamental periods are averaged the result would be 0.63 seconds.

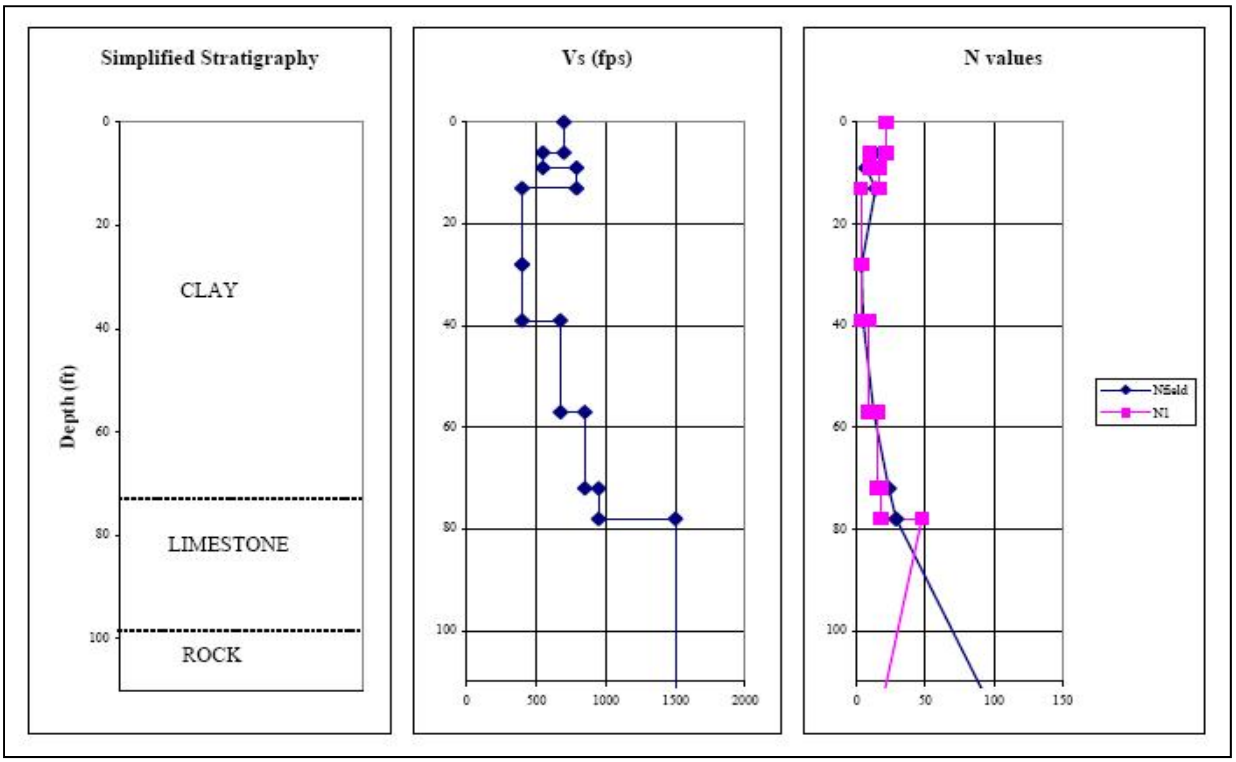

Figure CHAPTER 3.2: (a) soil type, (b) shear wave velocities, and (c) N values for “el Viaducto” (from Pérez, 2005)

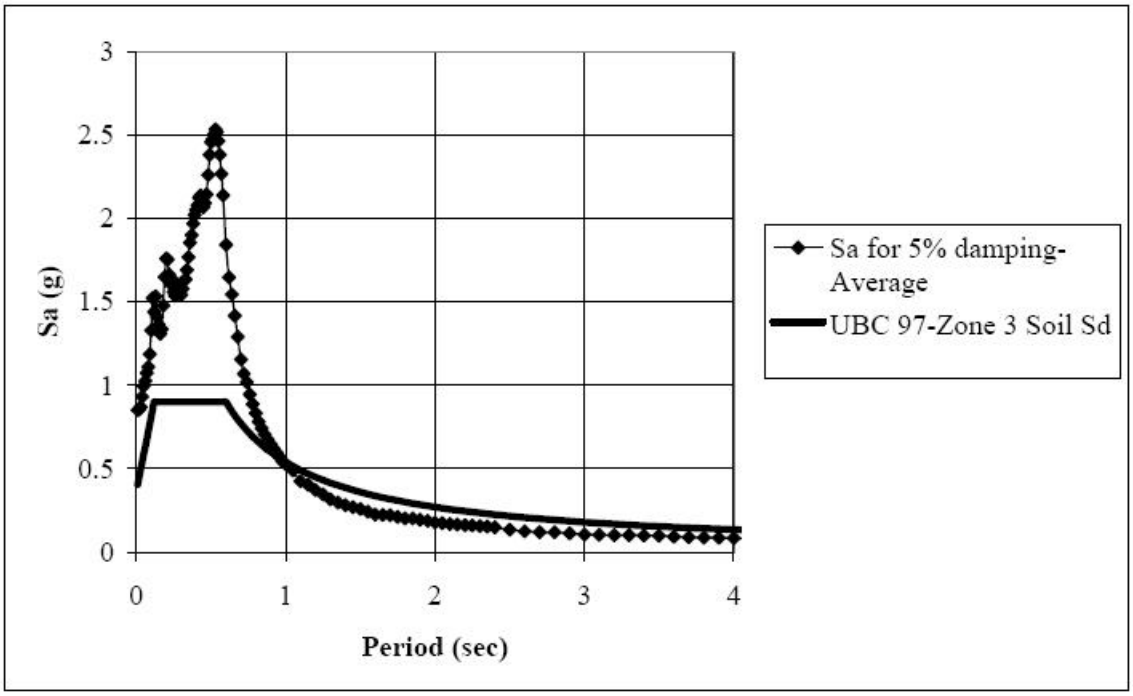

Figure CHAPTER 3.3: Surface response spectrum from the linear analysis and design spectrum according to UBC 97 for artificial earthquakes at "el Viaducto" (from Pérez, 2005)

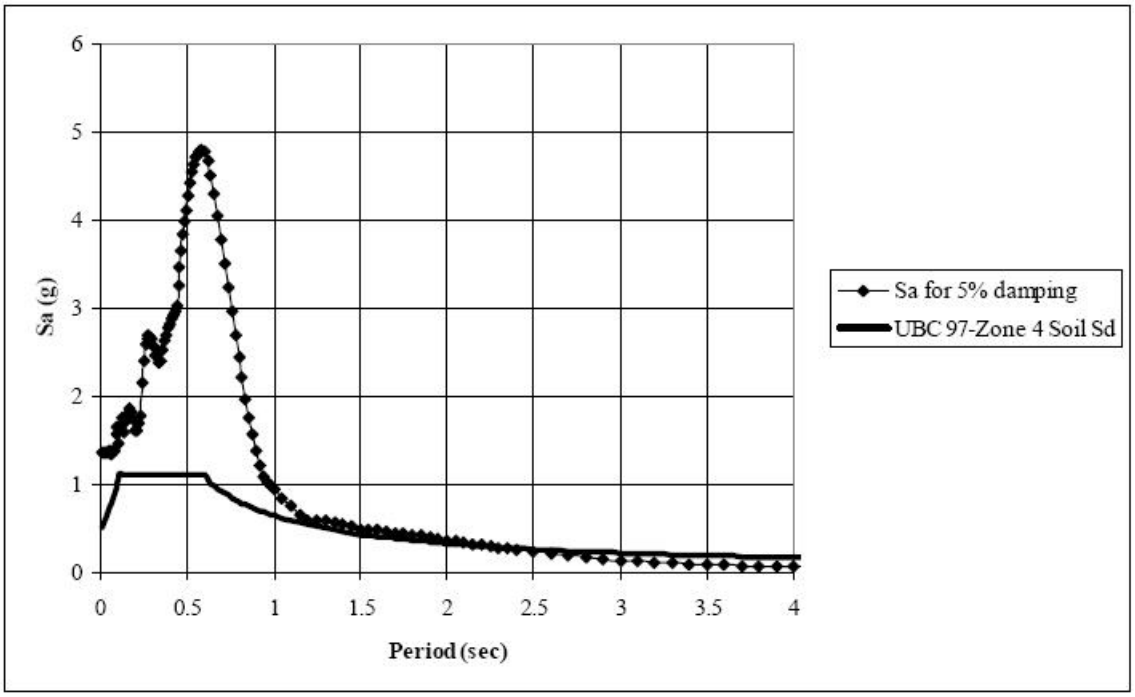

Figure CHAPTER 3.4: Surface response spectrum from the linear analysis and design spectrum according to UBC 97 (El Salvador earthquake)at "el Viaducto" (from Pérez, 2005)

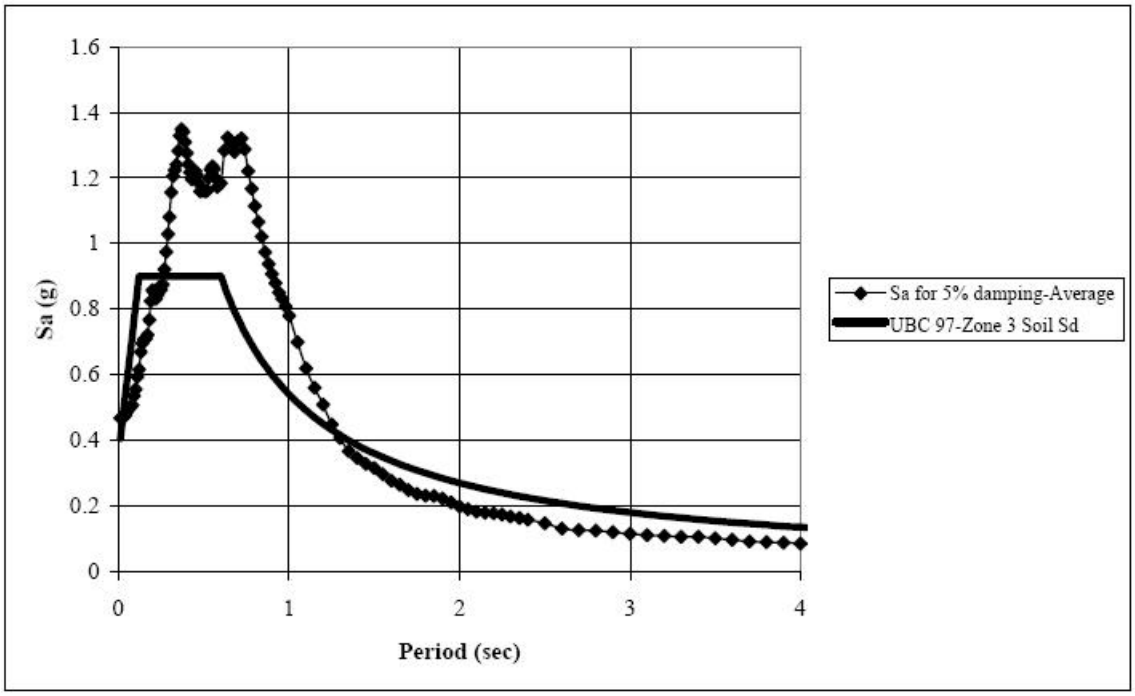

Figure CHAPTER 3.5: Surface response spectrum from the non linear analysis and design spectrum according to UBC 97 for artificial earthquakes at "el Viaducto" (from Pérez, 2005)

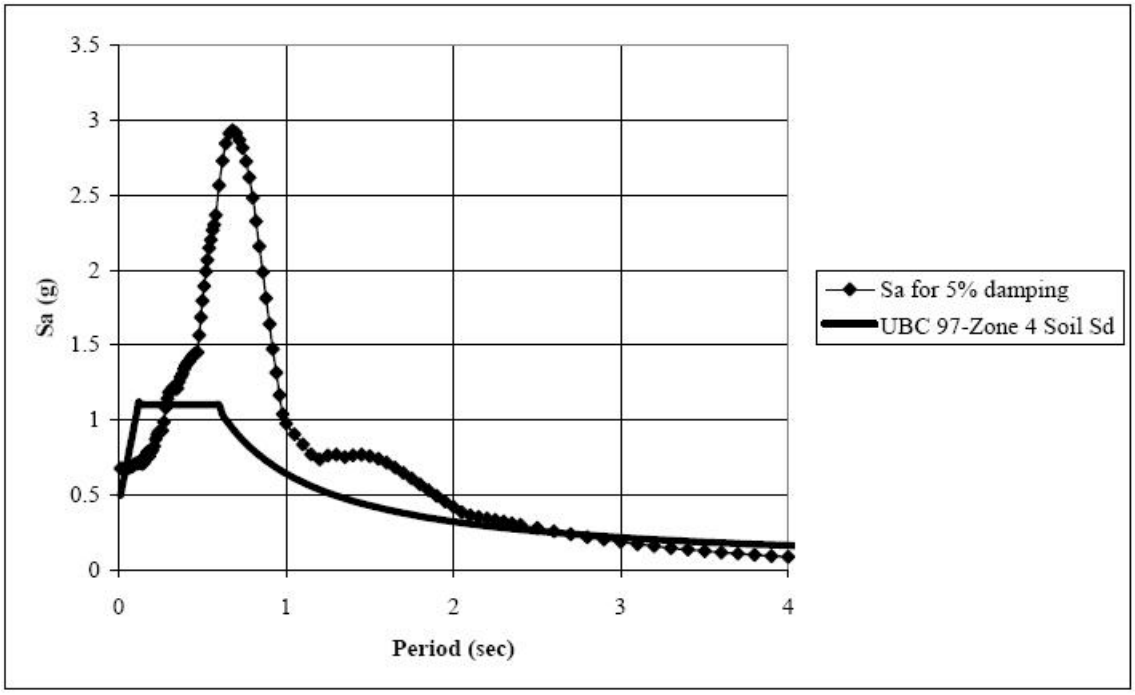

Figure CHAPTER 3.6: Surface response spectrum from the non linear analysis and design spectrum according to UBC 97 (El Salvador earthquake)at "el Viaducto" (from Pérez, 2005)

In conclusion, this chapter explained the feasibility of using microtemblors and weak earthquake motion to estimate predominant site periods using records from five seismic stations instrumented with strong motion accelerometers EpiSensor in Mayagüez, Puerto Rico. For each type of ground motion, several methods were investigated. In general, all methods provided estimates of the predominant frequency period in reasonable similar manner, except as discussed above for the MY05 station. Being able to predict reliably the predominant site periods from microtemblors is an advantage for seismic regions such as Puerto Rico where there is a low recurrence rate and no historical data of strong motion.

CHAPTER 4 APPLICATION OF THE METHODOLOGY TO MAYAGÜEZ, PUERTO RICO

4.1 *Introduction*

This chapter presents the analysis of the microtemblor spectral ratio technique (Horizontal/ Vertical), conducted for micro-zoning of the city of Mayagüez, Puerto Rico, which location can be seen in Figure 1.5. The beginning of the chapter presents a description of the measurements to be performed. Finally, details regarding ambient vibration measurements processing is provided. An analysis of the influence of various parameters involved in the measurement processing, a stability analysis of the Horizontal/Vertical spectral ratio method and a comparison between Horizontal/Vertical spectral ratio and transfer function modeling obtained from the soil deposit is also performed.

4.2 *General description of the city of Mayagüez*

4.2.1 *Location and city division*

The island of Puerto Rico is located in plate of the Caribbean Sea between latitudes 18º and 18.5º N and longitudes 65.25° and 67.25° W. The study area for this work is concentrated on the city of Mayagüez, which is located on the west side end of the island as shown in Figure 1.5. Figure 2.1 shows the city of Mayagüez map and its neighborhoods.

4.2.2 *Seismic characteristics*

The island of Puerto Rico is located on a very active and complex tectonic region in the northeastern Caribbean Sea. Most seismic activity in the area is produced by the convergence and lateral translation of the North America and the Caribbean plates beneath the Puerto Rico platelet (Tuttle et al., 2003), as shown in figure 2.2.

Figure 4.1: Map of Mayagüez

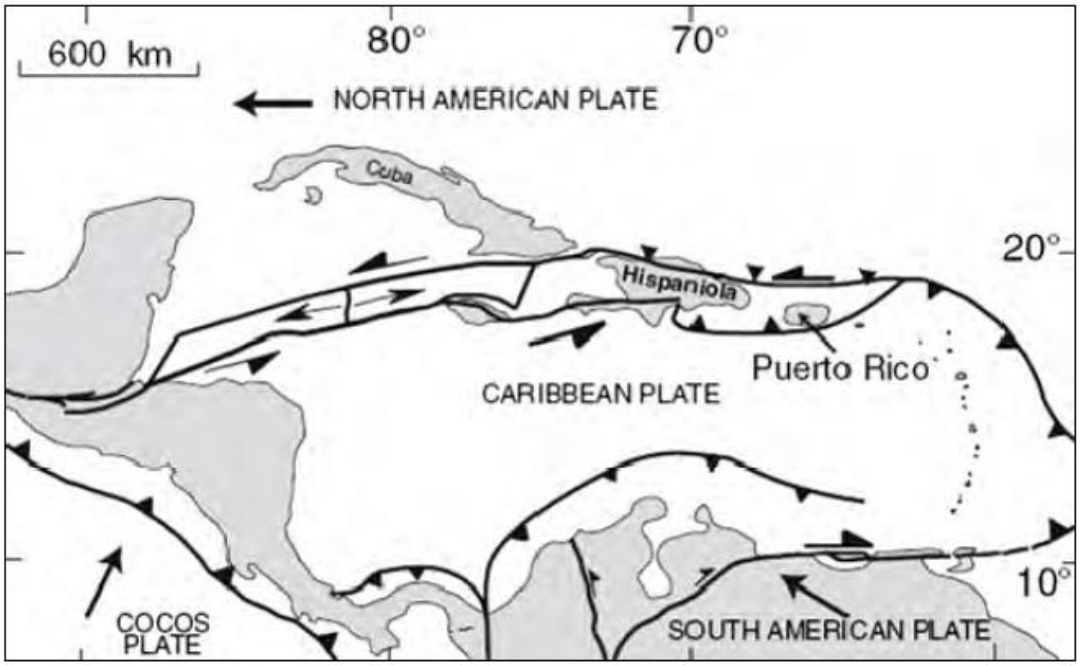

Figure 4.2: Seismic and plate tectonics for the Caribbean region (from Tuttle et al., 2003).

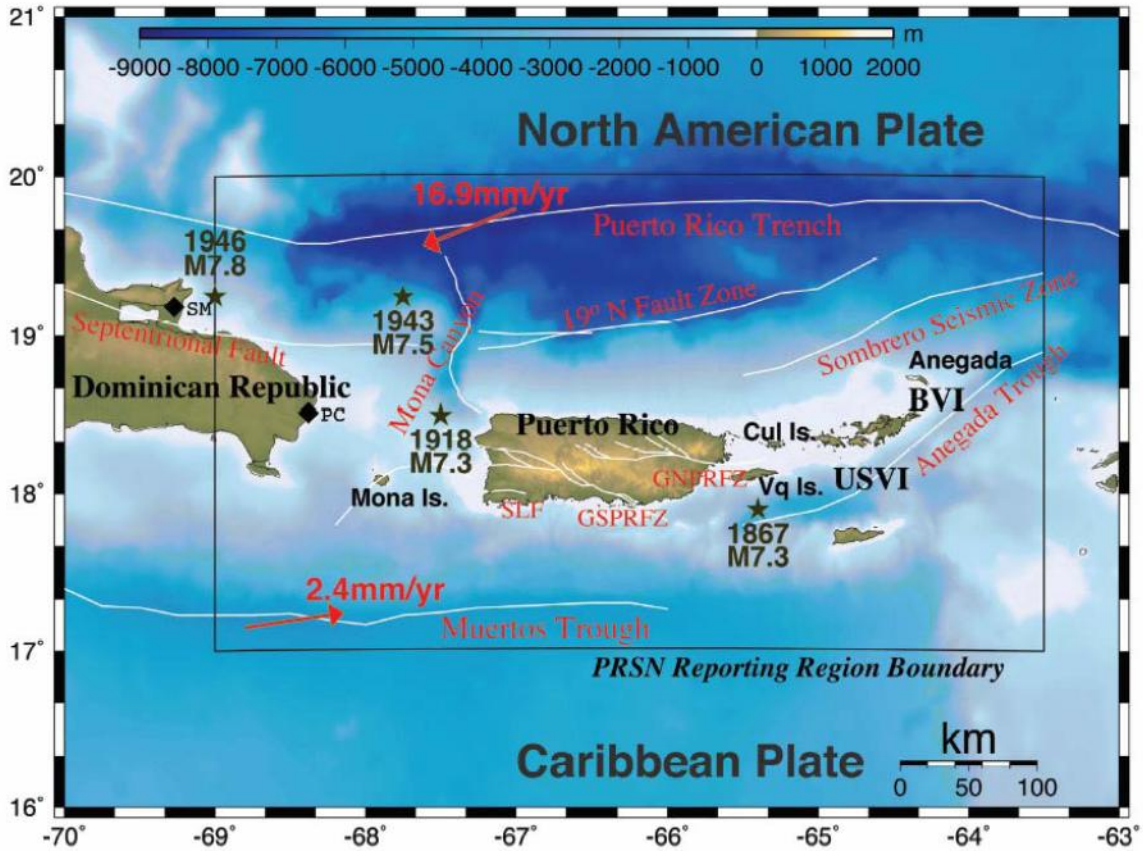

Figure 4.3: Seismic activity and major faults of Puerto Rico (from Clinton et al., 2006).

In addition to the aforementioned seismic sources, a new seismic source was recently identified as capable of generating events with a magnitude M7.0 (Prentice et al.2000; Prentice and Mann, 2005). This fault, located in the interior of the island, is identified in Figure 4.3 as SLF (South Lajas fault) which is located on the southwest corner of Puerto Rico.

The most important potential seismic sources to the area of Mayagüez is the Puerto Rico Trench, the Muertos Trough and the Mona Canyon (McCann, 1987).Historical records show that there have been major earthquakes in the Puerto Rico Trench (Sykes et al., 1982 and McCann, 1993). It is believed that this source is capable of generating events with a magnitude up to M ~ 8, since there is evidence that in 1943 there was an event of magnitude M ~ 7.75 (McCann, 1987). According to McCann (1987) Muerto Trough is considered capable of producing events of M ~ 7.5 to 8.0. However, the seismicity produced by La Mona Canyon is considered the greatest threat to the West Coast because of the proximity to this area. This area is capable of generating earthquakes of M ~ 7.5 to 8.0 (McCann, 1987). In 1918, this source generated the most devastating event for the Mayagüez area, with an estimated magnitude of 7.3. Approximately 116 people died and an estimated four million dollars loss in property were the consequences of this event (Reid and Taber, 1919).

4.2.3 *Geology*

The general geology for the Mayagüez area has been mapped by Curet (1986). Figure 2.4 shows the different geological units identified by Curet while Table 2.1 provides a brief description of these units. Overall, the Mayagüez area lies between the contact of two different geological units: the Sierra Bermeja complex and a volcanic complex (Moya and McCann, 1992).Sierra Bermeja complex is composed mainly of volcanic and metamorphic rocks from Cretaceous to pre-Early Cretaceous age and is considered the oldest rock formation on the island (Moya and McCann, 1992). The volcanic complex consists of sedimentary and volcanic rocks from the late Cretaceous to the early Tertiary age and covers the Sierra Bermeja complex (Moya and McCann, 1992).

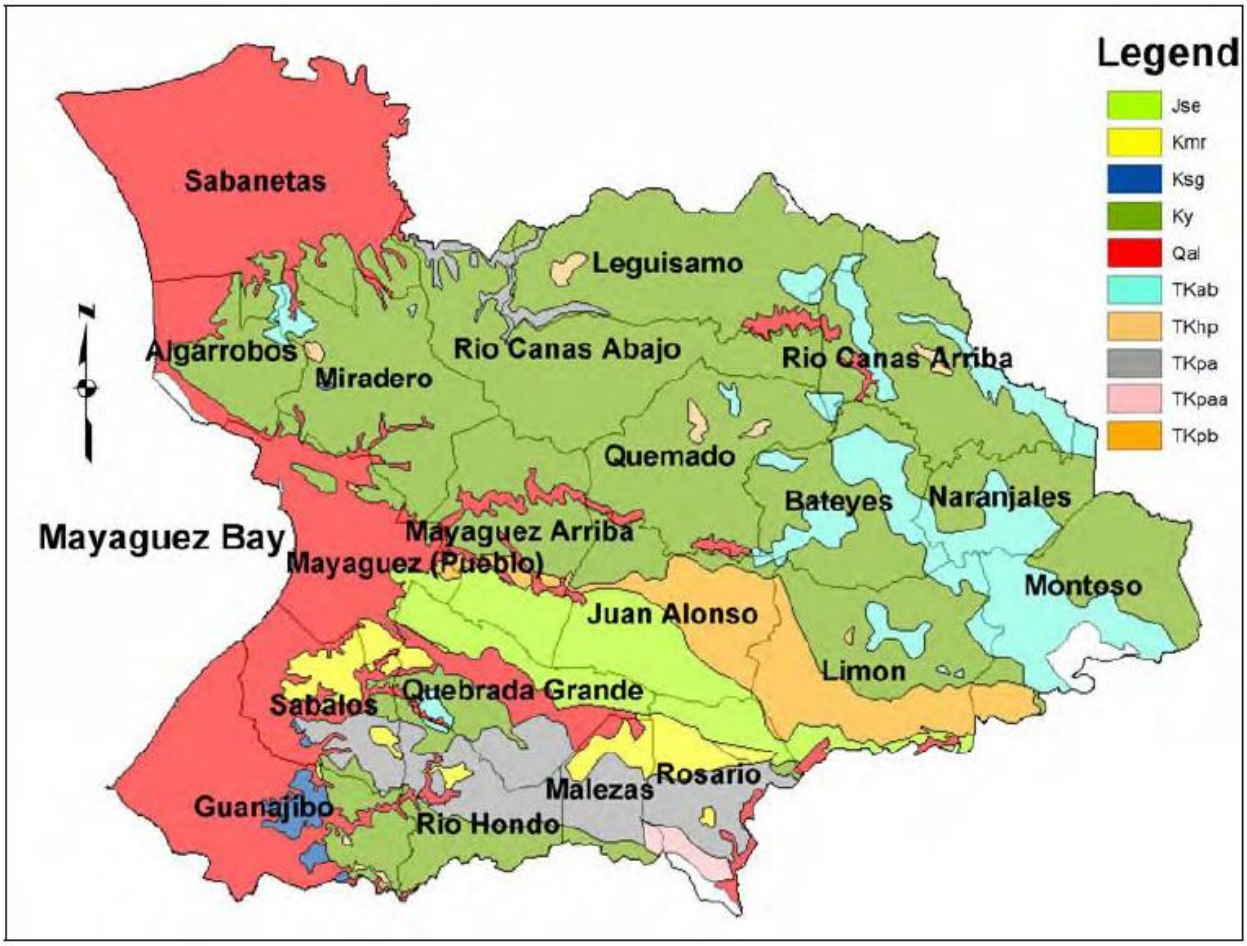

Figure 4.4: Geological map of Mayagüez (from Curet, 1986)

The areas near the coastline are mainly beach sand deposits. These sands are mainly composed of quartz sand formed in the Holocene and are described as rounded, medium to small size and small amount of gravel (Moya and McCann, 1992). Alluvial deposits are found near rivers areas (Guanajibo River for example) which date from the late Pleistocene and Holocene. The thickness of alluvial deposits in the Guanajibo River varies from 50 to 100 ft (Colón-Dieppe et al., 1985). Deposits near Añasco river typically have more than 100 ft thick (Columbus-Dieppe et al., 1985), while it is believed thickness ranges from 170 ft to 300 ft are found in the Mayagüez floodplains (McGuinness, 1946, Rodriguez and Helmet, 1988). Residual soils in the area of Mayagüez are located in mountainous terrain away from river and creeks.

Table 4.1: Geological stratigraphy table for Mayagüez area (from Curet, 1986)

Age	Stratigraphy	Description
Holocene	Qal alluvium	Sand, silt and gravels, includes rock falls and landslide deposits
Early Tertiary Maestrictian (Maest.)	TKpb Basalts	Basalts and basalts weathered
	TKpa Andesite-diorite	Porphyritic andesite-diorite
	TKpaa Andesite-diorite	Altered porphyritic andesite-diorite
	TKhp Diorite	Porphyritic hornblende diorite (massive)
	TKab Basalt	Porphyritic augite basalt (massive)
Maestrictian and Campanian	Kmr Maricao Formation	Massive breccia, conglomerate sandstone and limestone
	Ky Yauco Formation	Calcareous volcanoclastic sandstone, siltstone, claystone and limestone
Maestrictian and Turonian	Ksg Sábana Grande Formation	Massive breccia, conglomérate sandstone, siltstone, claystone and limestone
Pre. Late Kimmeridgian	Jse Serpentinite	Massive and weathered serpentinite

4.2.4 *Topography*

Mayagüez topography can be described as coastal deposits from Holocene age and alluvial valleys with gentle slopes to flat. Mountainous terrains are predominant on the east and northeast part of the city.

The coastal deposits are found along the Mayagüez Bay coastline. Other low lying areas of the region, are in the alluvial valleys of the principal rivers of the area, e.g., Yaguez and Guanajibo River. A large flat line is located at the mouth of the Guanajibo River, which is located at the south part of the Mayagüez city. The mountainous terrain is related to the central range of mountains located n the east part of the city starting near the coastal area and rapidly rising to 350 meters above mean sea level.

To illustrate the topography of Mayagüez, an elevation cross section was generated to show the topographic profile in the north to south direction. The location of the cross section is shown in figure 2.5. The resulting topographic profile for this cross section is shown in figure 2.6. This figure shows that the Sabanetas and the Mayagüez downtown (Pueblo) neighborhoods

are low lying lands in which the elevation ranges mostly between 2 m and 15 m above the mean sea level. As mentioned in the previous section, these two regions are mainly composed of alluvial deposits which potentially make them susceptible to liquefaction.

According to the U.S census Bureau (2000) almost 33 percent of the Mayagüez population lives in the Mayagüez downtown (Pueblo) area and 38 percent of the Mayagüez housing units are located in this area. On the other hand, only 2.7 percent of the population, and 2.5 percent of the housing units are located on the Sabanetas area. Population and housing unit values for the other Mayagüez neighborhoods intersected by the topographic cross section of figure 2.6 are listed in table 2.2.

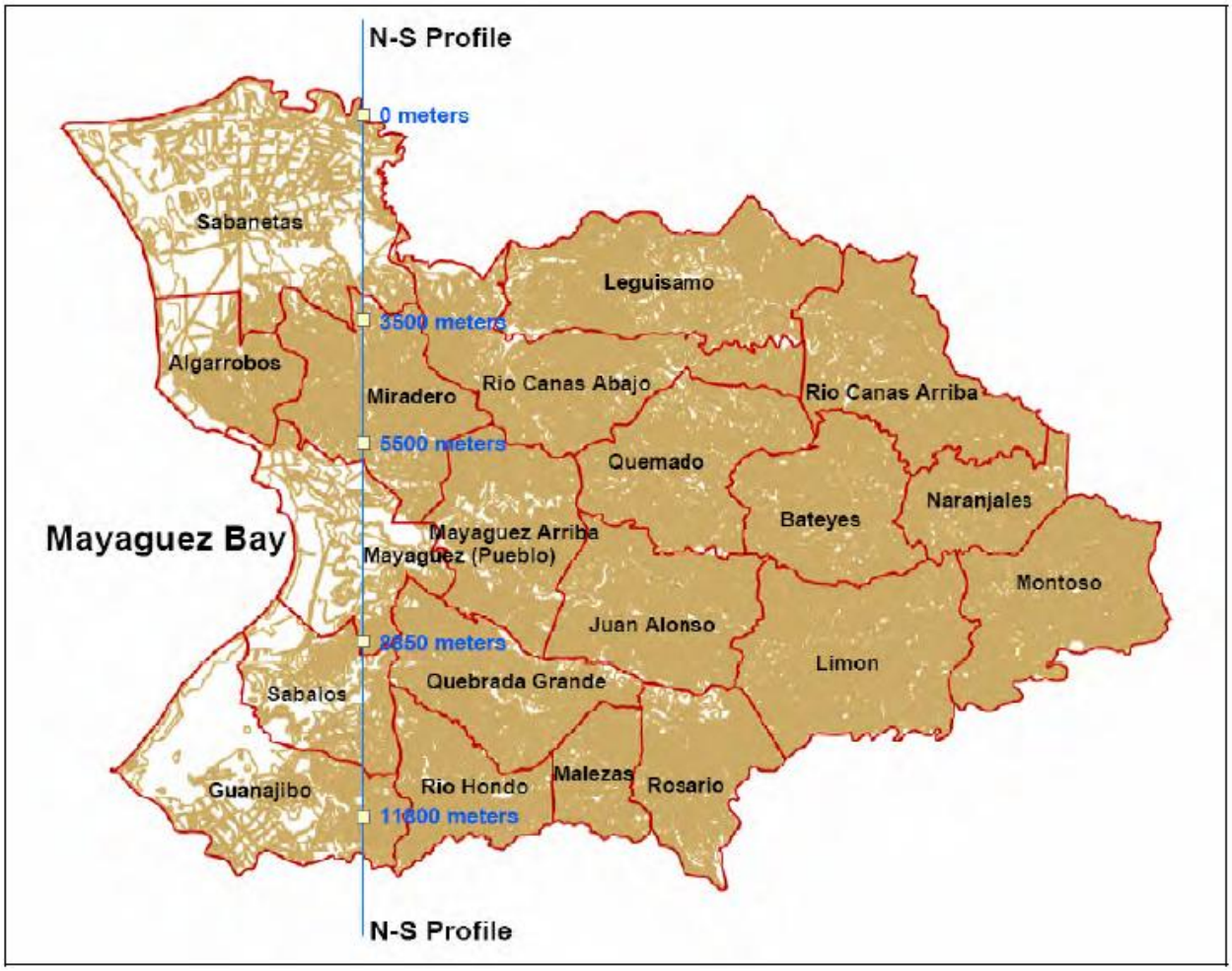

Figure 4.5: Location of N-S topographic profile (from Lugo, 2004)

Table 4.2: Population data for areas along the N-S topographic profile (from US Census Bureau, 2000)

N-S Geographical Area	Estimated Population	Housing Units	% Total Population	% Total Housing Units
Sabanetas	2645	985	2.7	2.5
Miradero	5510	2155	5.6	5.5
Mayagüez (Pueblo)	32043	14932	32.6	37.9
Sábalos	10271	3773	10.4	9.6
Guanajibo	7165	2754	7.3	7.0

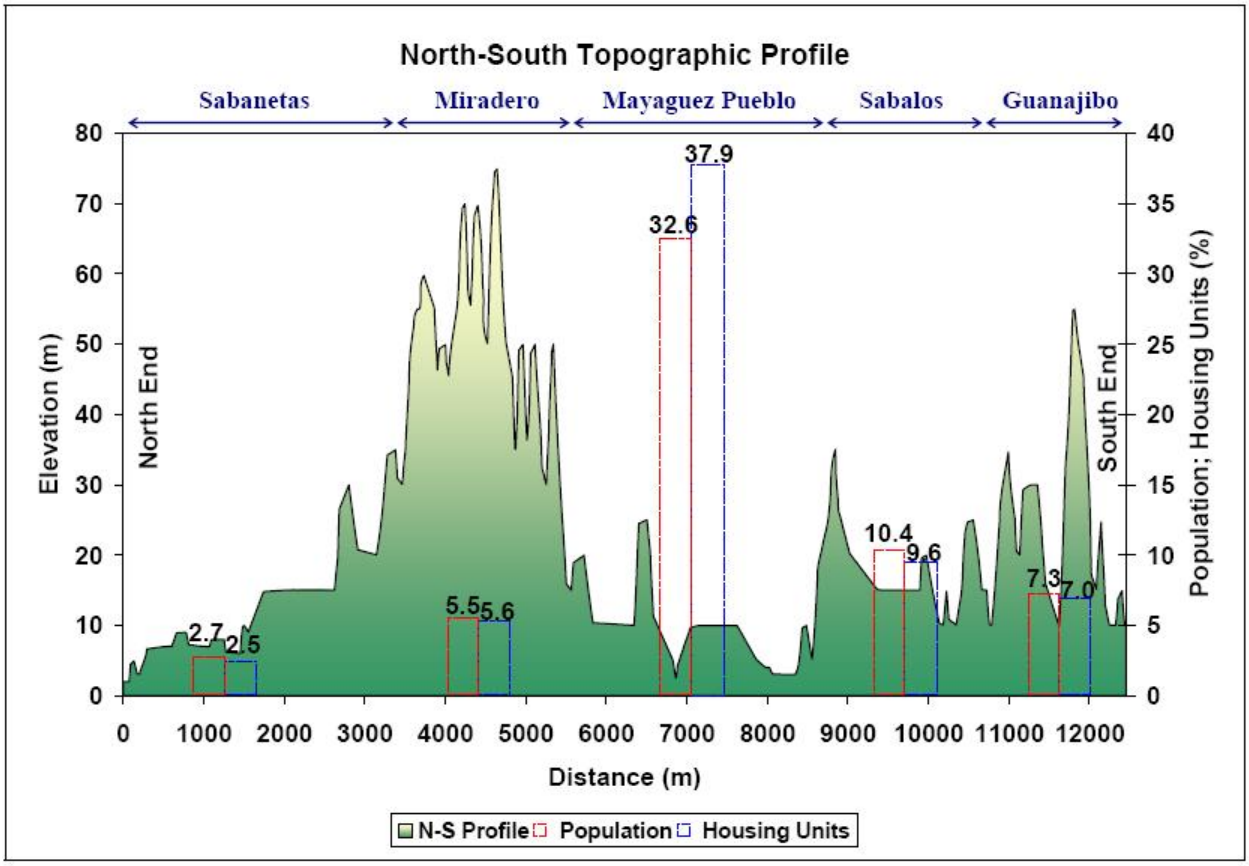

Figure 4.6: Topographic profile and associated population data for N-S section

4.3 *Ambient vibration measurements within study area*

This section presents a brief description related to ambient vibration measurements made in the area of Mayagüez. The type of instrumentation and the protocol followed for taking measurements are described.

4.3.1 *Instrumentation*

Ambient vibration measurements were made using ETNA accelerographs manufactured by Kinemetrics Company. Etna includes an internal force balanced accelerometer (EpiSensor ES-T) and a system of GPS (Global Positioning System). Figure 4.7 shows the instrument and the location of its principal parts such as a triaxial sensor, battery, memory card spaces and connection plugs.

Figure CHAPTER 4.7: ETNA accelerograph used for ambient vibrations

Two types of ETNA instruments were used, one with a dynamic range of ± 2.0g (g is the acceleration of gravity) and another with a dynamic range of ± 0.25g. Measurements were first

taken using the instrument with greater dynamic range. Then, it was decided to perform a test to determine the possible type of instrument influence on the measurement. Two sites were chosen to perform ambient measurements using both types of instruments at the same time for a period of one hour. The locations of sites are shown in Figure 4.8 which corresponds to the Biology faculty parking lot (P # 1) and the courtyard of the Civil Engineering Department (P # 2). The results for each site after processing the measurements are presented in Figure 4.9 (for the P site # 1) and Figure 4.10 (for the P site # 2). The comparison is done using spectral ratios H / V obtained with the two instruments mentioned above.

Figure CHAPTER 4.8: Biology parking lot (P#1) and Civil Engineering courtyard (P#2)

As shown in Figures 4.9 and 4.10, the shape of the spectral ratios remained unchanged for both instruments, but the amplitudes obtained with the 0.25g instrument were higher than those obtained with the instrument of 2.0g which is due to the higher sensitivity of the 0.25g instrument. It should be noted that all measurements were taken at 100 samples per second, equivalent to a folding frequency (Nyquist frequency) of 50 Hz and they were processed using the same processing parameters (parameters which will be explained later).

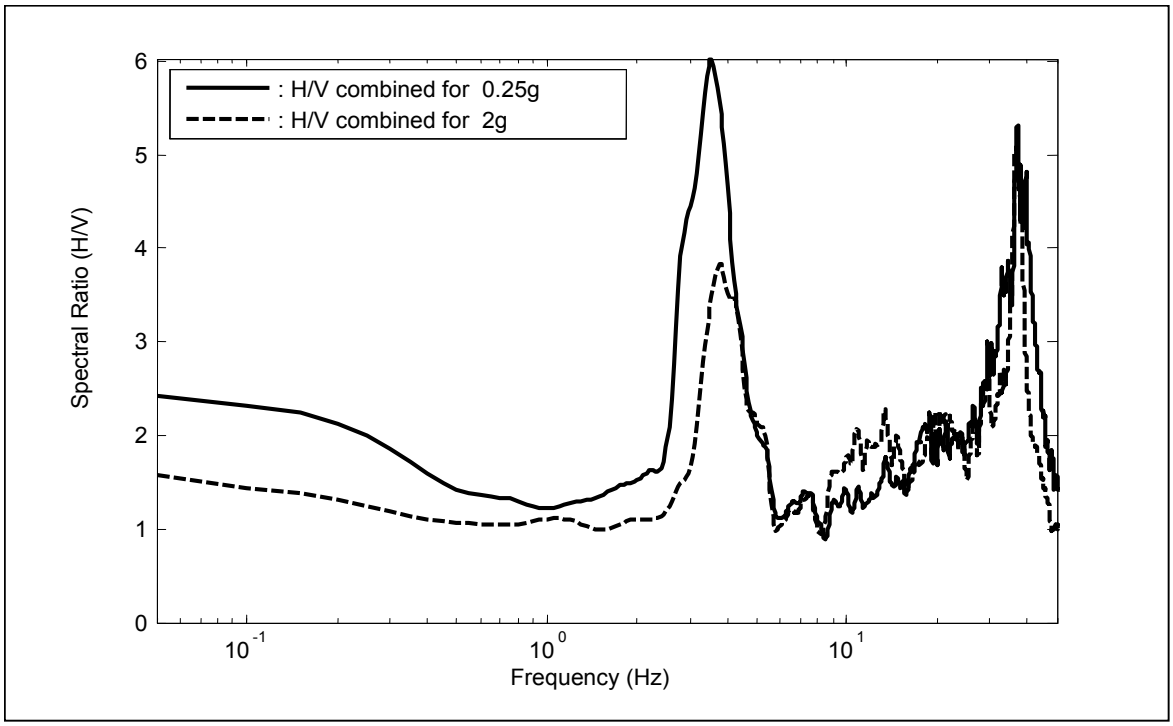

Figure CHAPTER 4.9: Spectral ratio H/V for P#1 using both instruments

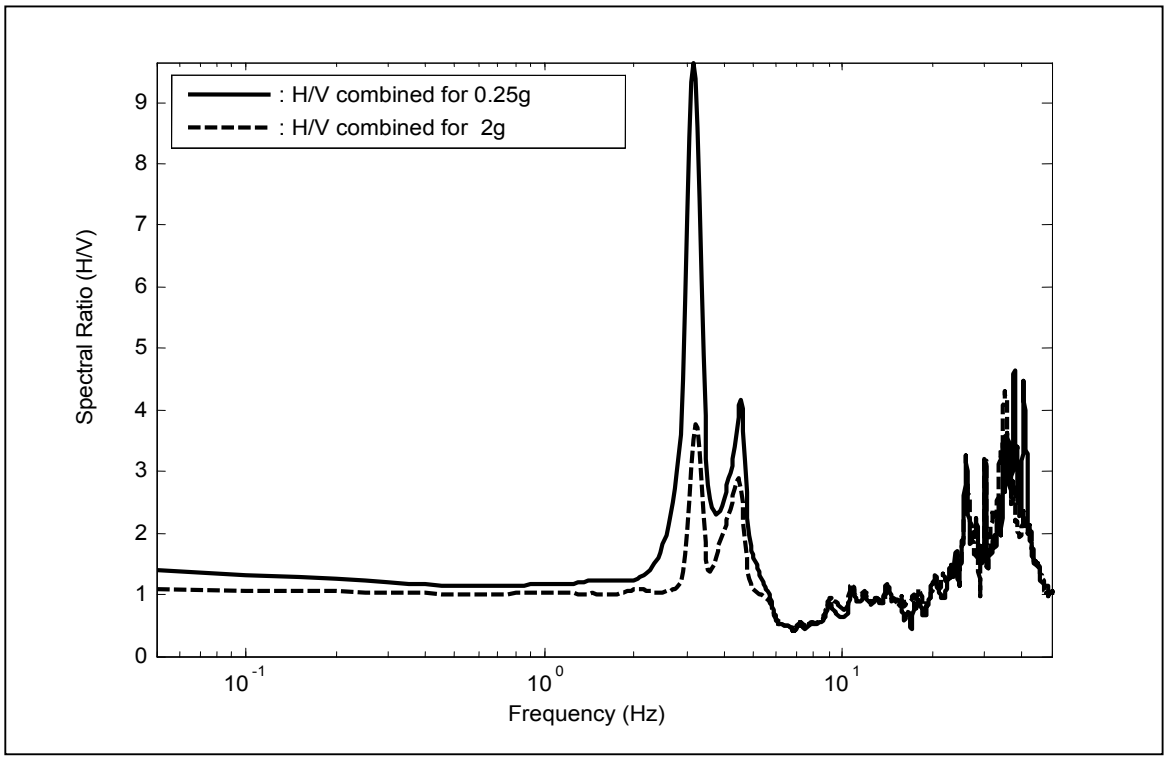

Figure CHAPTER 4.10: Spectral ratio H/V for P#2 using both instruments

4.3.2 *Protocol followed for taking measurements*

In order that all measurements were conducted under conditions as similar as possible, a protocol was designed to be followed the instrument during measurements. The main objective was to prevent the operator had influence over the results. This protocol basically indicated how to prepare the ground where the instrument would be located, how to put the instrument on the ground, its orientation according to the cardinal points and the configuration. On the other hand, a field sheet was developed to be completed at each measurement site in order to know the conditions under which each measurement was performed by determining the possible influence of certain parameters such as traffic, wind, proximity to buildings, etc. Appendix A presents the developed protocol which could be also used for future measurements.

4.3.3 *Measurements in the area of Mayagüez*

An ambient vibration measurements program was conducted in order to make a seismic micro-zoning study in the City of Mayagüez, and the construction of an isoperiod map. Initially measurements were concentrated in the most densely populated area of the city and then spread to the countryside of town. Measurements were performed at 111 sites in the city of Mayagüez as per Figures 4.11 and 4.12.

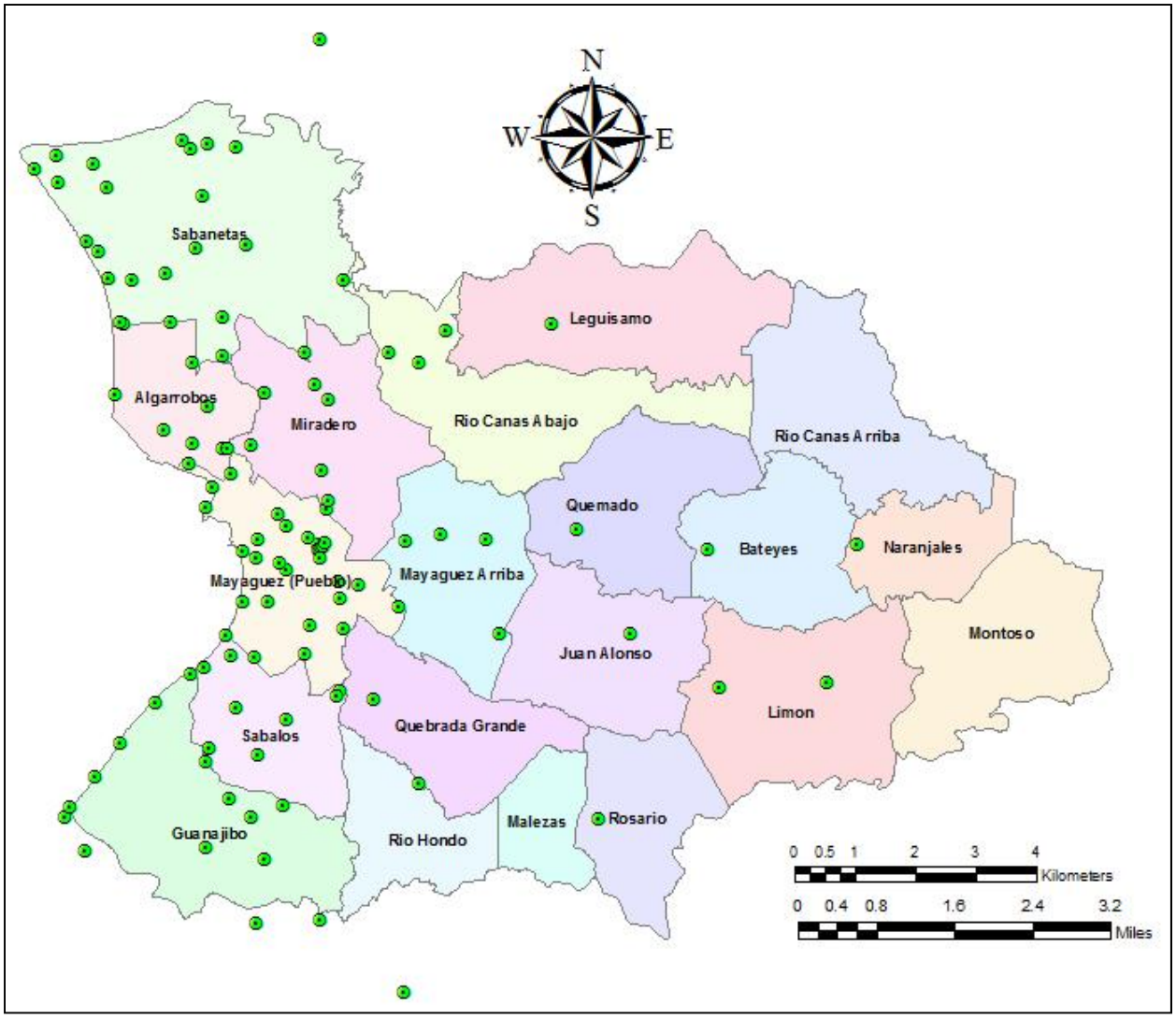

Figure CHAPTER 4.11: Location of measurement sites at Mayagüez city

As seen in Figures 4.11 and 4.12, there is a high density of measurement sites in the west region t of the city. Subsequently, a second set measurements were added to the east area as will be shown bellow. The first measurements were taken using accelerometers with a dynamic range of ± 2.0g and then replacing them with dynamic range accelerometers of ± 0.25g. All measurements were performed for an hour and using a sampling rate of 100 samples per second (mps). Figure 4.13 shows the accelerometer with the laptop used to configure and manually operate the equipment.

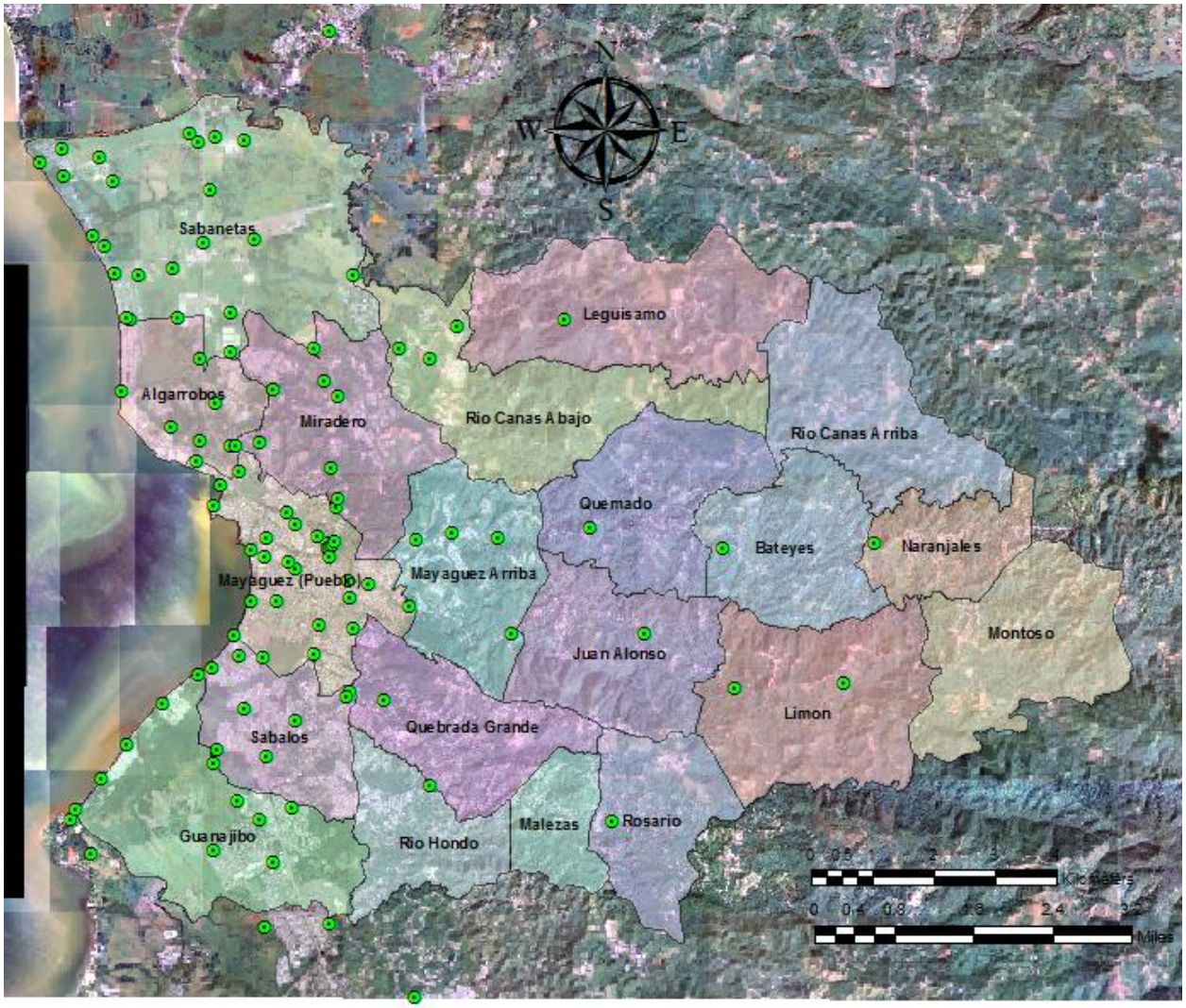

Figure CHAPTER 4.12: Location of measurement sites at Mayagüez city with topography

As shown in Figure 4.13, the equipment is mounted on a steel plate. The aim of this was a better instrument-field coupling. In all places where grass was found on the ground, it was removed in order to place the equipment directly on the ground surface and avoid possible errors in measurements, as recommended by Chatelain et al. (2008). Appendix C includes an analysis to determine the possible influence of high voltage power lines on the measurements; this appendix also presents results of measurements made with a seismometer and broadband accelerometer balanced force on the same site.

Figure CHAPTER 4.13: ETNA accelerometer setting

4.4 *Ambient vibration measurement analysis*

A program written in Matlab (HVSRAV.m) was used to analyze ambient vibration. Th program code is included in the Appendix D. Basically, the program processes the registration of each channel instrument by performing the following tasks: removal of the record mean , automatic selection of windows based on parameters defined by the user, multiplication of each window by a Hanning window, Fourier transform calculation and its smoothing for each window, all windows Fourier spectra average and finally, calculation of spectral ratios NS / V, EO / V Hc / V (where Hc is the combined horizontal components). The combination of the horizontal components was calculated as follows:

$$\frac{Hc}{V} = \sqrt{\frac{H_{E-O}^2 + H_{N-S}^2}{2 \times V^2}} \tag{4.1}$$

where H_{E-O}, H_{N-S} and V are respectively the Fourier spectral amplitudes in the EO, NS and vertical direction respectively.

4.4.1 *Hanning window*

A window function (or tapering function) is a function whose value is zero outside a certain range in signal processing. For example, a function that is constant within the interval and zero outside the window is known as rectangular window and is defined as:

$$h(t) = \begin{cases} 1 \; if \; t \in [0, T] \\ 0 \; otherwise \end{cases} \tag{4.2}$$

When another signal or function is multiplied by a window function, the obtained function is also zero outside the range is zero, and the remaining is what is seen through the window. These window functions are widely used in spectral analysis, filter design, etc.

In the case of spectral analysis, if a finite time segment is taken from a sampled signal and its Fourier transform is calculated, the result is called spectral “leakage” which means that when the lengths of wave does not divide exactly the size of the window, they are "poured" into a contiguous range of frequencies (Figure 4.14). This can be interpreted as a consequence of the frequency response of the rectangular filter, which corresponds to the truncation of the signal. Thus, when a signal $s(t)$ is multiplied by a window; for example the rectangular window defined by Equation 4.2, only the first T seconds of the signal are obtained (the signal is observed at an interval T). Instead of studying the signal $s(t)$, the truncated signal $s_h(t) = s(t) \bullet h(t)$ is studied. If $S_h(t)$ switches to frequency domain through Fourier transform, the convolution product $S_h(f) = S(f) * H(f)$ is obtained, where $H(f)$ the Fourier transform of the window is. It must be noted note that the asterisk represents the convolution of two functions $S(f)$ and $H(f)$, and not the direct product of both.

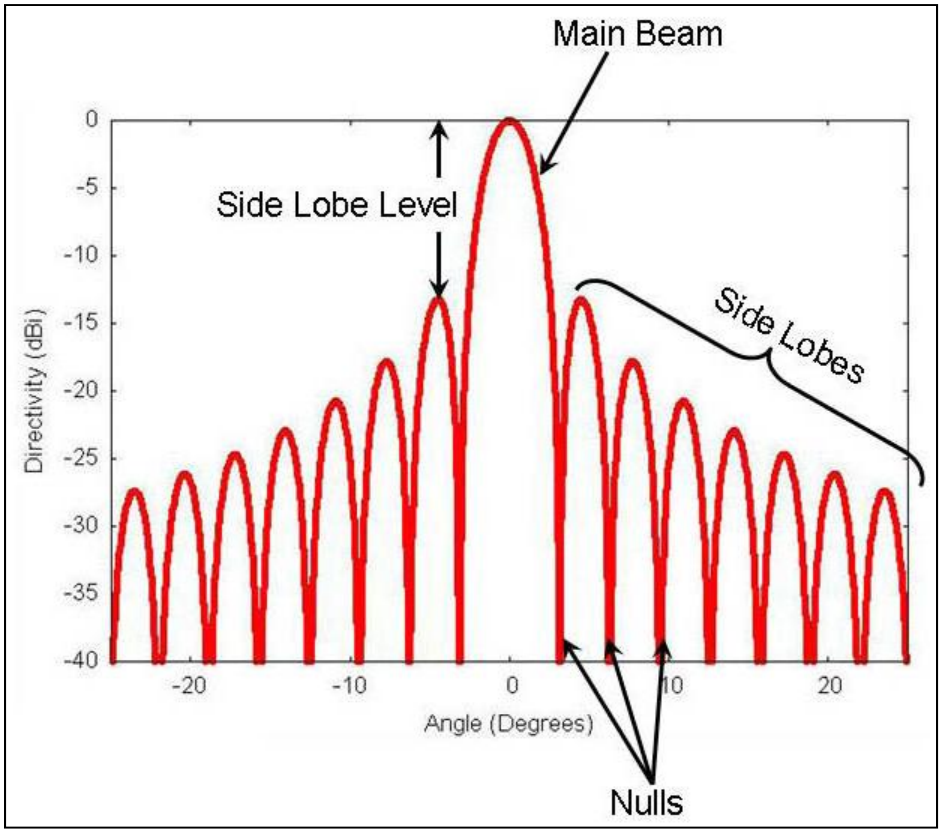

Figure CHAPTER 4.14: Frequency response of a typical window function (from http://en.wikipedia.org/wiki/Window_function).

Using a window changes the frequency spectrum in frequency of the signal. There are different types of windows that allow getting different results in the domain of frequencies. If instead of applying a simple truncation, the signal is multiplied by a window function such that diminishes towards zero, the effects of spectral leakage can be reduced. The Hanning window is commonly used in seismic signal analysis and its mathematical expression is:

$$w(n) = 0.5\left[1 - \cos\left(\frac{2\pi n}{N-1}\right)\right] \tag{4.3}$$

where N represents the width of the discrete window function (typically this is a integer power of 2, as 2^{10} = 1024) and n an integer, with values $0 \le n \le N-1$. A graph of this type of window can be seen in Figure 4.15. The term "Hanning window" is sometimes used to refer to the Hann window. This type of window was used for processing ambient vibration records in this project.

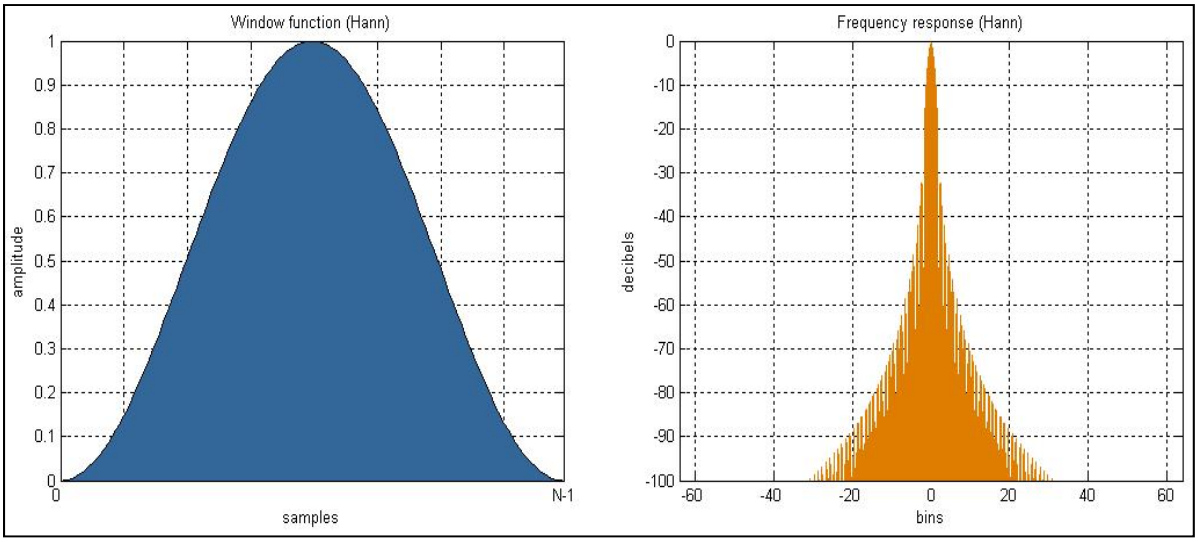

Figure CHAPTER 4.15: Hanning window function (left) and its response in frequency (right)

4.4.2 *Automatic window selector module*

In order to preserve the stationary parts of the noise and avoid transients factors often associated with point sources (pedestrians, nearby traffic, operating machinery, etc.), an automatic window selector module was incorporated in the Matlab program used for processing the ambient vibration records. This module consists of an algorithm known as "antitrigger", which detects and removes transient factors.

The procedure to detect transients is based on a comparison between two averages of the analyzed signal amplitudes. One is a short term average (STA) which is the average of the signal amplitude for a short period of time, denoted "TSTA" (typically 0.5 - 2.0 s) . The other is a long-term average (LTA) which is the average amplitude of the signal over a long period of time, denoted "TLTA" (typically several tens of seconds). When the ratio STA / LTA exceeds a predetermined threshold, it is considered that an “event” has been detected.

For this project, it was desirable to select windows completely free of transient energy which makes necessary to keep the ratio STA / LTA below a certain maximum value smax (typically 1.5 - 2.0). Simultaneously, it is also necessary to avoid windows with extremely low amplitudes; therefore, a minimum value smin was introduced which should not be reached by the selected window. This approach was taken from JSesame program, a program that emerged from the SESAME European project mentioned above in Chapter 3. Figure 4.16 shows the

window selection a given record. This procedure is also done by the program HVSRAV.m developed for this research using the program Matlab.

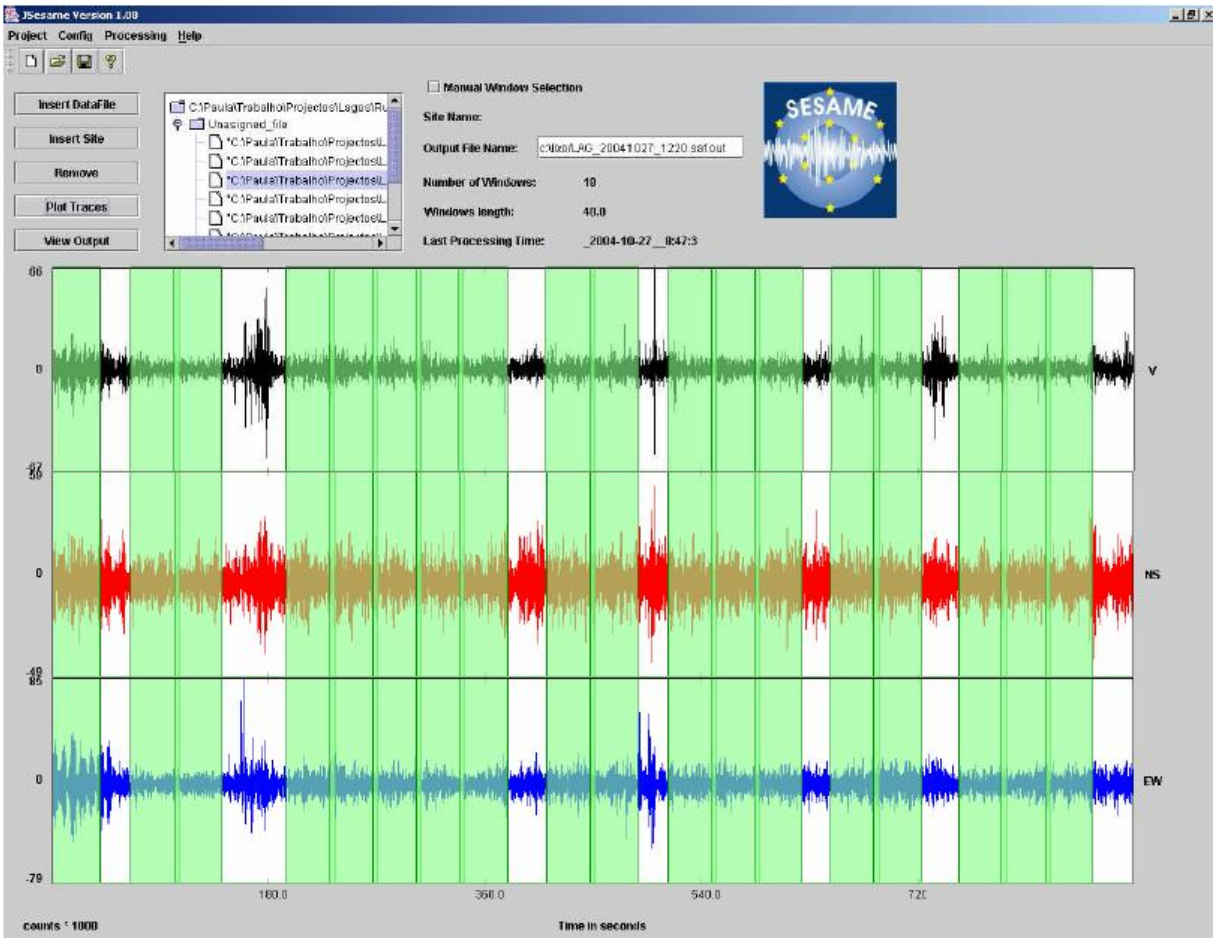

Figure CHAPTER 4.716: JSesame graphical interface. Selected windows are shown in green.

It also introduced another criterion for the selection of windows, optional. One may wish to avoid saturation of the signal, since it affects the Fourier spectrum. This criterion consists in detecting the maximum amplitude reached during the entire period of measurement, and automatically excludes those windows in which the peak amplitude exceeds the 99.5% of this maximum amplitude. It can be seen in Figure 4.16 as the program JSesame excludes certain regions of records. If we look closely at this figure, we see that the excluded regions contain, in some cases, acceleration values that are generally significantly higher than the average record. This indicates the presence of a transient. For data processing, certain parameters were chosen, whose values are summarized in Table 4.3.

Default J-Sesame parameters values were used for data processing (see Table 4.3). These values were used as a starting point and then slightly modified as needed. Appendix C presents a comparison between the results obtained when processing certain records of ambient vibration using the programs JSesame and HVSRAV.m.

Table CHAPTER 4.3: Parameters used in data processing

Window Length (sec.)	20
Overlap Window (% Window Length)	10
Window Length for the short term average (sec.)	1
Window Length for the long term average (sec.)	25
Minimum level for sta/lta threshold	0.5
Maximum level for sta/lta threshold	2

4.3.3 Influence of parameters involved in the automatic selection of windows

The following section is an analysis to determine the influence of various parameters involved in the processing of environmental vibration records to obtain spectral ratios. Site # 3 (old running track at the University of Puerto Rico, Mayagüez Campus) was chosen to perform this analysis. The first analysis was carried out using the parameters shown in Table 4.3 and then they were varied one at a time. Figure 4.17 shows the uncorrected ambient vibrations records (AV), Figure 4.18 shows the corrected records, and Figure 4.19 shows the spectral ratio H / V obtained using the parameters in Table 4.3. The site fundamental frequency was found to be 2.6-Hz as seen in Figure 4.19.

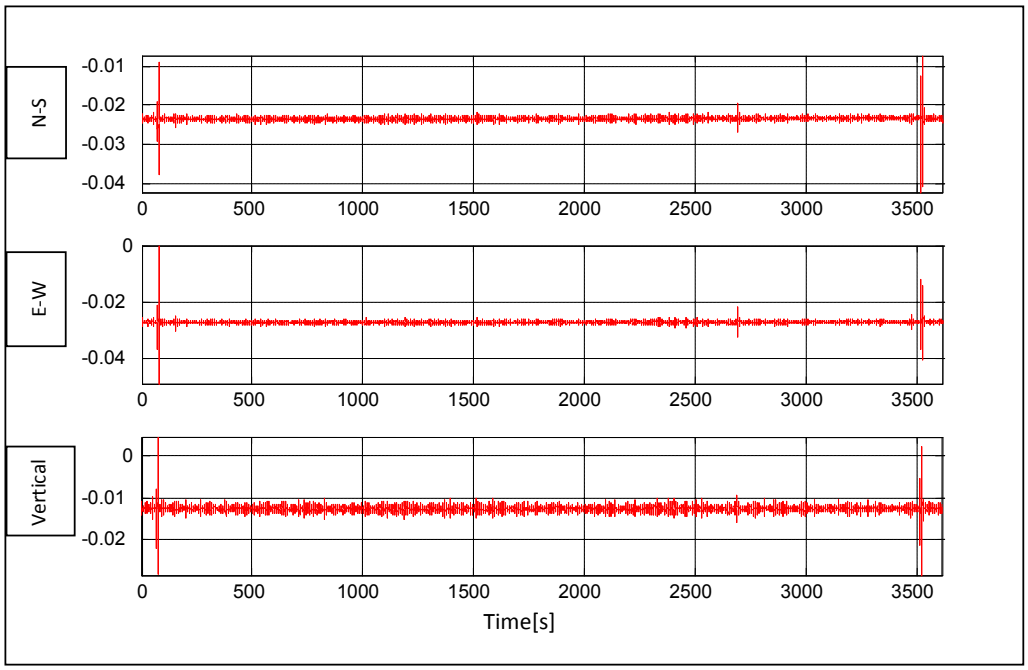

Figure CHAPTER 4.8: Ambient vibration records without correcting for site P#3

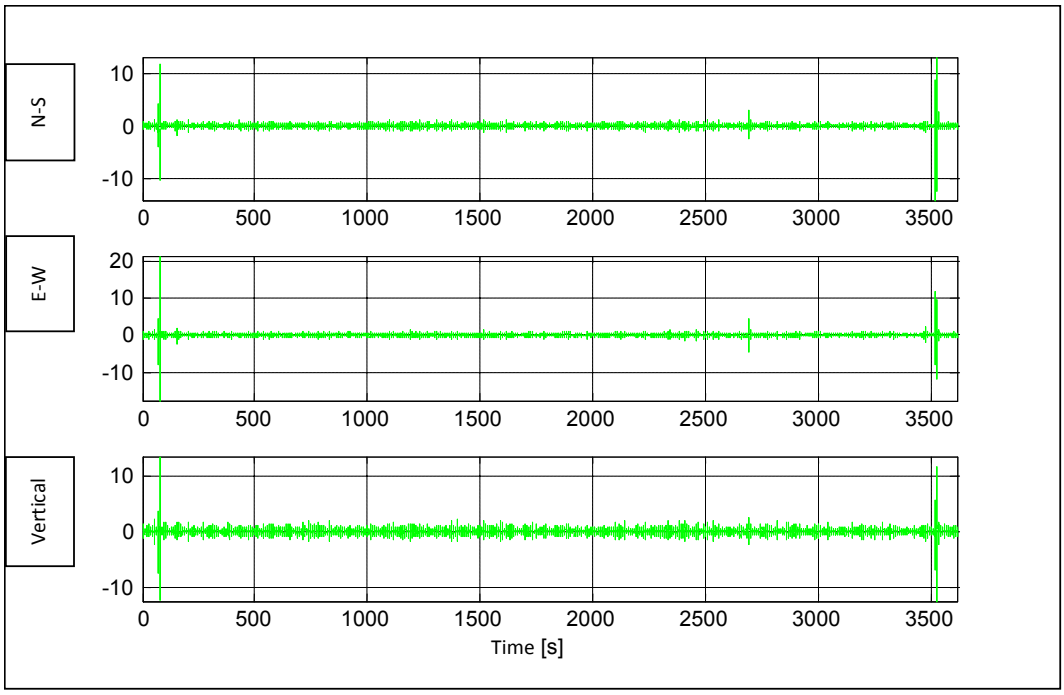

Figure CHAPTER 4.9: Corrected ambient vibration for site P#3

Acceleration peaks appear both at the beginning and end of the measurements (Figures 4.17 and 4.18). These peaks are generated by the instrument operator, when turning on and off the equipment. In order to take only the stationary part of the measurement, these peaks are manually removed before further processing.

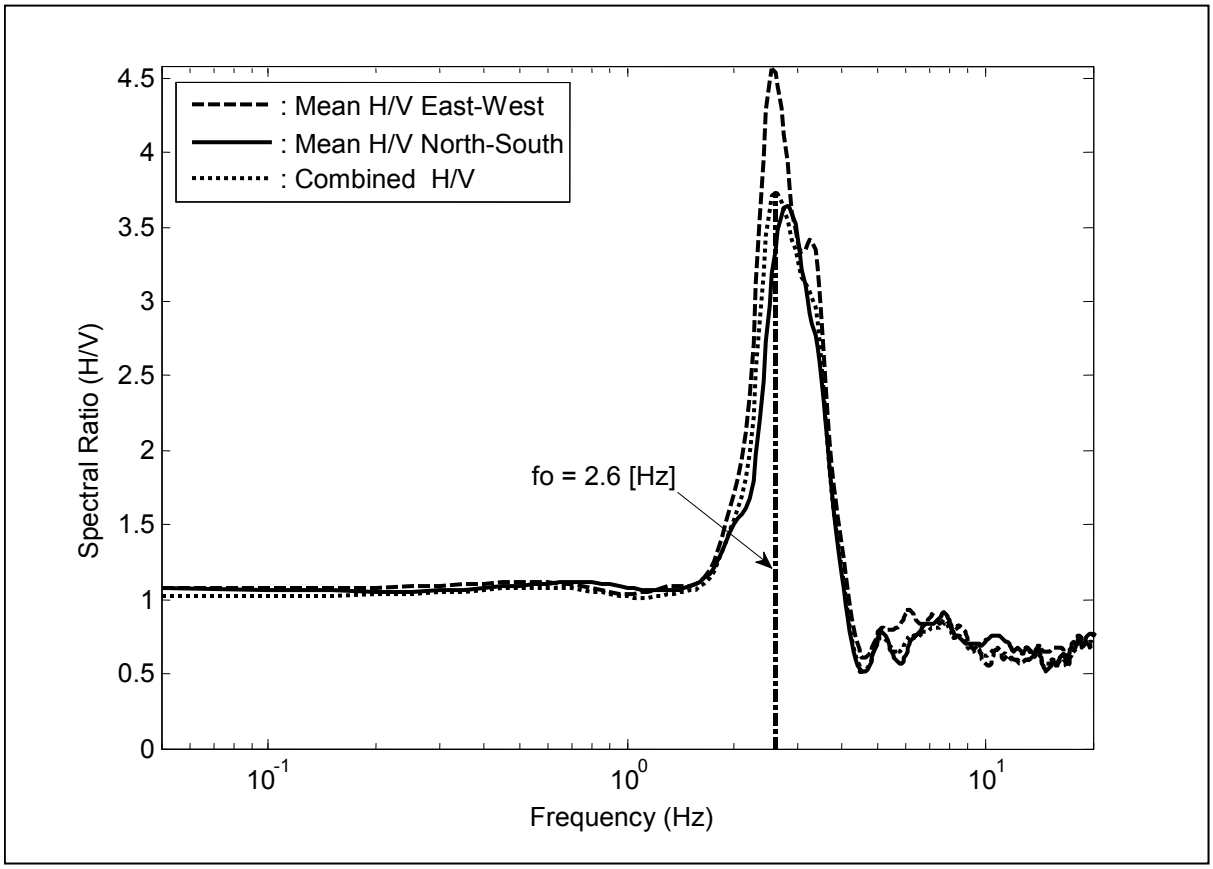

Figure CHAPTER 4.10: Spectral ratio H/V for site P#3

4.5 *Window Length (WL) Variation*

The variation of the window length in seconds is explained in this subsection. It was decided to perform two runs, one with a window length of 10 seconds and another with a window length of 30 seconds. Figures 4.20 and 4.21 show the results obtained with WL = 10 s and WL= 30 s.

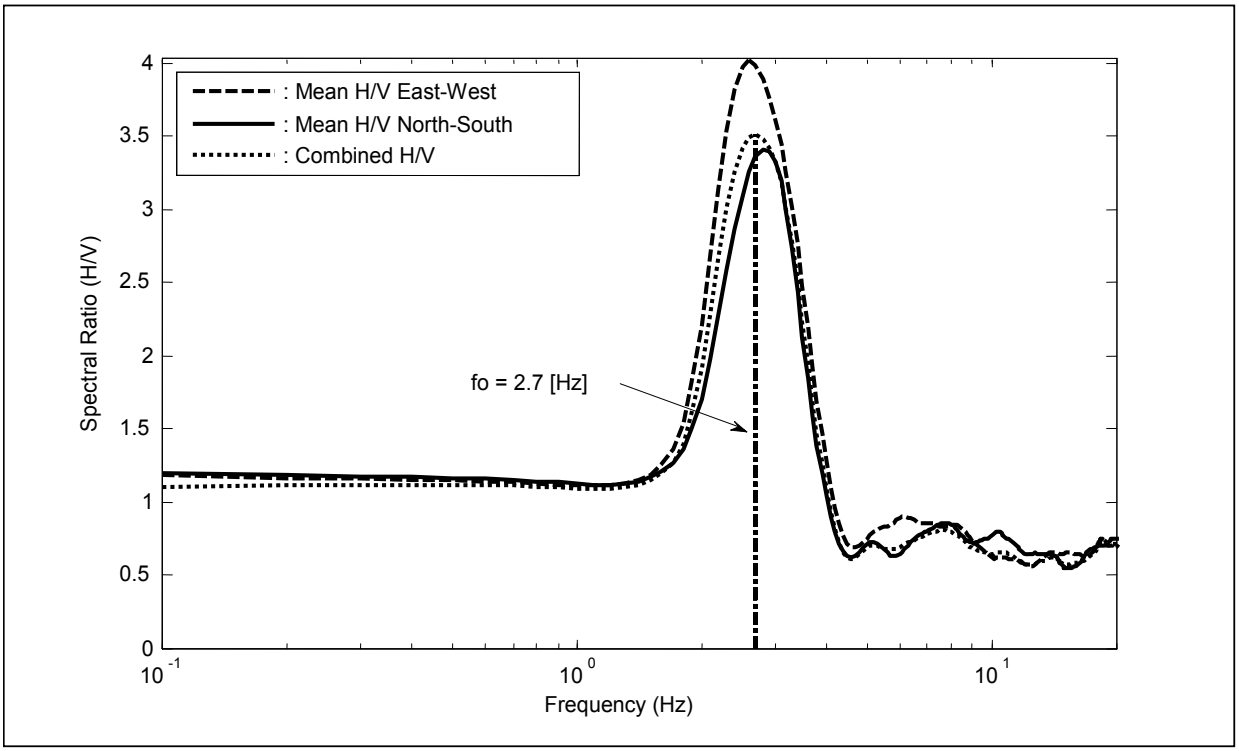

Figure CHAPTER 4.20: Spectral ratio H/V for site P#3 with WL = 10 seconds

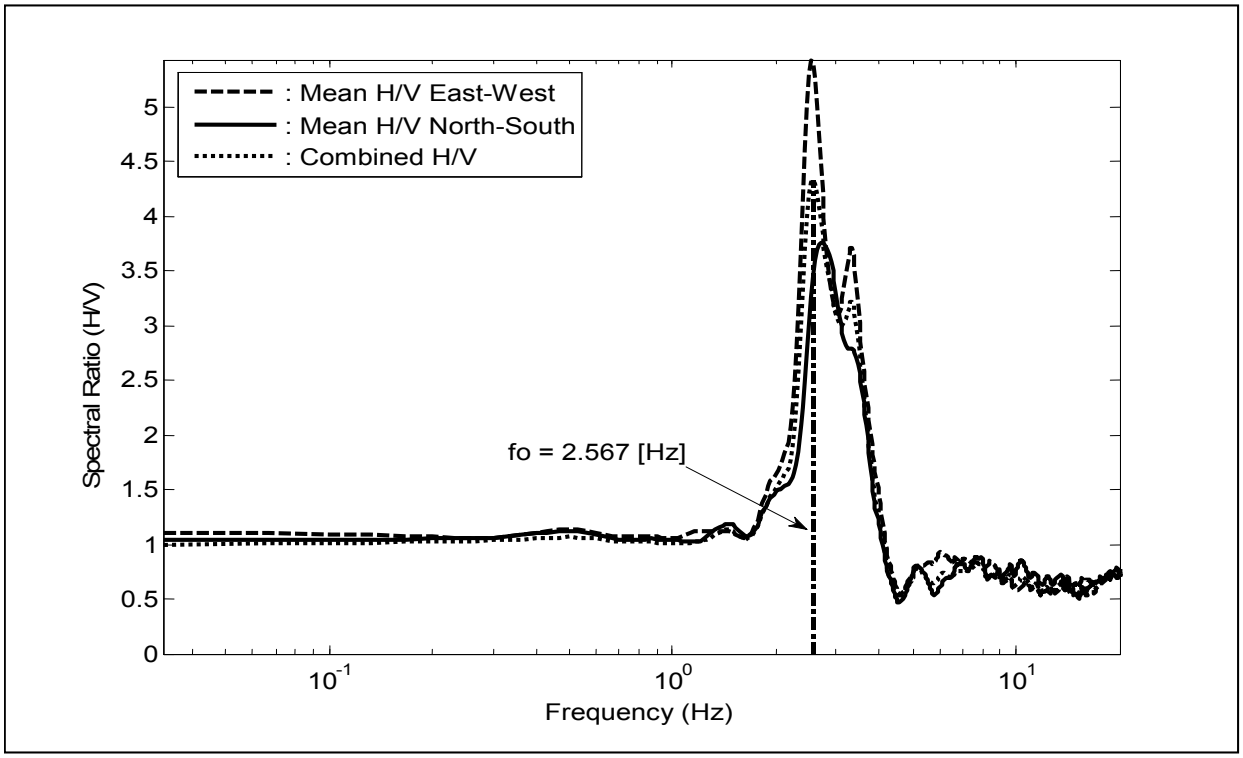

Figure CHAPTER 4.11: Spectral ratio H/V for site P#3 with WL = 30 seconds

Comparing Figures 4.20 and 4.21, a window length decrease produced a slight shift of the site fundamental frequency to the right with respect to that obtained with the parameters in Table 4.3, while an increase in the window length produced a slight shift of the site fundamental frequency to the left compared to that obtained with the parameters in Table 4.3. Therefore, it can be concluded that changing the length of the window does not have a marked effect; however, it is recommend using the value set by default.

4.6 *Percentage of overlap between windows (OW) variation*

Windows are not chosen one after the other during the automatic selection process. There is some overlap between them, as shown schematically in Figure 4.22.

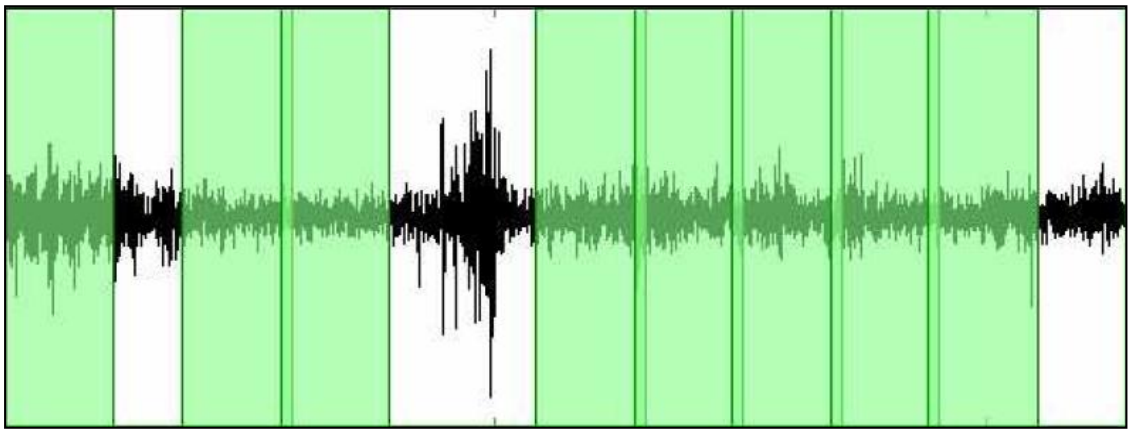

Figure CHAPTER 4.22: Overlapping between adjacent windows

Two runs were performed in order to analyze the effect of overlapping in the results, one with a 5% overlapping of the window length, and the other with a 50% overlapping of the length of the window. Figures 4.23 and 4.24 show the results obtained for this analysis (where OW is the acronym for Overlapping Window).

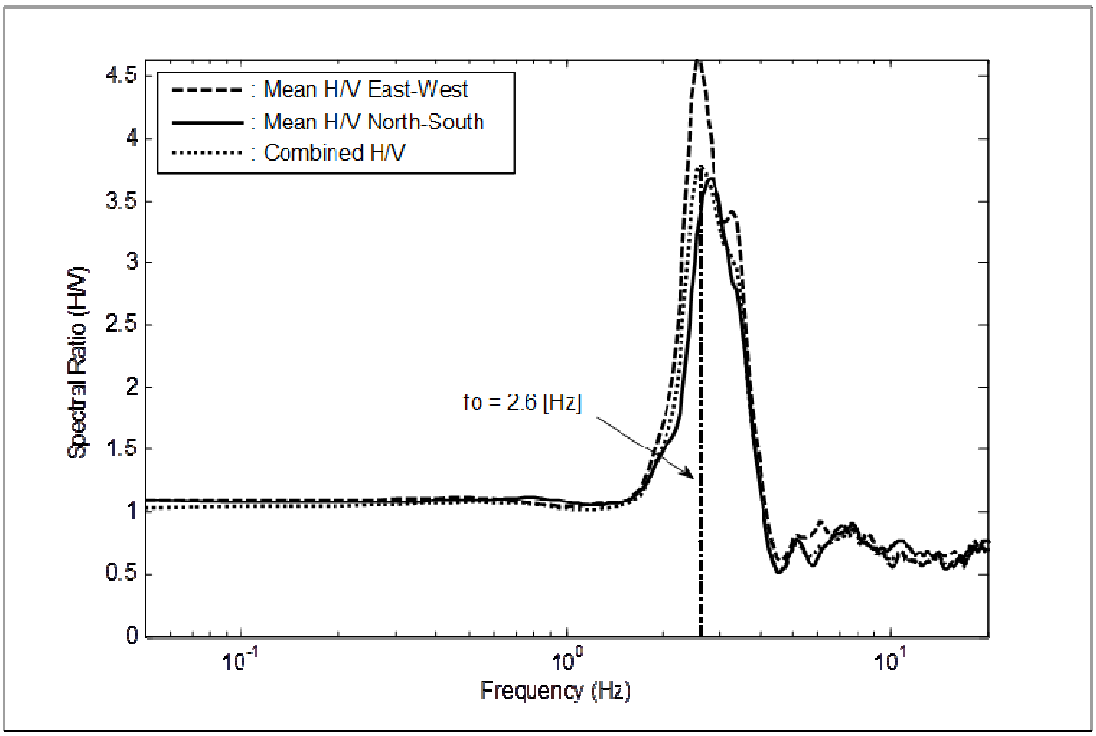

Figure CHAPTER 4.12: Spectral ratio H/V for site P#3 with OW = 5%

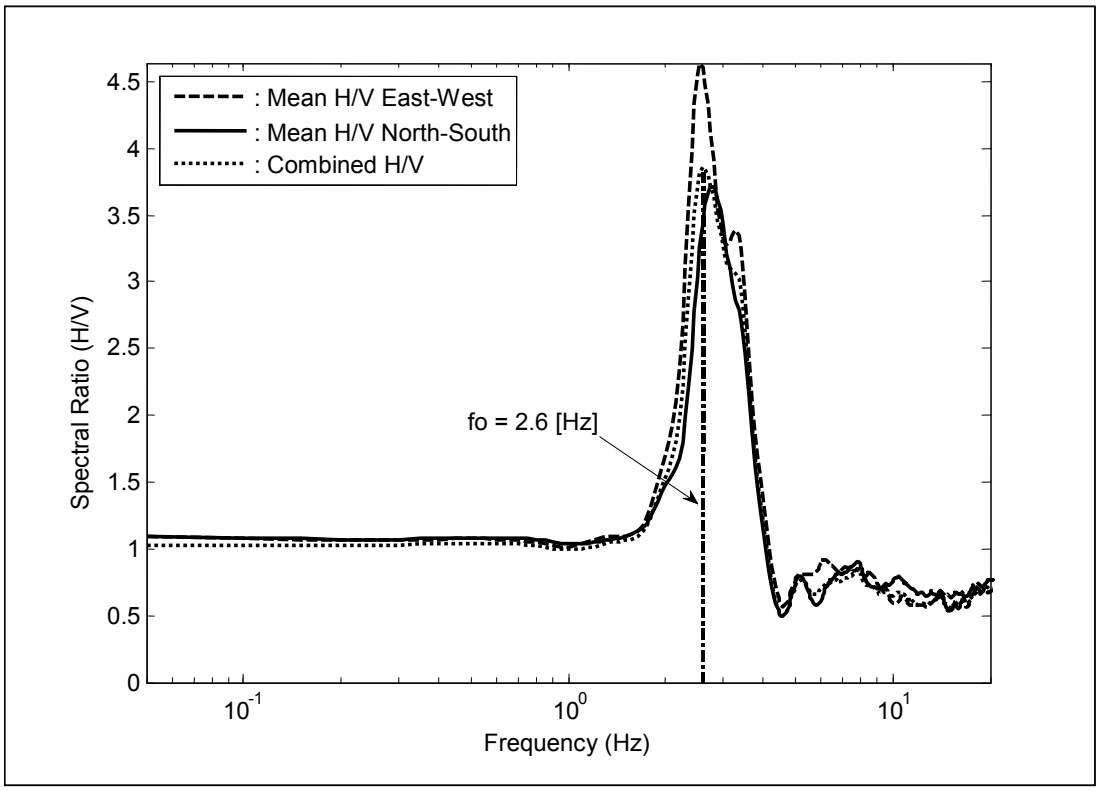

Figure CHAPTER 4.13: Spectral ratio H/V for site P#3 with OW = 50%

A variation in the overlapping window percentage does not change the fundamental frequency as seen in Figures 4.23 and 4.24. However, it is advisable to use a certain percentage of overlapping to obtain a better average across all windows that have met the selection parameters.

4.7 *Modification of time for the average short-period (tsta)*

This subsection presents the results obtained at the P # 3 site by changing the length of the window used to calculate the average acceleration short period (TSTA). JSesame suggests TSTA values between 0.5 and 2 seconds. Two runs using were performed with these two extreme values, and Figure 4.25 and 4.26 shows the results obtained. The value of TSTA, within the limits recommended by the program does not produce major Jsesame changes.

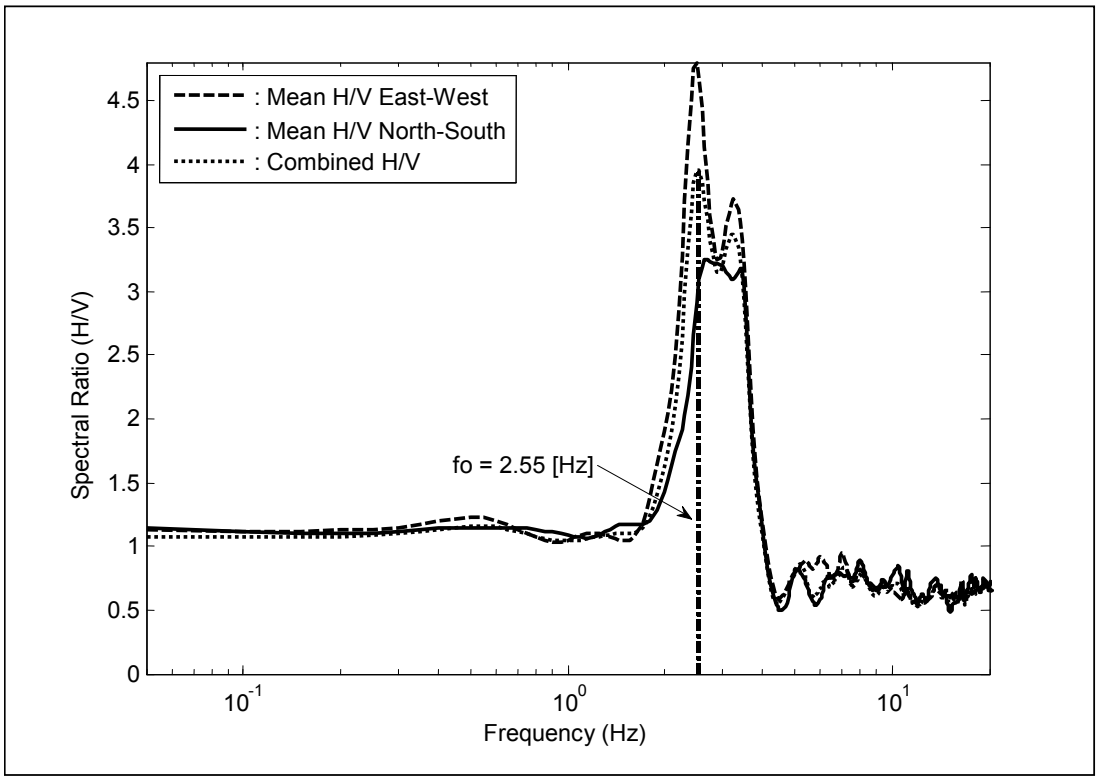

Figure CHAPTER 4.14: Spectral ratio H/V for site P#3 with TSTA = 0.5 seconds

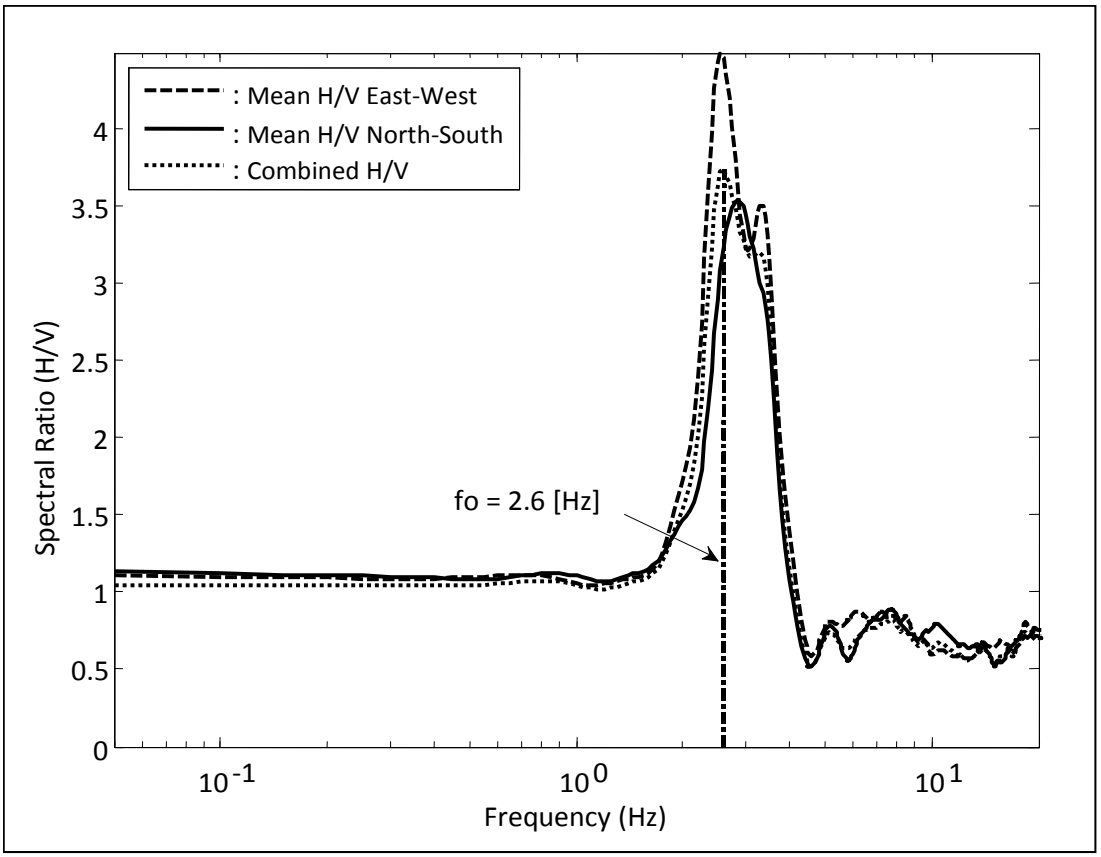

Figure CHAPTER 4.156: Spectral ratio H/V for site P#3 with TSTA = 2 seconds

4.8 *Modification of time for the average long-period (TLTA)*

The window length used to calculate the long period average acceleration (TLTS) was also analyzed. The Jsesame program suggests using several tens of seconds as a value for this parameter. Figures 4.27 and 4.28 show the ratios H / V obtained using TLTA equals to 20 and 40s respectively. It is observed that different TLTA values do not produce important changes in the value of the fundamental frequency, and lead to negligible changes in the spectral ratio.

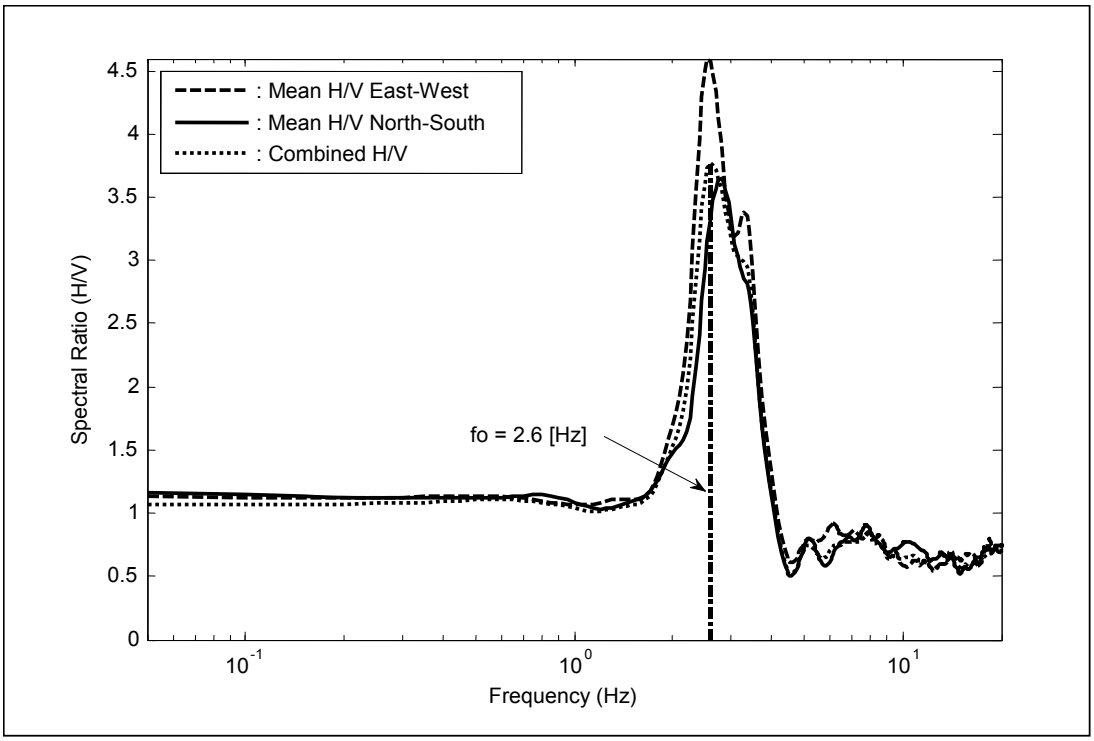

Figure CHAPTER 4.16: Spectral ratio H/V for site P#3 with TLTA = 20 seconds

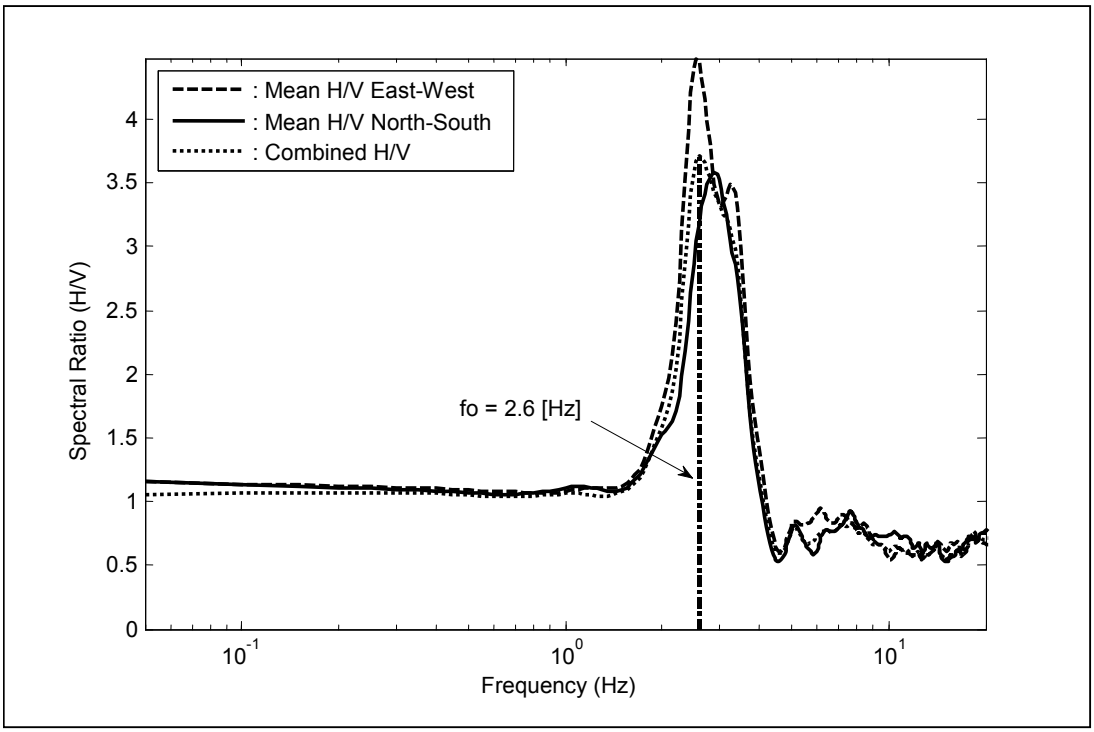

Figure CHAPTER 4.17: Spectral ratio H/V for site P#3 with TLTA = 40 seconds

4.9 *Minimum sta/lta ratio variation*

This subsection examines the effect produced by modifying the minimum value of the ratio between the average short-period and the average long period (denoted sta / lta) on the fundamental frequency. The JSesame program uses 0.5 as default value for this parameter. Figures 4.29 and 4.30 show the spectral ratios H / V and the natural frequencies obtained with sta/lta = 0.1 and 0.8 respectively. A variation of the sta/lta ratio has influence on the shape of the spectral ratio obtained, but not on the value of natural frequency which is kept unchanged.

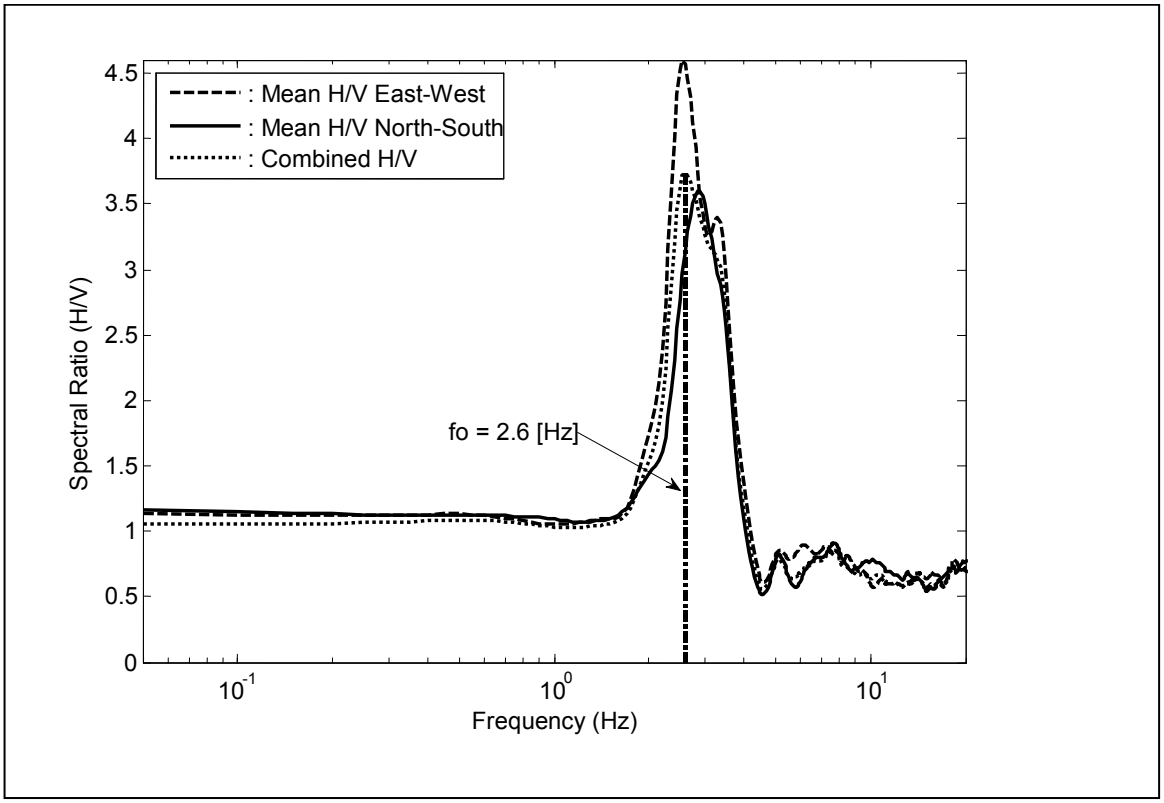

Figure CHAPTER 4.29: Spectral ratio H/V for site P#3 with sta/lta = 0.1

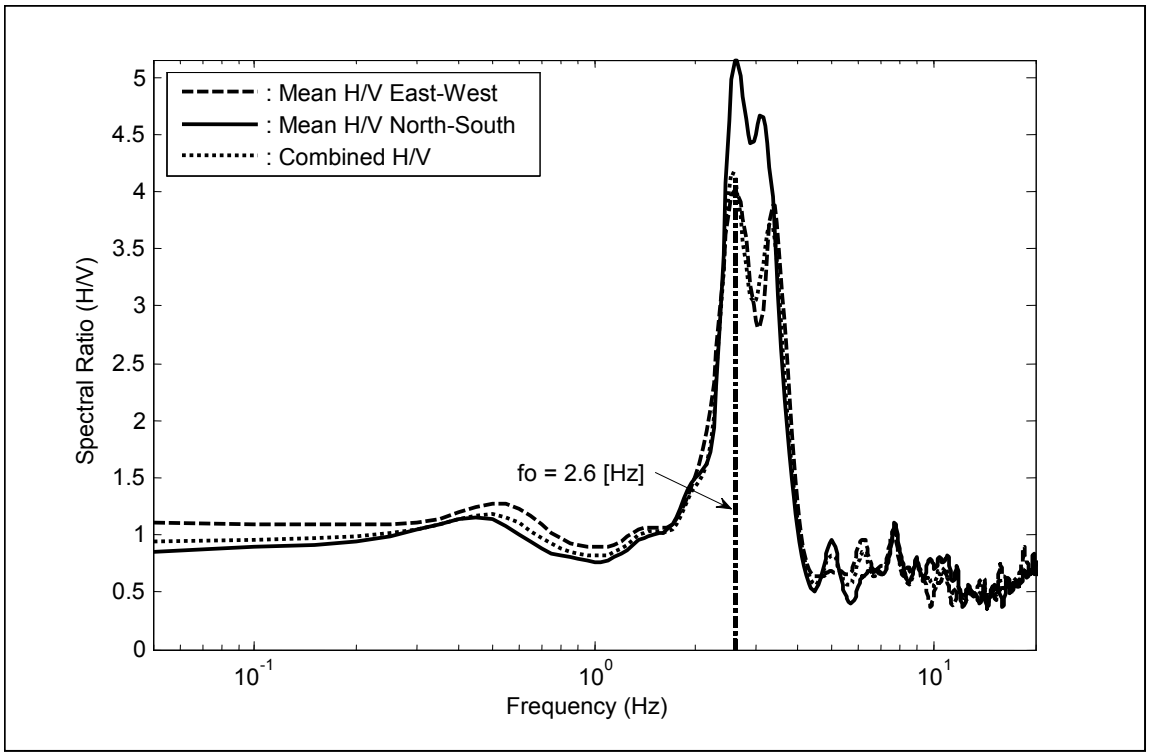

Figure CHAPTER 4.30: Spectral ratio H/V for site P#3 with sta/lta = 0.8

4.10 *Maximum sta/lta ratio variation*

A variation of the maximum ratio sta / lta values was also analyzed. The JSesame program uses a value of 2 by default. Figures 4.31 and 4.32 show the results obtained with sta / lta = 1.5 and 10 respectively. From Figure 4.32, it is observed that for a sta/lta ratio equal to 10 there is a slight change in the shape of the spectral ratios, mainly in the low frequencies. The change in the shape of the spectral ratios is due to the fact that an increase or decrease in the minimum and maximum value of sta / lta is produces an increased, respectively, the number of windows that meet the selection criteria, while increase or decrease the number of windows that meet the selection criteria. The value of the fundamental frequency remained unchanged.

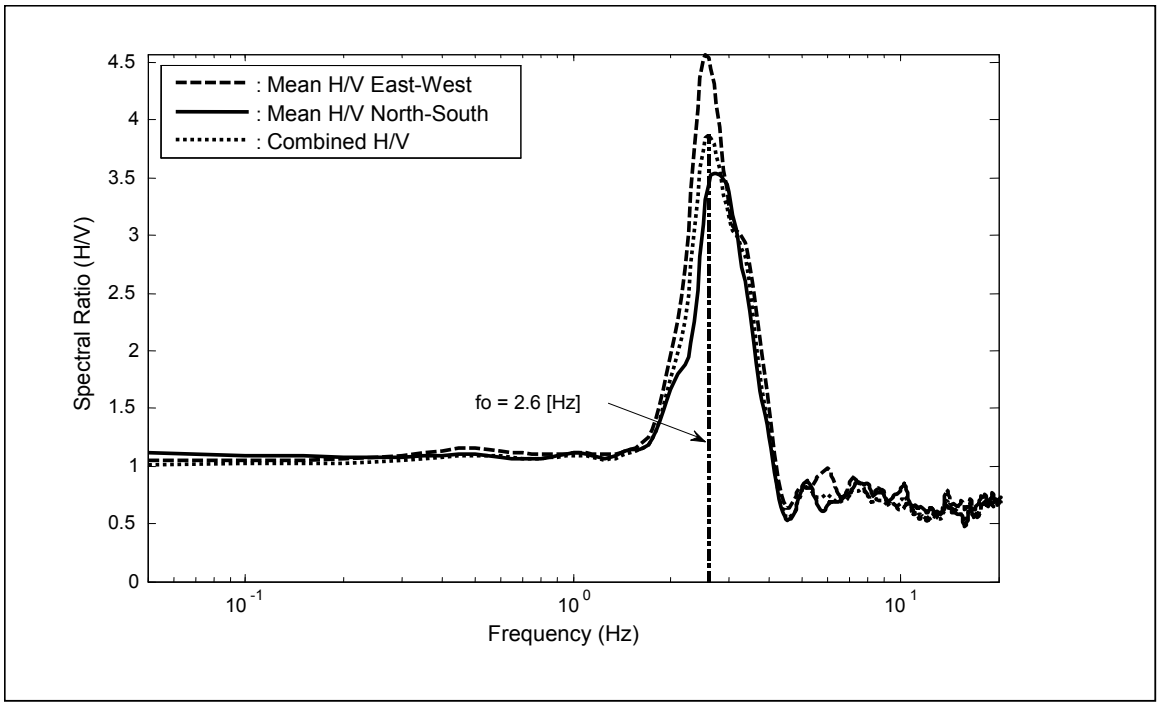

Figure CHAPTER 4.31: Spectral ratio H/V for site P#3 with sta/lta = 1.5

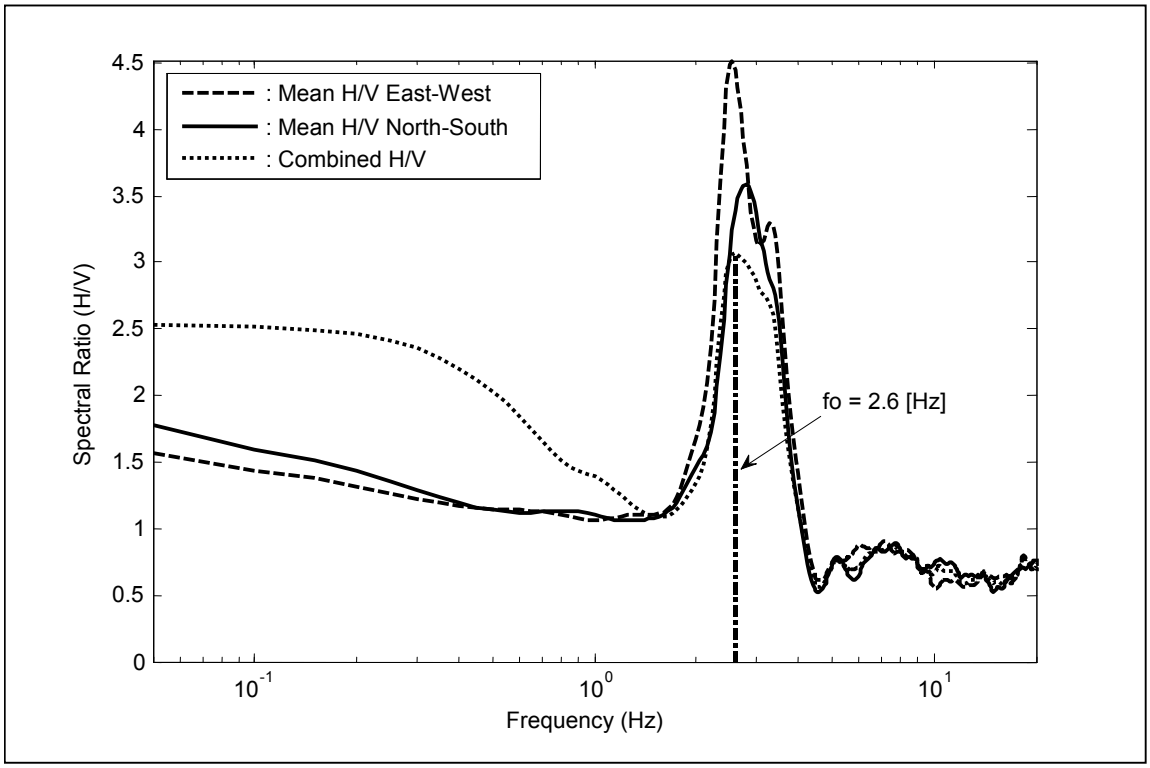

Figure CHAPTER 4.32: Spectral ratio H/V for site P#3 with sta/lta = 10

4.11 *Stability analysis of the spectral ratio method H / V*

In order to demonstrate the stability of the spectral ratio method using ambient vibration measurements to determine the fundamental frequency of a given site, it was decided to take a complete record during one day and then processed data at different times of the day. The site for this analysis was the Mayagüez Cathedral seismic station (P # 79), which belongs to the Strong Motion Program of Puerto Rico. The instrument used to take the measurement was a ± 2g ETNA accelerometer at a rate of 100 samples per second. Different times were processed using the parameters indicated in Table 4.1. A total number of 12 hours were considered (odd hours). Figure 4.33 shows the ratios H / V for different times processed.

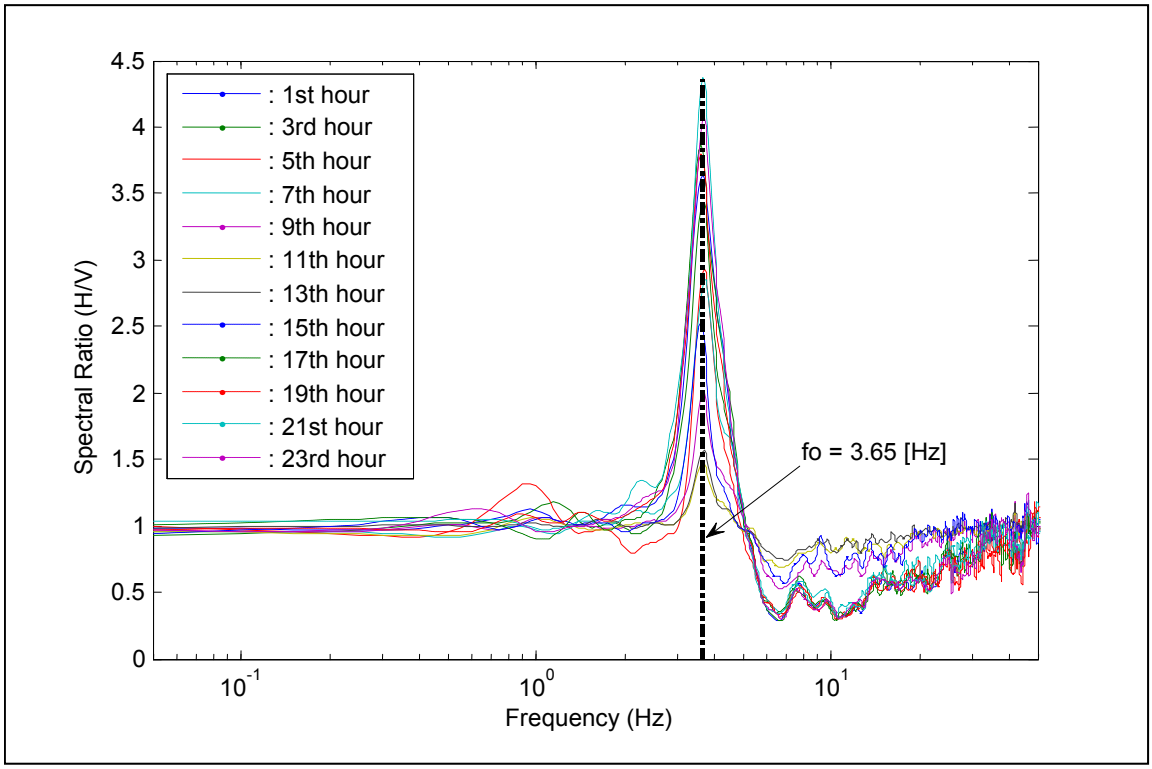

Figure CHAPTER 4.3318: Spectral ratio H/V for different times during a day for site P#79

As shown in Figure 4.33, the fundamental frequency of the ground was the same regardless of the time during the day. This demonstrates the stability of the method and that the fundamental frequency is a property of the ground, which depends on the kind of excitation to which it is subjected. It is also observed that the spectral ratio amplitude varies depending on the time the measurement was taken which is consistent with studies reported by Kanai and Tanaka,

(1961), Nakamura, (1989) and Alfaro (2006). The lowest amplitudes occur at night, when the human and industrial activity is reduced, while the highest amplitudes occur during the day.

4.12 *Ground modeling and spectral ratio comparison*

This section presents a comparison between the site fundamental frequency obtained using spectral ratio technique (Horizontal / Vertical) applied to microtemblors and that obtained by calculating the theoretical transfer functions of superficial rock-surface and basal rock-surface for site P # 17. SASW test results (English acronym for Spectral Analysis of Surface Waves) from the report "Ground Motions Evaluation and Geotechnical Database for the City of Mayagüez, Puerto Rico" (Pando et al., 2006) was used for this analysis. The result obtained using spectral ratios can be observed in Figure 4.34 resulting in a site fundamental frequency 2.15 Hz. The thickness and shear wave velocity for each layer were obtained from a previous report (Pando et al., 2006), and are shown in Table 4.4.

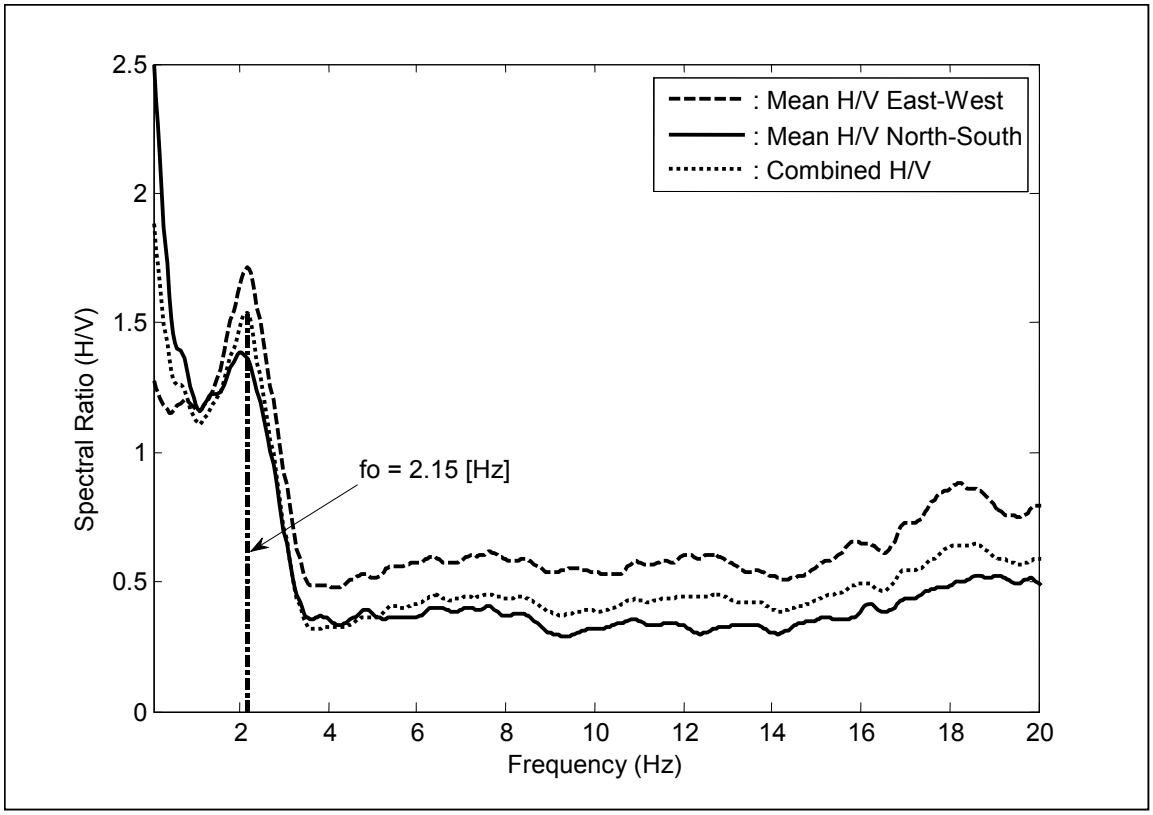

Figure CHAPTER 4.34: Spectral ratio H/V for site P#17

Using the Matlab program FTransf.m developed for the course UPRM Soil Dynamics (Suarez, 2007) and the parameters indicated in Table 4.4, the transfer functions were calculated and they are displayed in Figure 4.35. As can be seen by comparing Figures 4.34 and 4.35, the values of the fundamental frequency for the site P # 17 using both techniques correlate quite well.

Table CHAPTER 4.4: Soil properties for site P#17

Layer	Thickness [ft]	Unit Weight [lb/ft^3]	V_S [ft/seg]
1	3.94	125	770
2	6.23	120	1061
3	18	125	511
4	21	100	646
5	13.78	110	953
6	13.12	115	1725
7	22.31	100	2555
8 (rock)	200	140	10000

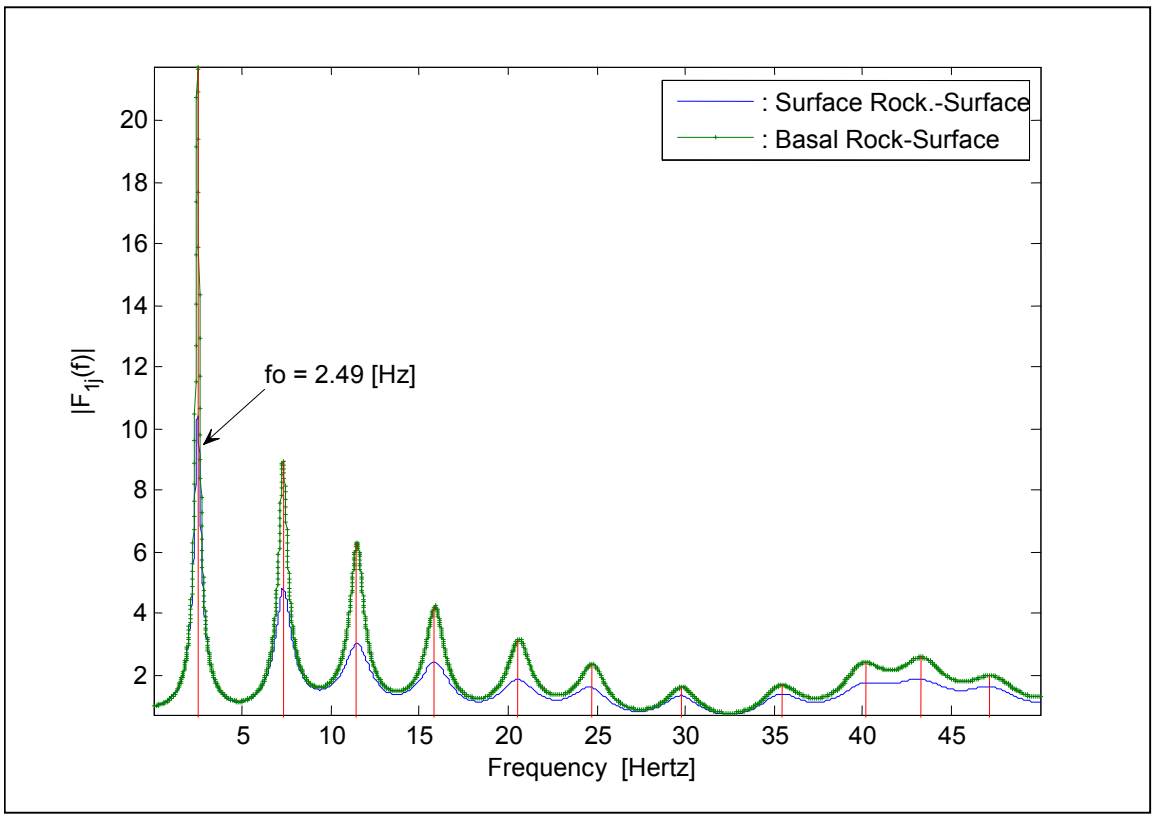

Figure CHAPTER 4.19: Transfer function between surface and basal rock for site P#17

CHAPTER 5 ISOPERIOD MAP FOR THE CITY OF MAYAGÜEZ

5.1 *Introduction*

This chapter presents the results obtained from processing ambient vibration measurements and the construction of isoperiod soil maps for the City of Mayagüez. Results obtained during the first set of measurement are initially discussed at the beginning of this chapter followed by data taken in a second set of measurements in certain sites where fundamental periods were not clearly identified from the first set of measurements. Subsequently, new data obtained during the second set of measurement are presented in order to achieve a higher density of points in certain areas of the City of Mayagüez. Finally, isoperiod soil map for the City of Mayagüez are illustrated.

5.2 *Results obtained from the first measurements*

After performing the first set of measurement; which consisted of a total of 111 ambient vibration measurements over a period of one hour per each, measurement, only 89 of these 111 measurements were taken into account to determine the site fundamental frequency. Table 5.1 shows the geographic coordinates (decimal degrees) for 111 sites and the fundamental period for the 89 sites that could be determined. It was not possible to determine the fundamental period in 22 sites since soils found at some of them were too rigid and therefore not being able to obtain amplifications at any frequency, while at other sites it was not possible to find a dominant frequency.

Table CHAPTER 5.1: First set of ambient vibration measurement results

Site	Latitude (N)	Longitude(W)	Frequency [Hz]	Period [Sec]
P#1	18.21323056	67.13986389	3.450	0.290
P#2	18.21433333	67.13944722	3.200	0.313
P#3	18.20786667	67.14105833	2.600	0.385
P#3_1	18.20704000	67.14098000	2.050	0.488
P#3_2	18.20719000	67.14083000	2.240	0.446
P#3_3	18.20741000	67.14059000	3.375	0.296
P#3_4	18.20770000	67.14028000	2.350	0.426
P#3_5	18.20805000	67.13993000	NA	NA
P#4	18.20404167	67.14605000	1.875	0.533
P#5	18.20246667	67.13783889	2.550	0.392
P#6	18.20189167	67.13480000	2.400	0.417
P#7	18.19540556	67.13703889	5.900	0.169
P#8	18.18606389	67.13766667	NA	NA
P#9	18.19163889	67.14318889	6.475	0.154
P#10	18.19596667	67.14231944	3.000	0.333
P#11	18.19926389	67.14886111	2.400	0.417
P#12	18.19107500	67.15088056	2.650	0.377
P#13	18.19443333	67.15532222	1.750	0.571
P#14	18.19933056	67.15285833	2.300	0.435
P#15	18.20682222	67.15278889	1.600	0.625
P#16	18.26776667	67.16260000	1.700	0.588
P#17	18.24730000	67.17405000	2.100	0.476
P#18	18.24063333	67.17143333	2.200	0.455
P#19	18.21320000	67.15850000	2.100	0.476
P#20	18.18950000	67.15871667	1.450	0.690
P#21	18.19135000	67.15450000	1.370	0.730
P#22	18.17550000	67.15851667	4.200	0.238
P#23	18.16266667	67.15851667	NA	NA
P#24	18.26433333	67.17625000	1.600	0.625
P#25	18.16213333	67.17721667	NA	NA
P#26	18.16721667	67.18053333	NA	NA
P#27	18.16873333	67.17951667	1.400	0.714

Table CHAPTER 5.1: First set of ambient vibration measurement results

Site	Latitude (N)	Longitude(W)	Frequency [Hz]	Period [Sec]
P#28	18.17315000	67.17560000	2.000	0.500
P#29	18.17836667	67.17191667	0.950	1.053
P#30	18.18431667	67.16636667	1.700	0.588
P#31	18.18851667	67.16093333	1.400	0.714
P#32	18.20583333	67.14066667	NA	NA
P#33	18.15200000	67.14066667	6.200	0.161
P#34	18.15150000	67.15050000	2.850	0.351
P#35	18.16116667	67.14936667	7.100	0.141
P#36	18.16915000	67.14651667	NA	NA
P#37	18.17000000	67.15470000	4.700	0.213
P#38	18.17661667	67.15023333	4.600	0.217
P#39	18.17743333	67.15801667	7.000	0.143
P#40	18.18191667	67.14583333	5.100	0.196
P#41	18.18360000	67.15368333	NA	NA
P#42	18.21055000	67.14605000	NA	NA
P#43	18.21240000	67.14748333	4.550	0.220
P#44	18.20883333	67.14266667	4.600	0.217
P#45	18.20850000	67.15050000	2.100	0.476
P#46	18.21840000	67.15466667	3.900	0.256
P#47	18.21633333	67.15756667	3.200	0.313
P#48	18.21973333	67.16116667	3.775	0.265
P#49	18.22261667	67.15161667	1.950	0.513
P#50	18.22996667	67.17278333	7.700	0.130
P#51	18.22281667	67.16065000	NA	NA
P#52	18.22836667	67.15831667	3.300	0.303
P#53	18.22475000	67.16525000	4.100	0.244
P#54	18.25135000	67.17546667	NA	NA
P#55	18.25283333	67.17733333	NA	NA
P#56	18.26146667	67.18175000	NA	NA
P#57	18.26340000	67.18548333	3.000	0.333
P#58	18.26541667	67.18203333	3.000	0.333
P#59	18.26075000	67.17431667	NA	NA

Table CHAPTER 5.1: First set of ambient vibration measurement results

Site	Latitude (N)	Longitude(W)	Frequency [Hz]	Period [Sec]
P#60	18.26655000	67.16108333	1.150	0.870
P#61	18.26731667	67.15858333	2.000	0.500
P#62	18.26678333	67.15408333	NA	NA
P#63	18.25956667	67.15930000	1.550	0.645
P#64	18.25173333	67.16028333	2.450	0.408
P#65	18.25241667	67.15260000	2.700	0.370
P#66	18.24805000	67.16501667	1.150	0.870
P#67	18.24710000	67.17030000	2.700	0.370
P#68	18.24705000	67.13735000	2.400	0.417
P#69	18.24070000	67.16428333	2.200	0.455
P#70	18.24170000	67.15610000	2.600	0.385
P#71	18.23641667	67.14330000	4.300	0.233
P#72	18.23166667	67.14155000	2.800	0.357
P#73	18.23475000	67.16075000	4.000	0.250
P#74	18.23575000	67.15616667	6.200	0.161
P#75	18.23033333	67.14958333	5.800	0.172
P#76	18.23031667	67.14958333	NA	NA
P#77	18.22933333	67.13948333	3.150	0.317
P#78	18.28300000	67.14100000	1.900	0.526
P#79	18.20000000	67.13750000	3.650	0.274
P#80	18.16720000	67.15140000	6.000	0.167
P#81	18.14130000	67.12750000	1.050	0.952
P#82	18.18540000	67.13800000	NA	NA
P#83	18.22215500	67.11560600	NA	NA
P#83_1	18.22210000	67.15522000	NA	NA
P#84	18.20516000	67.14700000	1.500	0.667
P#85	18.24080000	67.17220000	2.150	0.465
P#86	18.20950000	67.12190000	NA	NA
P#87	18.20580000	67.15080000	NA	NA
P#88	18.23980000	67.12130000	NA	NA
P#89	18.19870000	67.12852000	7.400	0.135
P#90	18.19483000	67.09226000	7.300	0.137

Table CHAPTER 5.1: First set of ambient vibration measurement results

Site	Latitude (N)	Longitude(W)	Frequency [Hz]	Period [Sec]
P#91	18.18688000	67.07844000	10.750	0.093
P#92	18.18760000	67.06167000	2.950	0.339
P#93	18.19471000	67.11274000	9.650	0.104
P#94	18.20843000	67.12750000	4.050	0.247
P#95	18.20872000	67.11485000	10.700	0.093
P#96	18.21015000	67.10085000	3.050	0.328
P#97	18.20734000	67.08041000	5.750	0.174
P#98	18.20811000	67.05701000	4.250	0.235
P#99	18.21883000	67.14070000	5.100	0.196
P#100	18.23486000	67.12553000	4.300	0.233
P#101	18.23634000	67.13024000	5.700	0.175
P#102	18.24079000	67.10488000	2.350	0.426
P#103	18.18483000	67.13242500	9.400	0.106
P#104	18.17244000	67.12531000	7.550	0.132
P#105	18.16727000	67.09715000	12.900	0.078

A soil classification was performed using the fundamental periods obtained from the 89 sites indicated on table 5.1. This classification was based on site fundamental periods within the half-open interval [0 - 0.1) seconds [0.1 - 0.2) seconds, etc. Once sites were classified, maps were built using the program ArcMap 9.3. Site fundamental periods are indicated in a circle as seen figure 5.1. The purpose of this map is to observe the distribution of the obtained site periods in order to determine the location of possible new sites to be measured.

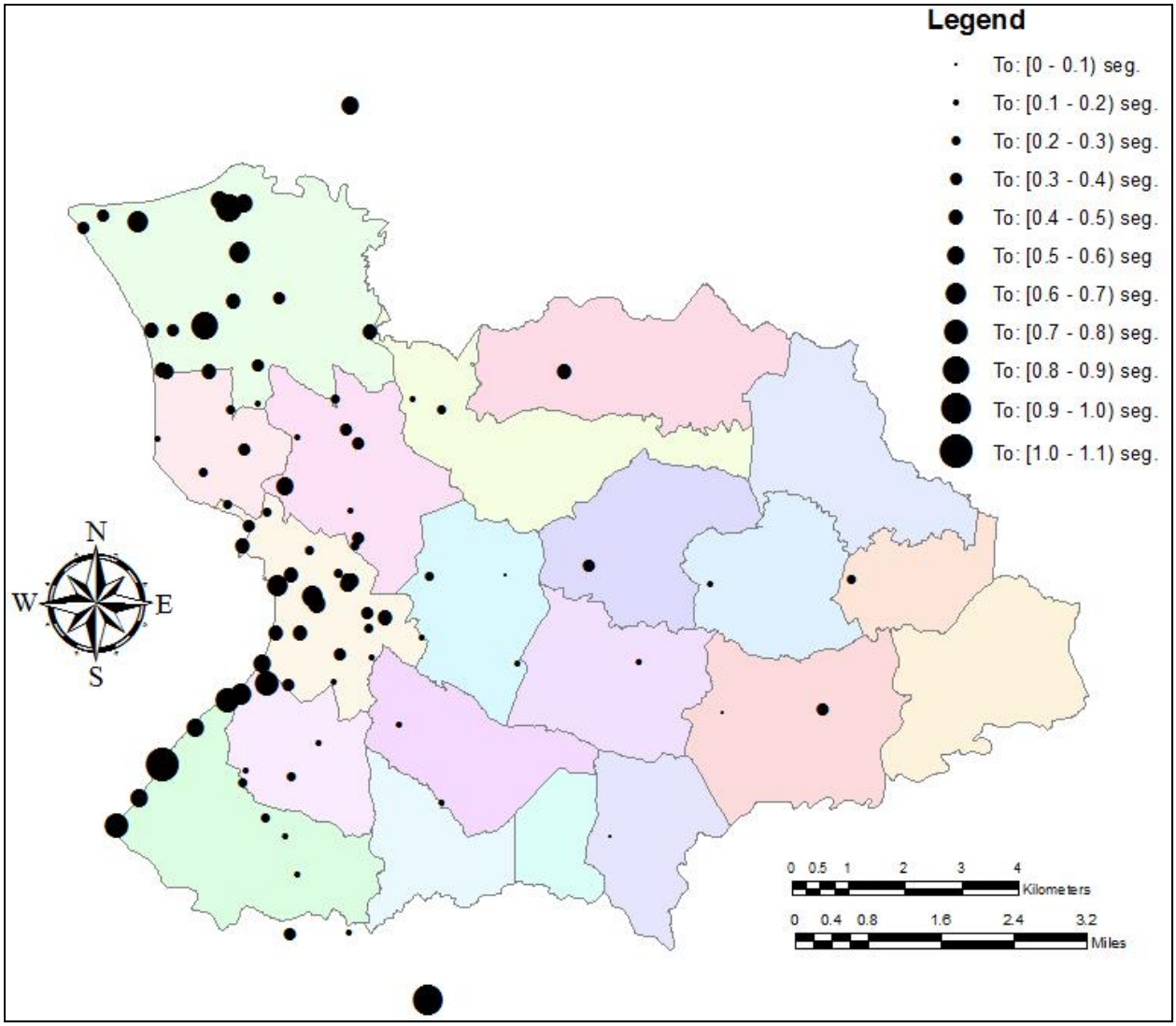

Figure CHAPTER 5.1 Preliminary map of fundamental periods for the city of Mayagüez

After processing the first set ambient vibration measurements, it was found that 22 of these measurements did not show a clear fundamental frequency value of the site. All these measurements were taken using a ± 2.0g ETNA accelerometer, which was described, demonstrated in section 4.3. It was decided to carry out a second set of measurements in these 22 sites, but this time using accelerometers ± 0.25g. Each measurement was taken during a period of one hour at 100 samples per second. Figure 5.2 shows the location of these 22 sites. These new measurements were processed in the same manner as the original measurements using the program HVSRAV.m. Table 5.2 shows the results obtained from these measurements.

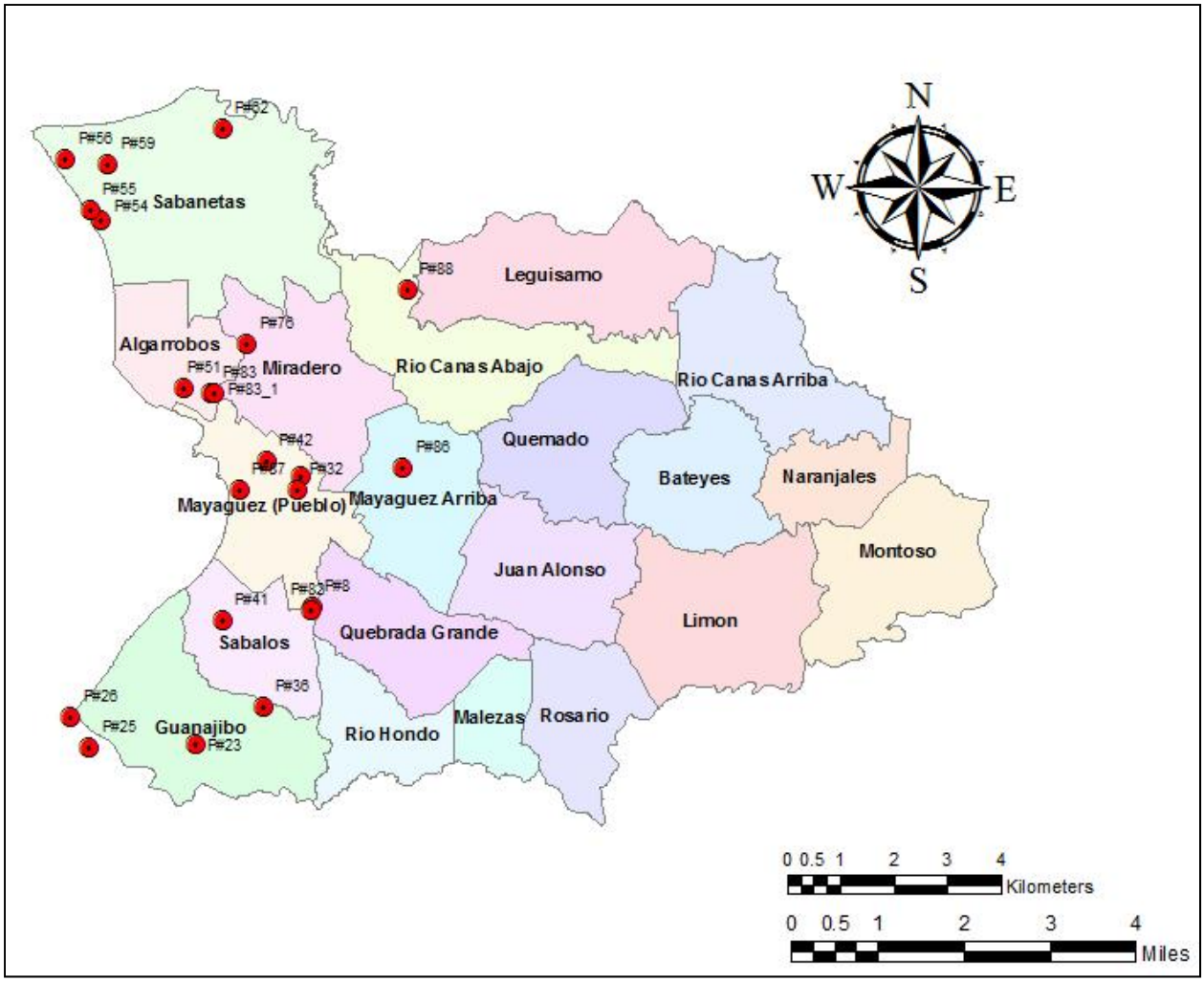

Figure CHAPTER 5.2: Sites where new ambient vibration measurements were taken

Repeated measurements in the 22 selected sites were successful since only four of these did not resulted in an adequate fundamental frequency for the site as indicated in table 5.2. This confirms the fact that 0.25g accelerometer is more sensitive and therefore more convenient than 2.0g. In summary, from a total of 111 measurements, it was possible to determine the fundamental period from 107 measurements, while only 4 did not yield a clear result.

Table CHAPTER 5.2 Repetition of ambient vibration measurement at selected sites results

Site	Latitude (N)	Longitude(W)	Frequency [Hz]	Period [Sec]
P#3_5	18.20805000	67.13993000	4.950	0.202
P#8	18.18606389	67.13766667	8.200	0.122
P#23	18.16266667	67.15851667	13.500	0.074
P#25	18.16213333	67.17721667	9.225	0.108
P#26	18.16721667	67.18053333	18.050	0.055
P#32	18.20583333	67.14066667	1.600	0.625
P#36	18.16915000	67.14651667	6.350	0.157
P#41	18.18360000	67.15368333	NA	NA
P#42	18.21055000	67.14605000	NA	NA
P#51	18.22281667	67.16065000	3.250	0.308
P#54	18.25135000	67.17546667	0.950	1.053
P#55	18.25283333	67.17733333	0.950	1.053
P#56	18.26146667	67.18175000	0.70	1.428
P#59	18.26075000	67.17431667	1.250	0.800
P#62	18.26678333	67.15408333	1.600	0.625
P#76	18.23031667	67.14958333	NA	NA
P#82	18.18540000	67.13800000	6.550	0.153
P#83	18.22215500	67.11560600	NA	NA
P#83_1	18.22210000	67.15522000	6.350	0.157
P#86	18.20950000	67.12190000	3.350	0.298
P#87	18.20580000	67.15080000	1.550	0.645
P#88	18.23980000	67.12130000	3.600	0.278

5.3 *Second set of ambient vibration measurements*

First set of measurement were primarily focused on the most populated area of the city (west area). In order to increase in order to increase the density of measured points, it was decided to carry out a second set of measurements toward the east side of the city which is characterized by a mountainous topography and low density low population. A total of 23 new sites were selected as shown in figure 5.3. Measurements were taken using ± 0.25g ETNA accelerometers at a rate of 100 samples per second over a period of 1 hour for each measurement.

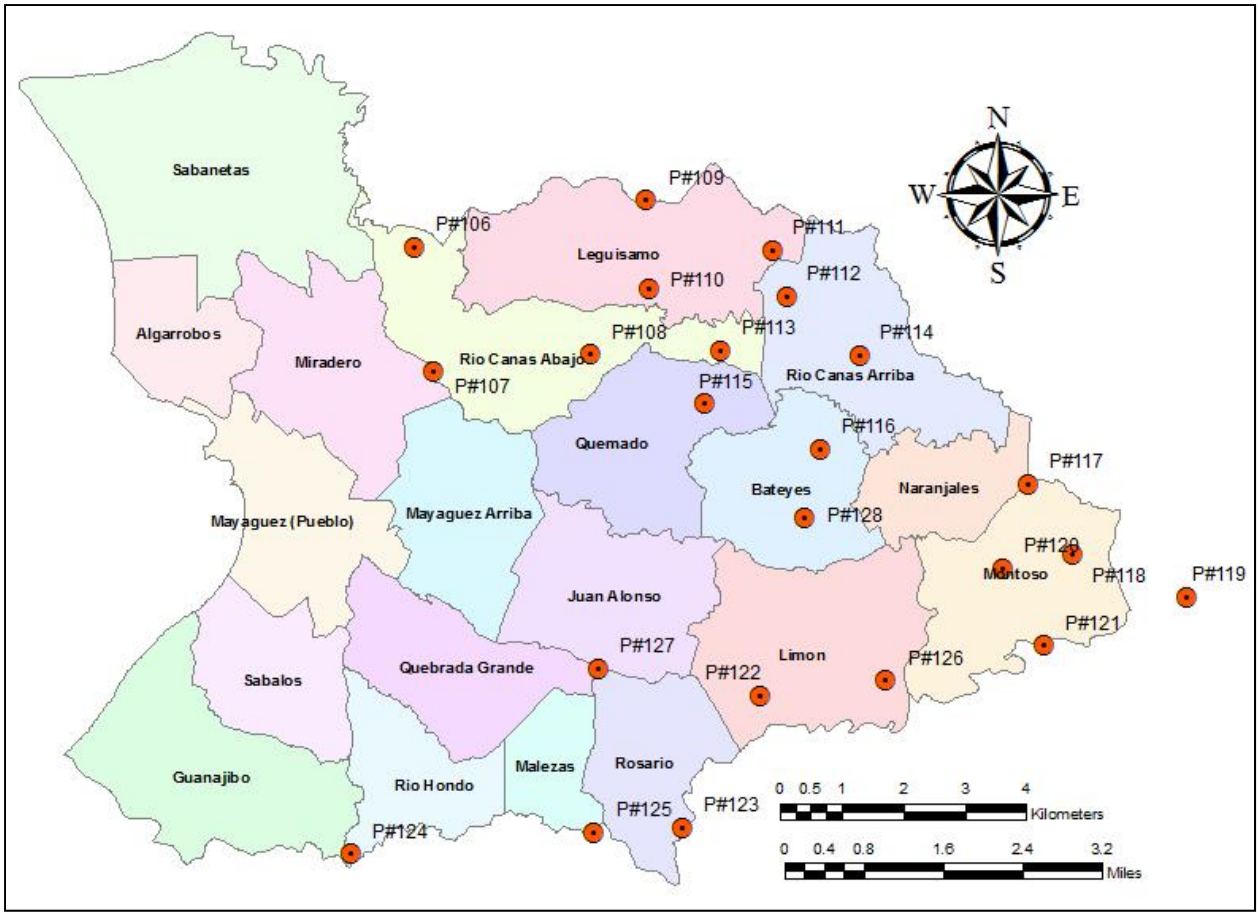

Figure CHAPTER 5.3: New ambient vibration measurement located at the east area of Mayagüez

5.4 *Second measurement analysis*

After completing the measurements in the 23 new sites, the analysis of the data was performed using the program HVSRAV.m. Table 5.3 shows the results obtained after processing the data.

Examining the data shown in table 5.3, it is concluded that from the new 23 measurements, 19 of them resulted in reliable results for the site fundamental period; therefore, out of a total of 134 environmental vibration measurements recorded at different locations in the City of Mayagüez, 126 resulted in reliable fundamental frequency of the soil, while only 8 failed to produce a clear value of fundamental frequency. Table 5.4 summarizes all sites measured with the corresponding frequencies and periods while figures 5.4, 5.5 and 5.6 all measured sites, the sites where fundamental frequencies where measured, and the sites where fundamental frequency was not obtained respectively.

Table CHAPTER 5.3: Repetition of ambient vibration measurement at selected sites results

Site	Latitude (N)	Longitude(W)	Frequency [Hz]	Period [Sec]
P#106	18.24258000	67.12713000	3.4	0.294
P#107	18.22431000	67.12418000	2.65	0.377
P#108	18.22705000	67.10004000	NA	NA
P#109	18.24955000	67.09155000	2.3	0.435
P#110	18.23660000	67.09106000	2.75	0.364
P#111	18.24236000	67.07226000	2.55	0.392
P#112	18.23558000	67.07006000	3.55	0.282
P#113	18.22769000	67.08012000	4.65	0.215
P#114	18.22702000	67.05878000	3.45	0.290
P#115	18.21982000	67.08241000	3.65	0.274
P#116	18.21330000	67.06464000	3	0.333
P#117	18.20830000	67.03291000	3.75	0.267
P#118	18.19793000	67.02610000	3	0.333
P#119	18.19189000	67.00857000	6	0.167
P#120	18.19599000	67.03686000	NA	NA
P#121	18.18473000	67.03039000	11.9	0.084
P#122	18.17730000	67.07388000	13	0.077
P#123	18.15796000	67.08582000	4.1	0.244
P#124	18.15393000	67.13653000	10.55	0.095
P#125	18.15717000	67.09921000	NA	NA
P#126	18.17952000	67.05458000	NA	NA
P#127	18.18114000	67.09874000	6	0.167
P#128	18.20317000	67.06709000	4.22	0.237

Table CHAPTER 5.4: Summary of all ambient vibration measurements

Site	Latitude (N)	Longitude(W)	Frequency [Hz]	Period [Sec]
P#1	18.21323056	67.13986389	3.450	0.290
P#2	18.21433333	67.13944722	3.200	0.313
P#3	18.20786667	67.14105833	2.600	0.385
P#3_1	18.20704000	67.14098000	2.050	0.488
P#3_2	18.20719000	67.14083000	2.240	0.446
P#3_3	18.20741000	67.14059000	3.375	0.296
P#3_4	18.20770000	67.14028000	2.350	0.426
P#3_5	18.20805000	67.13993000	4.950	0.202
P#4	18.20404167	67.14605000	1.875	0.533
P#5	18.20246667	67.13783889	2.550	0.392
P#6	18.20189167	67.13480000	2.400	0.417
P#7	18.19540556	67.13703889	5.900	0.169
P#8	18.18606389	67.13766667	8.200	0.122
P#9	18.19163889	67.14318889	6.475	0.154
P#10	18.19596667	67.14231944	3.000	0.333
P#11	18.19926389	67.14886111	2.400	0.417
P#12	18.19107500	67.15088056	2.650	0.377
P#13	18.19443333	67.15532222	1.750	0.571
P#14	18.19933056	67.15285833	2.300	0.435
P#15	18.20682222	67.15278889	1.600	0.625
P#16	18.26776667	67.16260000	1.700	0.588
P#17	18.24730000	67.17405000	2.100	0.476
P#18	18.24063333	67.17143333	2.200	0.455
P#19	18.21320000	67.15850000	2.100	0.476
P#20	18.18950000	67.15871667	1.450	0.690
P#21	18.19135000	67.15450000	1.370	0.730
P#22	18.17550000	67.15851667	4.200	0.238
P#23	18.16266667	67.15851667	13.500	0.074
P#24	18.26433333	67.17625000	1.600	0.625
P#25	18.16213333	67.17721667	9.225	0.108
P#26	18.16721667	67.18053333	14.600	0.068
P#27	18.16873333	67.17951667	1.400	0.714

Table CHAPTER 5.4: Summary of all ambient vibration measurements

Site	Latitude (N)	Longitude(W)	Frequency [Hz]	Period [Sec]
P#28	18.17315000	67.17560000	2.000	0.500
P#29	18.17836667	67.17191667	0.950	1.053
P#30	18.18431667	67.16636667	1.700	0.588
P#31	18.18851667	67.16093333	1.400	0.714
P#32	18.20583333	67.14066667	1.600	0.625
P#33	18.15200000	67.14066667	6.200	0.161
P#34	18.15150000	67.15050000	2.850	0.351
P#35	18.16116667	67.14936667	7.100	0.141
P#36	18.16915000	67.14651667	6.350	0.157
P#37	18.17000000	67.15470000	4.700	0.213
P#38	18.17661667	67.15023333	4.600	0.217
P#39	18.17743333	67.15801667	7.000	0.143
P#40	18.18191667	67.14583333	5.100	0.196
P#41	18.18360000	67.15368333	NA	NA
P#42	18.21055000	67.14605000	NA	NA
P#43	18.21240000	67.14748333	4.550	0.220
P#44	18.20883333	67.14266667	4.600	0.217
P#45	18.20850000	67.15050000	2.100	0.476
P#46	18.21840000	67.15466667	3.900	0.256
P#47	18.21633333	67.15756667	3.200	0.313
P#48	18.21973333	67.16116667	3.775	0.265
P#49	18.22261667	67.15161667	1.950	0.513
P#50	18.22996667	67.17278333	7.700	0.130
P#51	18.22281667	67.16065000	3.250	0.308
P#52	18.22836667	67.15831667	3.300	0.303
P#53	18.22475000	67.16525000	4.100	0.244
P#54	18.25135000	67.17546667	0.950	1.053
P#55	18.25283333	67.17733333	0.950	1.053
P#56	18.26146667	67.18175000	0.700	1.429
P#57	18.26340000	67.18548333	3.000	0.333
P#58	18.26541667	67.18203333	3.000	0.333
P#59	18.26075000	67.17431667	1.250	0.800

Table CHAPTER 5.4: Summary of all ambient vibration measurements

Site	Latitude (N)	Longitude(W)	Frequency [Hz]	Period [Sec]
P#60	18.26655000	67.16108333	1.150	0.870
P#61	18.26731667	67.15858333	2.000	0.500
P#62	18.26678333	67.15408333	1.600	0.625
P#63	18.25956667	67.15930000	1.550	0.645
P#64	18.25173333	67.16028333	2.450	0.408
P#65	18.25241667	67.15260000	2.700	0.370
P#66	18.24805000	67.16501667	1.150	0.870
P#67	18.24710000	67.17030000	2.700	0.370
P#68	18.24705000	67.13735000	2.400	0.417
P#69	18.24070000	67.16428333	2.200	0.455
P#70	18.24170000	67.15610000	2.600	0.385
P#71	18.23641667	67.14330000	4.300	0.233
P#72	18.23166667	67.14155000	2.800	0.357
P#73	18.23475000	67.16075000	4.000	0.250
P#74	18.23575000	67.15616667	6.200	0.161
P#75	18.23033333	67.14958333	5.800	0.172
P#76	18.23031667	67.14958333	NA	NA
P#77	18.22933333	67.13948333	3.150	0.317
P#78	18.28300000	67.14100000	1.900	0.526
P#79	18.20000000	67.13750000	3.650	0.274
P#80	18.16720000	67.15140000	6.000	0.167
P#81	18.14130000	67.12750000	1.050	0.952
P#82	18.18540000	67.13800000	6.550	0.153
P#83	18.22215500	67.11560600	NA	NA
P#83_1	18.22210000	67.15522000	6.350	0.157
P#84	18.20516000	67.14700000	1.500	0.667
P#85	18.24080000	67.17220000	2.150	0.465
P#86	18.20950000	67.12190000	3.350	0.299
P#87	18.20580000	67.15080000	1.550	0.645
P#88	18.23980000	67.12130000	3.600	0.278
P#89	18.19870000	67.12852000	7.400	0.135
P#90	18.19483000	67.09226000	7.300	0.137

Table CHAPTER 5.4: Summary of all ambient vibration measurements

Site	Latitude (N)	Longitude(W)	Frequency [Hz]	Period [Sec]
P#91	18.18688000	67.07844000	10.750	0.093
P#92	18.18760000	67.06167000	2.950	0.339
P#93	18.19471000	67.11274000	9.650	0.104
P#94	18.20843000	67.12750000	4.050	0.247
P#95	18.20872000	67.11485000	10.700	0.093
P#96	18.21015000	67.10085000	3.050	0.328
P#97	18.20734000	67.08041000	5.750	0.174
P#98	18.20811000	67.05701000	4.250	0.235
P#99	18.21883000	67.14070000	5.100	0.196
P#100	18.23486000	67.12553000	4.300	0.233
P#101	18.23634000	67.13024000	5.700	0.175
P#102	18.24079000	67.10488000	2.350	0.426
P#103	18.18483000	67.13242500	9.400	0.106
P#104	18.17244000	67.12531000	7.550	0.132
P#105	18.16727000	67.09715000	12.900	0.078
P#106	18.24258000	67.12713000	3.400	0.294
P#107	18.22431000	67.12418000	2.650	0.377
P#108	18.22705000	67.10004000	NA	NA
P#109	18.24955000	67.09155000	2.300	0.435
P#110	18.23660000	67.09106000	2.750	0.364
P#111	18.24236000	67.07226000	2.550	0.392
P#112	18.23558000	67.07006000	3.550	0.282
P#113	18.22769000	67.08012000	4.650	0.215
P#114	18.22702000	67.05878000	3.450	0.290
P#115	18.21982000	67.08241000	3.650	0.274
P#116	18.21330000	67.06464000	3.000	0.333
P#117	18.20830000	67.03291000	3.750	0.267
P#118	18.19793000	67.02610000	3.000	0.333
P#119	18.19189000	67.00857000	6.000	0.167
P#120	18.19599000	67.03686000	NA	NA
P#121	18.18473000	67.03039000	11.900	0.084
P#122	18.17730000	67.07388000	13.000	0.077

Table CHAPTER 5.4: Summary of all ambient vibration measurements

Site	Latitude (N)	Longitude(W)	Frequency [Hz]	Period [Sec]
P#123	18.15796000	67.08582000	4.100	0.244
P#124	18.15393000	67.13653000	10.550	0.095
P#125	18.15717000	67.09921000	NA	NA
P#126	18.17952000	67.05458000	NA	NA
P#127	18.18114000	67.09874000	6.000	0.167
P#128	18.20317000	67.06709000	4.220	0.237

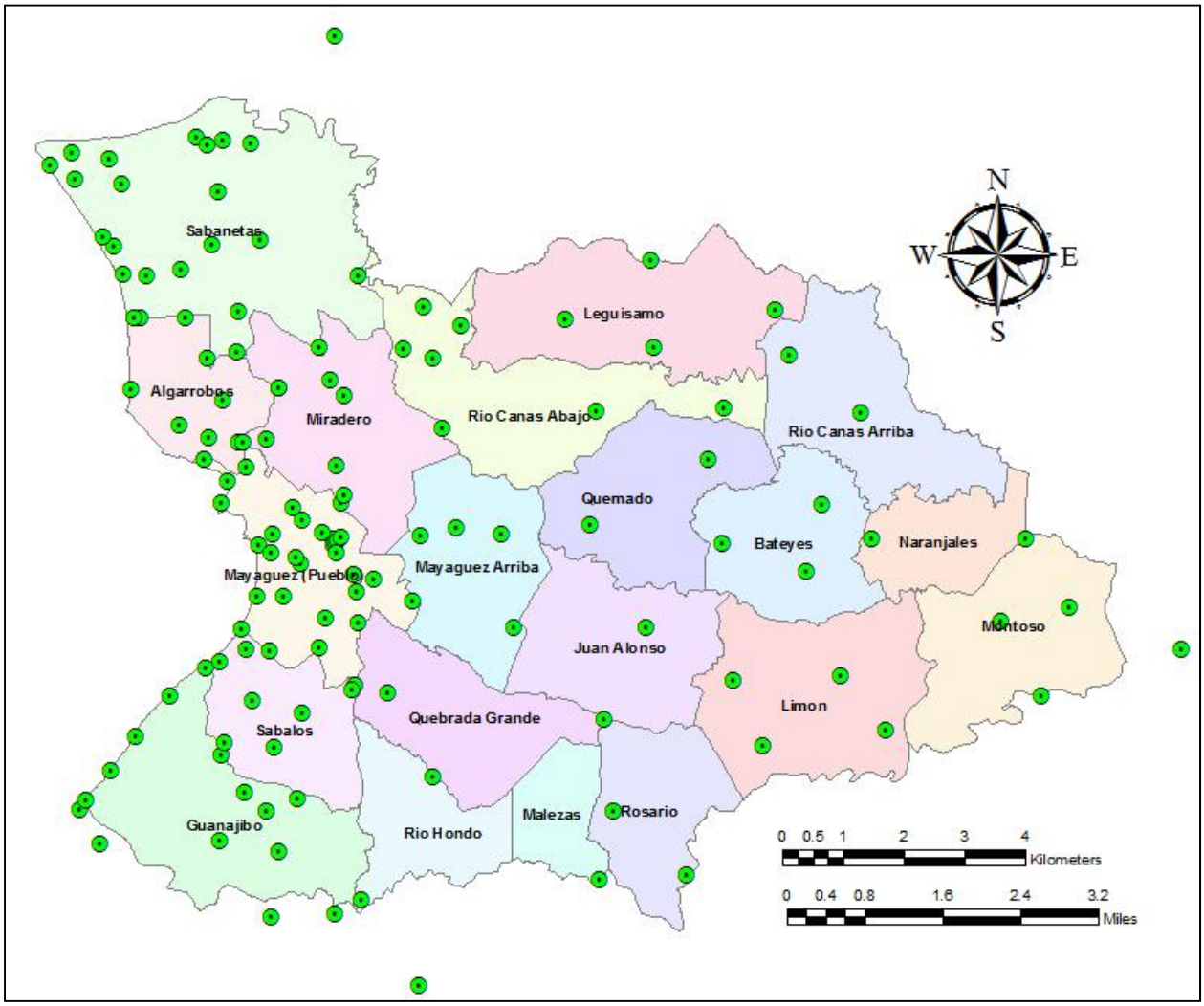

Figure CHAPTER 5.4: Location of all ambient vibration measurements sites

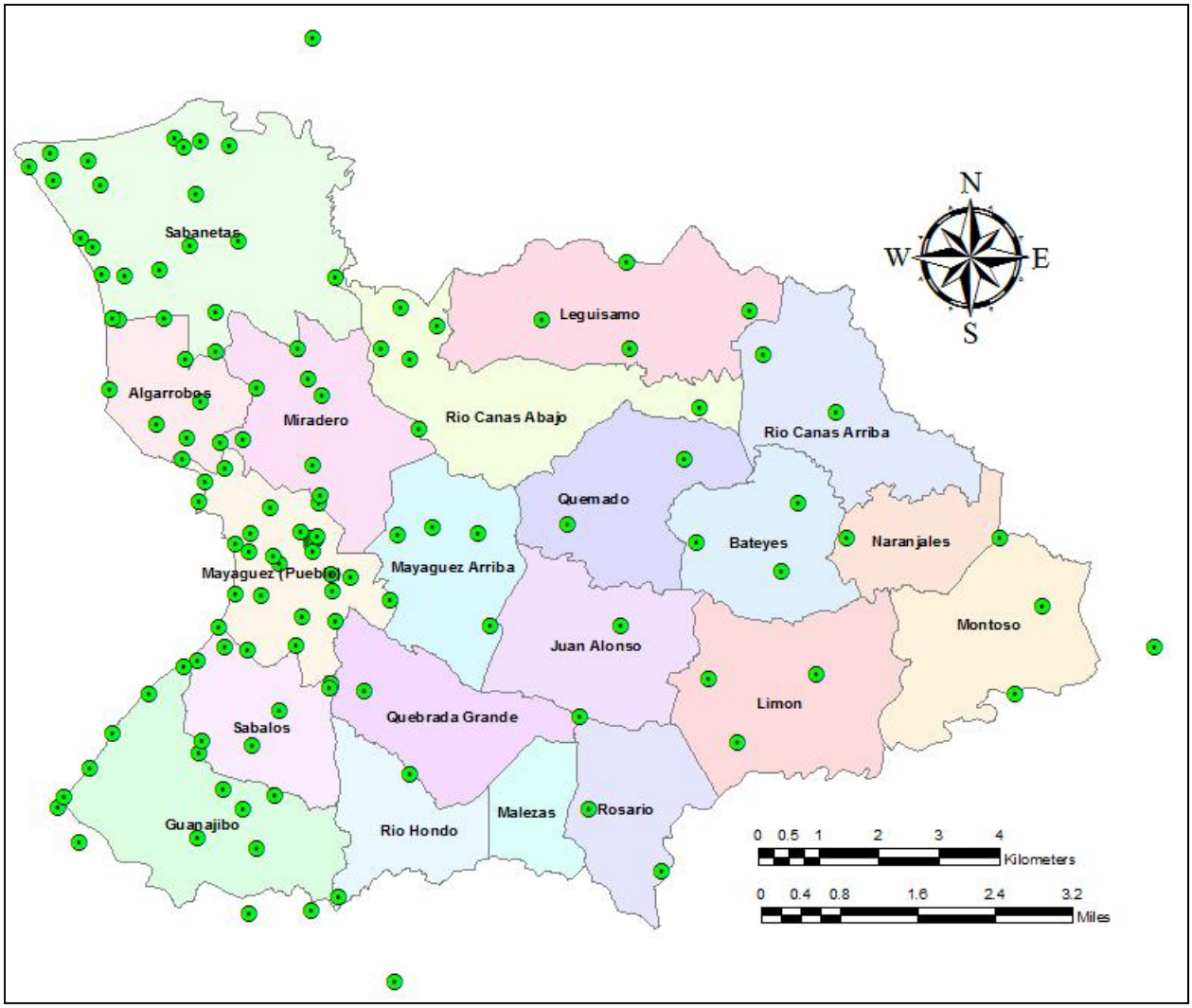

Figure CHAPTER 5.5: Sites where a reliable fundamental period was obtained

Comparing Figures 5.4 and 5.5, it is clear that it was possible to obtain the fundamental period at most of the sites. From a total of 134 measurements, 126 resulted in reliable a fundamental period which means that only 5.97% of the measurements were unsuccessful. Sites where it was not possible to obtain data are shown in figure 5.6 in case their location is needed for further research. Next section will illustrate the isoperiod maps developed for the city of Mayagüez from all these ambient vibration measurement.

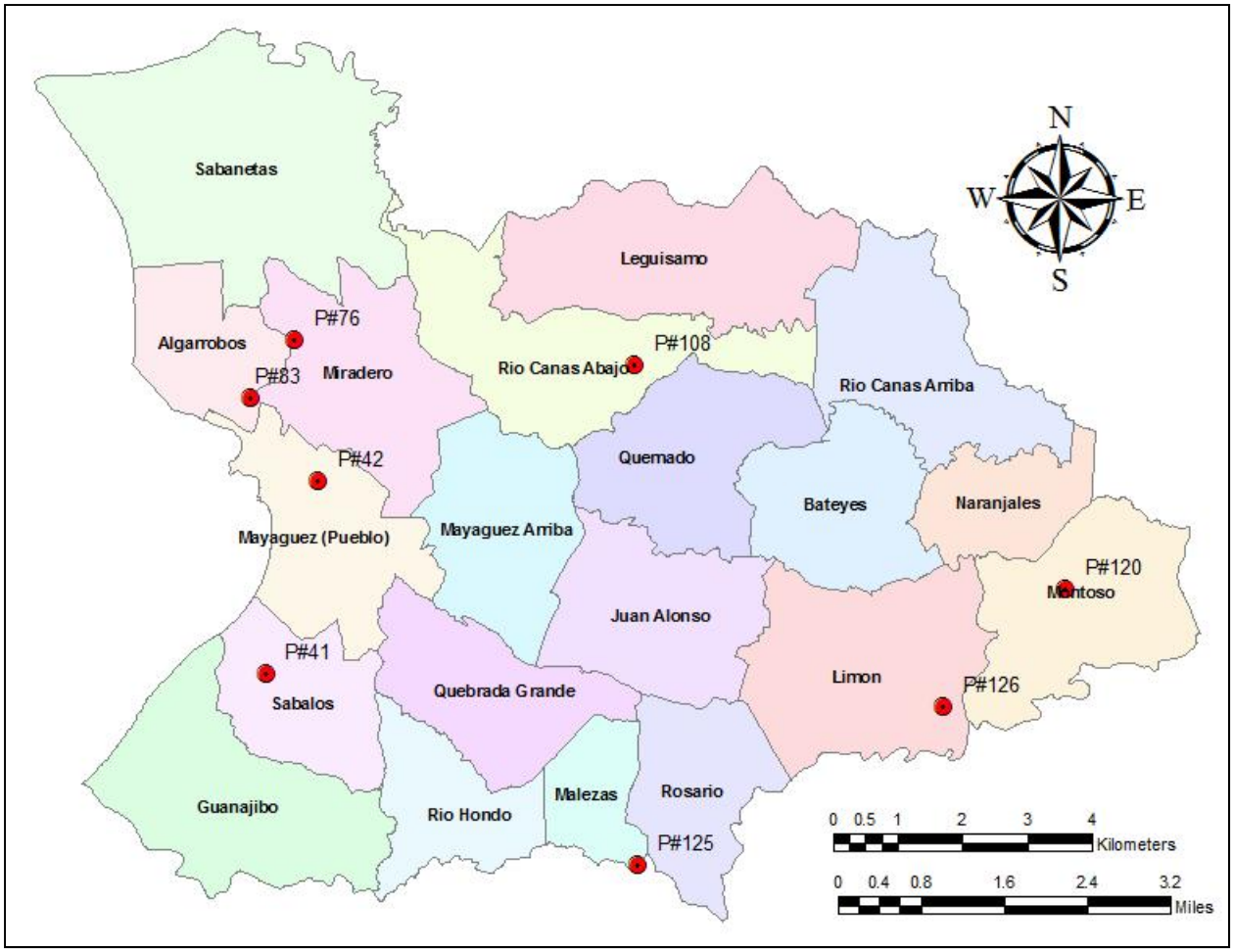

Figure CHAPTER 5.6: Location of sites where fundamental periods were not obtained

5.5 *Soil isoperiod maps for the city of Mayagüez*

From the results obtained during this research (summarized in Table 5.4) and with the aid of ESRI ® ArcMap 9.3 software (http://www.esri.com/), an isoperiod map for the City of Mayagüez was developed. The geotechnical data base compiled by Carmen Lugo (2007) in her master's thesis was used as a start point. Once the sites were located geographically on the map, it was decided to classify them according to their fundamental period within the half-open interval [0 - 0.1) seconds [0.1 - 0.2) seconds and etc. A black circle label whose size indicates the value of the fundamental period of the site was assigned to each group. Figure 5.7 shows the resulting map.

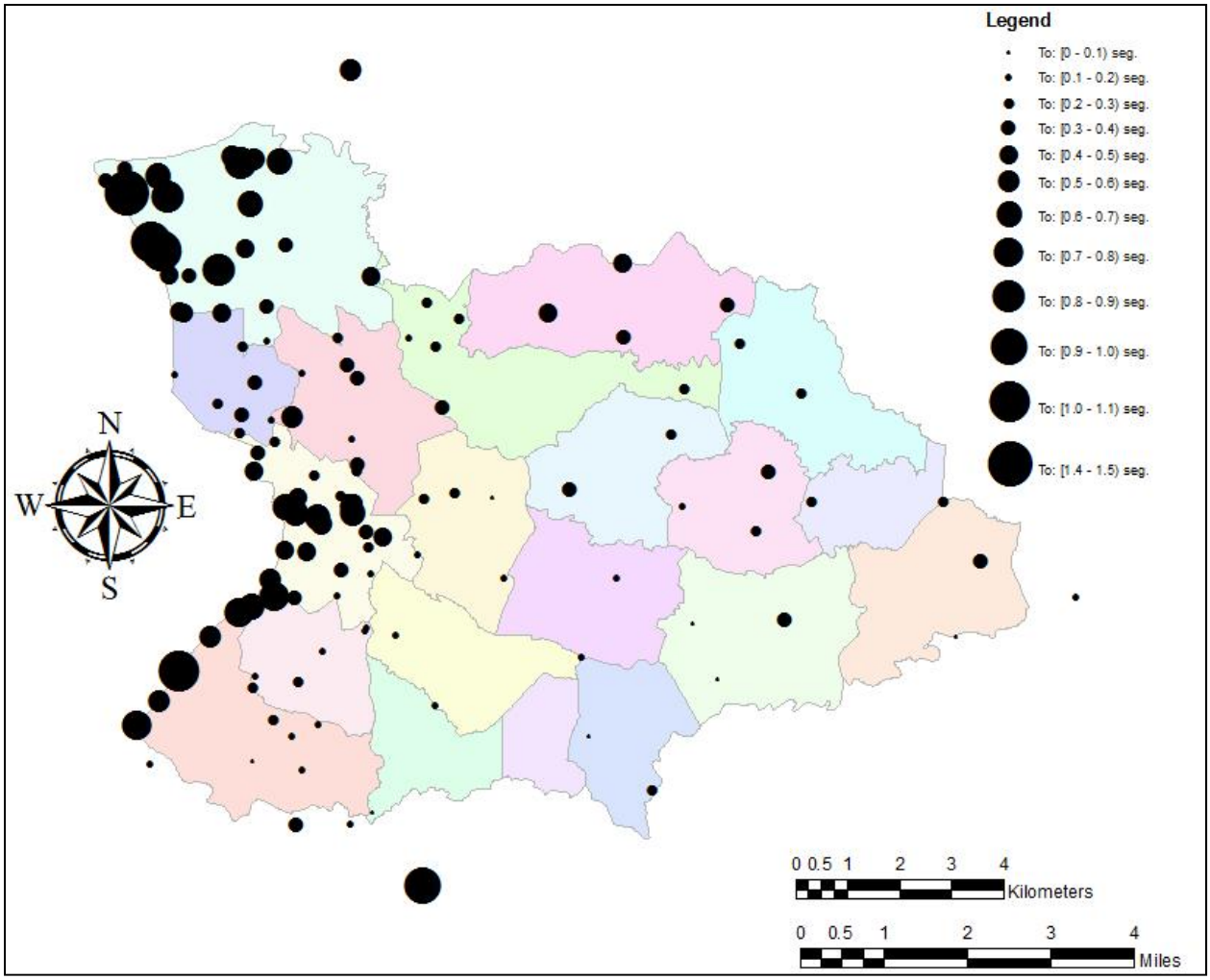

Figure CHAPTER 5.7: Site fundamental period map for the city of Mayagüez

An isoperiod map, a map of isolines where each line represents a constant value for the fundamental period of the soil, was successfully developed from the obtained data. Program ArcMap has tools for generating contour lines from a data set (the fundamental periods for this case).

The map was basically done by creating an interpolation surface for the site fundamental periods, which pass through all sites measured. This surface was generated using the "Spline Interpolation" found in the toolkit "Spatial Analyst". While there are various tools to perform the interpolation, it was decided to use the spline interpolation since it is the only one that actually goes through the known points. Figure 5.8 shows three types of interpolation available in the program ArcMap.

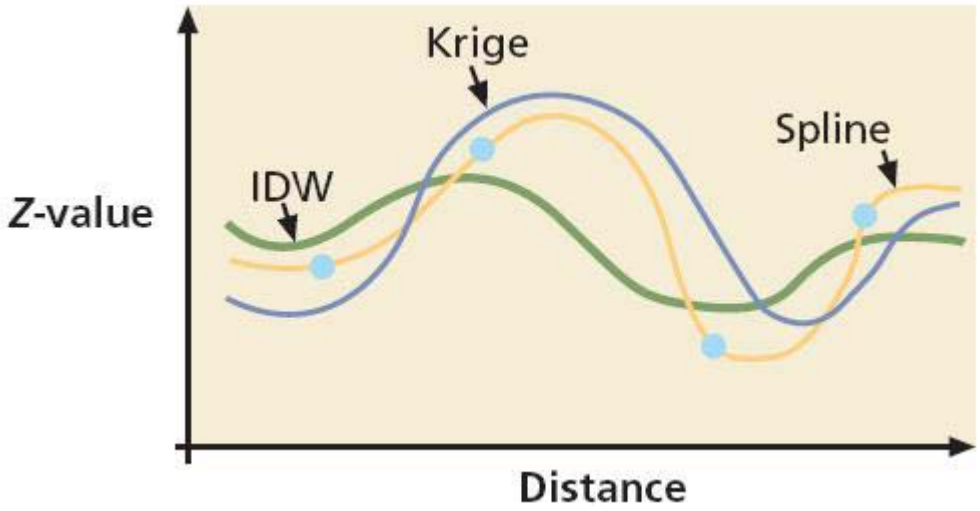

Figure CHAPTER 5.8: Interpolation types (Adapted from Colin Childs, 2004)

After performing the interpolation, the program generates regions or contours with different colors on the map. Each color represents a range of values for the interpolated fundamental period of the soil. The next step consisted on generating the isolines for the soil natural vibration period from the interpolation surface. The tool "contour", which is one of the tools for surface analysis interpolation, was used for this purpose. Figure 5.9 shows the resulting map, and the values of the ground fundamental period in seconds are illustrated on the right according to the color.

It can be observed that there is good correlation between Figures 5.7 and 5.9. Also there is an area of peak periods in the coastal region of Mayagüez (West), which is characteristic of soft deposits. The periods are shorter within the central and east area of the city where the topography is mountainous.

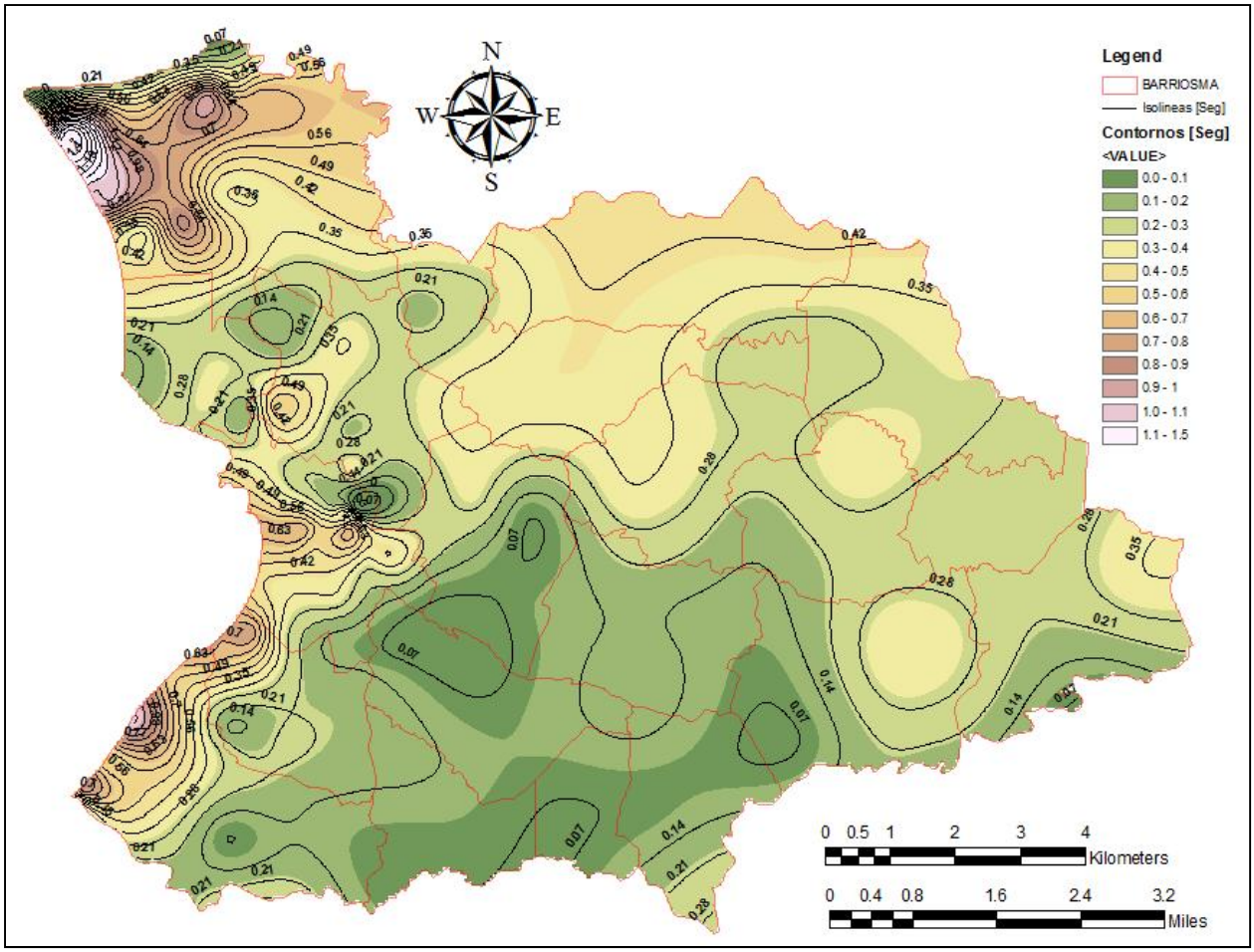

Figure CHAPTER 5.9: Isoperiod map for the city of Mayagüez

Comparing also the geological map of Mayagüez (Figure 4.4) with the isoperiod soil map (Figure 5.9) is found that there is some correlation between the fundamental periods and the geology of the various regions in the city . Figure 4.4 shows that the areas near the coastline are mostly beach sand deposits, characteristic of coastal environments (Qal). However there is an area on which this alluvial geology is invaded by the Yauco formation (Ky), which is composed mainly of volcaniclastic sandstone, limestone, siltstone, shale, claystones, limestone and subordinates conglomerate. Comparing the region that includes the Qal geology type with Figure 5.9, it is conclude that there is good correlation between both figures. The coastal area has high periods except in the region where Yauco formation invades Qal geology. Periods start to become smaller and smaller towards the east area, which was expected due to the mountainous topography.

CHAPTER 6 CONCLUSIONS AND RECOMMENDATIONS FOR FUTURE WORK

This report examined the horizontal / vertical spectral ratios (H / V) method applicability to microtemblor records or ambient vibration for determining the fundamental period of the ground. This technique was compared with other existing procedures, the influence of the instrument used to perform measurements was analyzed; and finally, constructed a soil isoperiod map for the city of Mayagüez was developed.

Comparing the different techniques for determining the fundamental period, it was concluded that the use of ambient vibration is an excellent alternative that provides very good results compared with those obtained with other techniques. Furthermore, it is clear that the use of ambient vibration is a very simple and inexpensive that can be applied at any time without waiting the occurrence of a seismic event as in other techniques. This is an important advantage, especially for those regions of low seismicity. Moreover, the spectral ratio H / V technique is stable over time which means that the fundamental period obtained does not depend on the time at which the measurement is taken.

Three types of instruments were available to take the measurements: two ETNA accelerometers (0.25g and 2 g), and one broadband seismometer. Certain sites were selected to take records with more than one instrument simultaneously. The findings suggest that while the three instruments are capable of determining the fundamental period in most places, it is preferable to use instruments with greater sensitivity in order to detect smaller variations in the measurements.

After processing the data obtained during the first set of measurement, it was found that many sites showed in addition to the fundamental frequency, high frequency peaks. Therefore, it was decided to perform a test that consisted of taking measurements in a perpendicular direction away from a line of power transmission lines. It was not possible to clarify from the data analysis

whether power lines have an influence on the instrument or not. However, because no other cause found to explain these peaks, it is likely that the power transmission lines affect the measurements.

Finally, after processing all ambient vibration measurements, a soil isoperiod map for the city of Mayagüez was developed. This map allows knowing the dynamic behavior of soil presented in Mayagüez through its fundamental period of vibration. This parameter is very useful for earthquake-resistant design of new structures. The map can also function as a guide to reduce the seismic risk from possible future earthquakes.

As future work, it is suggested to take new measurements at the eight sites where it was not possible to determine the fundamental period, but using more sensitive instrumentation, perform a theoretical study of the phenomenon which determines the fundamental period of the ground and the possibility of the amplification factor, since there is no consensus among authors on these issues.

REFERENCES

Alfaro, A. (2006). "Caracterización dinámica de suelos mediante microtemblores HVSR y arreglos," Universidad de La Salle, ISBN: 978-958-9290-73-6.

Asencio, E. (1980). "Western Puerto Rico Seismicity," USGS Open File Report 80-192.

Borcherdt, R. D. (1970). "Effect of the local geology on ground motion near San Francisco Bay," Bulletin of the Seismological Society of America, Vol. 60, pp. 29-61.

Borcherdt, R. D., Borcherdt, R. D., Wentworth, C. M., Janssen, A., Fumal, T. and Gibbs, J. (1991). "Methodology for predictive GIS mapping of special study zones for strong ground shaking in the San Francisco Bay Region," Proceedings of the 4th International Conference on Seismic Zonation, Vol. 3, pp. 545–552.

BSSC (2001). "NEHRP Recommended Provisions for Seismic Regulations for New Buildings and Other Structures," ***FEMA-368***, Federal Emergency Management Agency, Washington, D.C.

Capacete, J. L. and Herrera, A. (1972). "The 1918 earthquake: an engineering study," CIAA (Colegio de Ingenieros, Arquitectos y Agrimensores), Vol. 22, No. 1, Puerto Rico.

Chatelain, J.-L., Guillier, B., Cara, F., Duval, A.-M., Atakan, K., Bard, P.-Y., The WP02 SESAME team (2008). "Evaluation of the influence of experimental conditions on H/V results from ambient noise recordings," Bulletin of Earthquake Engineering, No. 6, pp. 33-74.

Clinton, J. F., Cua, G., Huérfano, C. V., von Hillerbrandt-Andrade, C. G., and Martínez-Cruzado, J. (2006). "The current state of seismic monitoring in Puerto Rico," Seismological Research Letters, Vol. 77, No. 5, 12 p.

Colin Childs (2004). "Interpolating Surfaces in ArcGIS Spatial Analyst," ESRI Education Services, ArcUser, July-September 2004, pp. 32-35, www.esri.com.

Colón-Dieppa, E. and Quiñonez-Martínez, F. (1985). "A Reconnaissance of the Water Resources of the Central Guanajibo Valley, Puerto Rico," USGS Water Resources Investigations Report 82-4050, 47 p.

Curet, A. F. (1986). "Geologic Map of the Mayagüez and Rosario Quadrangles, Puerto Rico," Map I-1657, US Geological Survey.

Guillier, B., Atakan, K., Chatelain, J.-L., Havskov, J., Ohrnberger, M., Cara, F., Duval, A.-M., Zacharopoulos, S., and Teves-Costa, P., The SESAME team (2008). "Influence of instruments on the H/V spectral ratios of ambient vibrations," Bulletin of Earthquake Engineering, No. 6, pp. 3-31.

Haghshenas, E., Bard, P.-Y. and Theodulidis, N. (2008). "Empirical evaluation of microtremor H/V spectral ratio," Bulletin of Earthquake Engineering, No. 6, pp. 75-108.

ICBO (1997). "Uniform Building Code, 1997 Edition," International Conference of Building Code Officials, Whittier, California, Vol. 2, Chap. 16, Div. IV.

Kagami, H., Duke, C. M., Liang, G. C. and Ohta, Y. (1982). "Observation of 1 to 5 second microtremors and their application to earthquake engineering. Part II. Evaluation of site effect upon seismic wave amplification due to extremely deep soil deposits," Bulletin of the Earthquake Research Institute, Vol. 72, pp. 987-998.

Kanai, K. and Tanaka, T. (1961). "On microtremors. VIII," Bulletin of the Earthquake Research Institute, Vol. 39, pp. 97-114.

Lachet, C. and Bard, P. Y. (1995). "Theoretical investigations on the Nakamura's technique," Proceedings of the Third International Conference on Recent Advances in Geotechnical Earthquake Engineering and Soil Dynamics, April 2-7, St. Louis, Missouri, Vol. II.

Lermo, J. and Chávez-García, F. J. (1994). "Are microtremors useful in site response evaluation?," Bulletin of the Seismological Society of America, Vol. 84, No. 5, pp. 1350-1364.

Llavona, A. (2004). "Clasificación de Suelos (UBC-97) del Municipio de Mayagüez," Master of Engineering thesis, Civil Engineering & Surveying Department, University of Puerto Rico at Mayagüez.

Lugo, C.Y. (2007). "Development of a Geotechnical Database for the City of Mayagüez, Puerto Rico," Master of Engineering thesis, Civil Engineering & Surveying Department, University of Puerto Rico at Mayagüez.

McCann, W.R. (1987). "Historic earthquakes and the earthquake hazard of Puerto Rico," Proceedings of Conference XXXVI, A Workshop on Assessment of Geologic Hazard and Risk in Puerto Rico, May 14-16, 1986, U.S. Department of the Interior Geological Survey, Open File Report 87-008.

McCann, W.R. (1993). "Seismic Hazard Map for Puerto Rico," Report to the Seismic Safety Commission of Puerto Rico.

Mercado, A. and McCann, W. R. (1998). "Numerical simulation of the 1918 Puerto Rico tsunami," Natural Hazards, No. 18, pp. 57-76.

Moya, J. C. and McCann, W. R. (1992). "Earthquake Vulnerability of the Mayagüez Area, Western Puerto Rico," presented at "Comisión de Seguridad Contra Terremotos", 43 p..

Nakamura, Y. (1989). "A method for dynamic characteristics estimation of subsurface using microtremors on the ground surface," Quaterly Report of Railway Technical Research Institute, Vol. 30, No. 1, pp. 25-33.

Nakamura, Y. (2000). "Clear identification of fundamental idea of Nakamura's technique and its applications," Proceedings of the 12th World Conference on Earthquake Engineering, Auckland, New Zealand, paper 2656.

Nakamura, Y. (2008). "On the H/V Spectrum," Proceedings of the 14th World Conference on Earthquake Engineering, Beijing, China.

Nogoshi, M. and Igarashi, T. (1970). "On the propagation characteristics of microtremor," Journal of Seismic Society of Japan, No. 23, pp. 264-280.

Nogoshi, M. and Igarashi, T. (1971). "On the amplitude characteristics of microtremor (Part 2)," Journal of Seismic Society of Japan, No. 24, pp. 26-40.

Ohsaki, Y. (1972). "Japanese microzonation methods," Bulletin of the Earthquake Research Institute, Vol. 49, pp. 161-182.

Ordoñez, G.A. (2004). "SHAKE2000 a Computer Program for the 1D Analysis of Geotechnical Earthquake Engineering Problems." User's Manual, 306 pp.

Pacheco, J. F., and Sykes, L. R. (1992). "Seismic Moment Catalog of Large Earthquakes, 1900 to 1989," Bulleting of the Seismological Society of America, No. 82, pp. 1306-1349.

Pando, M.A., Cano, L., Suarez, L.E., Montejo, L., and *Ritta, R. (2008). "Comparison of Site Fundamental Period Estimates Using Weak-Motion Earthquakes", 14th World Conference on Earthquake Engineering, 12 to 17 October 2008, Beijing, China, Paper No. 02-0142, 10 p.

Pando, M., Suárez, L., Martínez-Cruzado, J., Lugo, C., Llavona, A., Pérez, E., Varela, W., and Asencio, E. (2006), "Ground Motions Evaluation and Geotechnical Database for the City of Mayagüez, Puerto Rico," USGS NEHRP Report 04HQGR0075, Available online at http://earthquake.usgs.gov/research/ , 121 p..

Panou, A. A., Theodulidis, N. P., Hatzidimitriou, P. M., Savvaidis, A. S., and Papazachos, C. B. (2005). "Reliability of ambient noise horizontal-to-vertical spectral ratio in urban environments: the case of Thessaloniki City (Northern Greece)," Pure and Applied Geophysics, Vol. 162, No. 5, pp. 891-912.

Panou, A. A., Theodulidis, N., Hatzidimitriou, P., Stylianidis, K., and Papazachos, C. B. (2005). "Ambient noise horizontal-to-vertical spectral ratio in site effects estimation and correlation with seismic damage distribution in urban environment: the case of the city of Thessaloniki (Northern Greece)," Soil Dynamics and Earthquake Engineering, Vol. 25, No. 4, pp. 261-274.

Pérez, E. (2005). "Ground response spectra at surface for Mayagüez considering in-situ Soil Dinamic Properties," Master of Science Thesis, Civil Engineering & Surveying Department, University of Puerto Rico at Mayagüez.

Prentice, C.S., Mann, P., and Burr, G. (2000). "Prehistoric Earthquakes Associated with a Late Quaternary Fault in the Lajas Valley, Southwestern Puerto Rico," Transactions of the American Geophysical Union 81, F 1182 (abstract).

Prentice, C.S., and Mann, P. (2005). "Paleoseismic Study of the South Lajas Fault: First Documentation of an Onshore Holocene Fault in Puerto Rico," Active Tectonics and Seismic

Hazards of Puerto Rico, the Virgin Island, and Offshore Areas, Geological Society of America, Special Paper 385, pp. 215-222.

Reid, H. F., and Taber, S. (1919). "The Porto Rico earthquakes of October – November, 1918," Bulletin of the Seismological Society of America, Vol. IX, p.p. 95-127.

Rodríguez, C.E., and Capacete, J.L. (1988). "Liquefaction potential in Puerto Rico," Revista Dimensión, Año 2, Vol. 8.

Rodríguez-Martínez, J., Santiago-Rivera, L., Guzmán-Ríos, S., Gómez-Gómez, F., and Oliveras-Feliciano, M.L. (2004). "Surface-Water, Water-Quality, and Ground-Water Assessment of the Municipio of Mayagüez, Puerto Rico, 1999-2002," USGS Water Resources Investigations Report 03-4317.

SESAME (2004). "Guidelines for the implementation of the H/V Spectral Ratio Technique on Ambient Vibrations," Research Report WP12, available online at: http://sesame-fp5.obs.ujf-grenoble.fr/index.htm.

Shimizu, P. and Suehiro, S. (1947). "Report of Survey in Nakamura Town, Interim Report on Nankaido Earthquake, Central Meteorological Observatory".

Sokolov, V. Y., Loh, C-H., and Jean, W-Y. (2007). "Application of horizontal-to-vertical (H/V) Fourier spectral ratio for analysis of site effect on rock (NEHRP-class B) sites in Taiwan," Soil Dynamics and Earthquake Engineering, Vol. 27, No. 4, pp. 314-323.

Sykes, L., McCann, W.R., and Kafka, A., 1982. "Motion of Caribbean Plate during last seven million years and implications for earlier Cenozoic movements," Journal of Geophysics Research, Vol. 87, pp. 10656-10676.

Theodulidis, N., Cultrera, G., De Rubeis, V., Cara, F., Panou, A., Pagani, M., Teves-Costa, P. (2008). "Correlation between damage distribution and ambient noise H/V spectral ratio: the SESAME Project results," Bulletin of Earthquake Engineering, No. 6, pp. 109-140.

US Census Bureau, Census 2000 Summary File 1, July 2000. http://www.census.gov/population/estimates/puerto-rico.prmunnet.txt

Yokoi, T., Kuwabara, T., and Horiuchi, T. (1965). "Studies of soil conditions and earthquakes damage in Nagoya, Part 2," Proceedings of the Architectural Institute of Japan.

APPENDIX A

Protocol followed for taking measurements

Required Equipment:

ETNA accelerometer.

Steel plate (17’’ length t by 12’’ width).

Compass.

GPS.

Digital thermometer.

Camera.

Communication cable between the computer and the instrument (R232).

Shovel to remove grass and level the ground.

Computer with required programs installed

#3 bar to identify the exact site after measurement.

Red Aerosol to paint # 3 bar.

Notebook to make annotations.

Steel plate to improve soil-instrument contact:

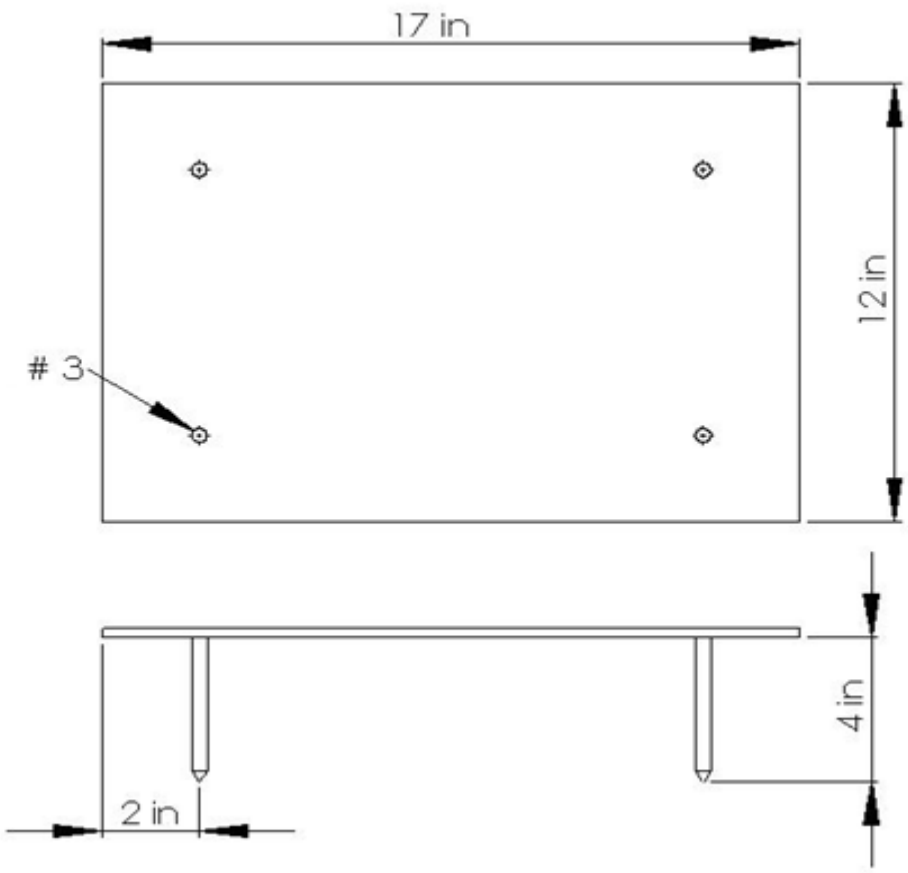

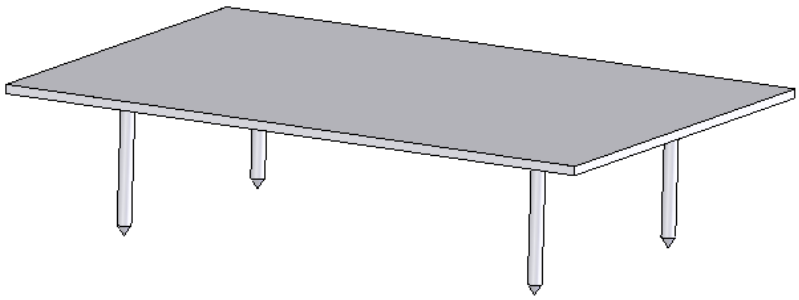

Procedure:

- Once the site is chosen, the best spot to place the instrument should be located. It is recommended to choose a place without grass and away from pavement and buildings.
- Get the geographic coordinates using the GPS. Temperature is also recorded.
- In case of grass presence, this should be removed so that the equipment is totally over the ground .
- Place the steel plate over the ground and orient it using the compass toward the magnetic north. Consider the deviation between magnetic north (indicated by the compass) and the actual indicated by the compass (about 11 degrees to the area of Puerto Rico). This will be useful when processing data.
- Place ETNA accelerometer over the steel plate.
- Carefully remove the ETNA lid and level it using the level indicator located in its interior. For this, use the screws that are at the bottom.
- Check that the orientation has not changed
- Place ETNA lid carefully.
- Turn on and connect the computer to ETNA using R232 cable.
- Open Kinemetrics-QuickTalk program to establish communication with ETNA.
- Select Port “COM 1” and press OK.
- Once the communication is established, the screen can be amplified by first pressing the central button which is located in the upper right and then clicking on "window"→ “Tile”.
- Press “Set Time” → “PC Time”. Which gives the equipment the computer time?

- Proceed to program the equipment. Press “recorder” and then “Acquisition Control”.
- Press “Stop Acquisition”.
- Press “Edit Parameters”. A window where all icons are off except those located to the left will be displayed. Press “From Recorder so that all icons are turned on.
- Press “Stream Parameters”. Make sure “Pre-event Time” and “Post-event Time” have unit values. “Sampling Rate” must be 100.
- Press “To Recorder” and then “Close”.
- Remove all local materials and tools in order make clear the area.
- Press “Start Acquisition” and then “Keyboard trigger” for equipment initialization. At this point the program will indicate the file name, which must be written down with the time when measurement starts.
- Once the recording time is finished, press “Keyboard Detrigger” to stop recording and after 5 to 10 minutes press “Stop Acquisition” to stop data acquisition collection.
- Turn off the equipment, disconnect the battery, remove the equipment, mark the site and collect all material and equipment to continue with the next site.

APPENDIX B

Matlab programs

Program for ambient vibration data analysis

```
%Program HVSRAV.m
% Objective 1: To file convertion from ETNA EVT file into MatLab or ASCII
% Objective 2: To obtain the site frequency to a soil using Microtremors
%              The processing method is the Nakamura's Spectral Ratios
%Varlist:
% Input:
% archi=  File Name of ETNA archive, (*.EVT)

% Program by: Raul J. Ritta - Puerto Rico Strong Motion Program
% Last Update: July 08 - 2009

clc
close all
clear all

%% Input data:
             % File Name
             % ETNA file (*.EVT without extension)

archi = input('==> ETNA file name (without extension): ','s');

% Instrument Information:
% Kinemetrics ETNA
% Channel 1: (Sensor x - EW Direction)
%           Episensor 31634
%           Sensitivity: 1.248
%           Natural Frequency: 210 Hz
%           Damping:    0.7
% Channel 2: (Sensor y - NS Direction )
%           Episensor 31635
%           Sensitivity: 1.248
%           Natural Frequency: 198 Hz
%           Damping:    0.7
% Channel 3: Sensor (z - Vertical Direction)
%           Episensor 31649
%           Sensitivity: 1.250
%           Natural Frequency: 198 Hz
%           Damping:    0.7

% Accelerograph Constants
% s1=1.248;          Full Scale Volts to Sensor 1 Default (1.248)
% s2=1.248;          Full Scale Volts to Sensor 1 Default (1.248)
% s3=1.248;          Full Scale Volts to Sensor 1 Default (1.248)

%% Preliminars
% Convert the *.EVT file to a three vectors Matlab structure
archi1=strcat(archi,'.EVT');
```

```
co=['kw2asc.exe ' archi1];
dos(co);  % Convert to ASCII the EVT file using kw2asc
xname=strcat(archi,'.001');
yname=strcat(archi,'.002');
zname=strcat(archi,'.003');
SHDname=strcat(archi,'.SHD');

['Loading the Uncorrected Acceleration Channels....Please Wait...']

xrec=load (xname);                % load the Uncorrected Channel x in Volts
yrec=load (yname);                % load the Uncorrected Channel y in Volts
zrec=load (zname);                % load the Uncorrected Channel z in Volts
%=========================================================================

% cut of archives to introduce them in J-SESAME program
x = xrec(1:end);
y = yrec(1:end);
z = zrec(1:end);
%=========================================================================

SHD=char(textread(SHDname, '%s', 'whitespace', '')); % Read the header file

['Searching to Sampling Ratio']
%Searching to Sampling ratio
for i=1:length(SHD)
    if (SHD(i)=='S')
        if (SHD(i+1)=='a')& (SHD(i+2)=='m')
            sr=str2num(strcat(SHD(i+14:i+17)));  % Sampling Ratio Found !
            dt=1/sr;                             % Samplig steep
            i=length(SHD);
            ['Sampling Ratio Founded']
        end;
    end;
end;
%=========================================================================
%% Ploting uncorrected accelerations time histories

np = length(x);                                  % new number of data points
tf = (np-1)*dt;                                  % final time of accelerogram
t = 0:dt:tf;                                     % row vector with time steps
t = t';                                          % column vector with time steps

figure; subplot(3,1,1),plot(t,y,'r'); grid on;
axis tight; title(['Uncorrected acceleration [Volts] time histories for ',archi1]);
ylabel('North-South');

subplot(3,1,2); plot(t,x,'r'); grid on;
axis tight; ylabel('East-West');

subplot(3,1,3); plot(t,z,'r'); grid on;
axis tight; xlabel('Time [s]'); ylabel('Vertical');
%=========================================================================

%% Baseline correction of complete files

['Executing Baseline Correction']

ns=length(x)/2^10;
g = 981;             % Acceleration of the gravity [cm/seg^2]
sens = 10;           % Sensitivity (Volts/g)--> [Instr. 0.25 g's]
cte = g/sens;        % Constant for convertion from Volts --> cm/seg^2
```

```
if (length(x)>2^10)
    for i=1:3
        if(i==1) x2=x;
            elseif (i==2)
                   x2=y;
            else x2=z;
        end;
        for j=1:floor(ns)
            x2(2^10*(j-1)+1:2^10*j)=detrend(x2(2^10*(j-1)+1:2^10*j));
        end;
        x2(2^10*j+1:length(x2))=detrend(x2(2^10*j+1:length(x2)));
        if(i==1) xcorr=x2*cte;
            elseif (i==2)
                    ycorr=x2*cte;
            else zcorr=x2*cte;
        end;
    end;
else
    xcorr=detrend(x)*cte;
    ycorr=detrend(y)*cte;
    zcorr=detrend(z)*cte;
end;

x = xcorr;
y = ycorr;
z = zcorr;
%==========================================================================

%% Ploting corrected accelerations time histories

figure; subplot(3,1,1),plot(t,y,'g'); grid on;
axis tight; title(['Corrected acceleration [cm/seg^2] time histories for ',archi1]);
ylabel('North-South'); axis([0 max(t) min(y) max(y)])

subplot(3,1,2); plot(t,x,'g'); grid on;
axis tight; ylabel('East-West'); axis([0 max(t) min(x) max(x)])

subplot(3,1,3); plot(t,z,'g'); grid on;
axis tight; xlabel('Time [s]'); ylabel('Vertical'); axis([0 max(t) min(z) max(z)])
%==========================================================================

%% Window Selection Module

% Input:
%        1- Window length for selected window in seconds.
%        2- Overlap percentage for selected window.
%        3- Window length for the short term average (sta) in seconds (0.5-2 sec.).
%        4- Window length for the long term average (lta) in seconds (several tens of sec.).
%        5- Minimum level for sta/lta threshold.
%        6- Maximum level for sta/lta threshold (1.5-2).

twl = input('Windows Length (sec.): ');
ow = input('Overlap Windows (% Window Length):');
tsta = input('Window length for the short term average (sta) in seconds (0.5-2 sec.):');
tlta = input('Window length for the long term average (lta) in seconds (several tens of
sec.):');
smin = input('Minimum level for sta/lta threshold:');
smax = input('Maximum level for sta/lta threshold:');

NPwl = sr*twl;
```

```
NPow = (ow/100)*NPwl;
NPsta = sr*tsta;
NPlta = sr*tlta;

Nwsta = floor(length(x)/NPsta);

for w = 1:Nwsta

    stax = mean(abs(x((w-1)*NPsta+1:w*NPsta)));
    stay = mean(abs(y((w-1)*NPsta+1:w*NPsta)));
    staz = mean(abs(z((w-1)*NPsta+1:w*NPsta)));

    if (w-1)*NPsta+NPlta <= length(x)
        ltax = mean(abs(x((w-1)*NPsta+1:(w-1)*NPsta+NPlta)));
        ltay = mean(abs(y((w-1)*NPsta+1:(w-1)*NPsta+NPlta)));
        ltaz = mean(abs(z((w-1)*NPsta+1:(w-1)*NPsta+NPlta)));
    else
        ltax = mean(abs(x(w*NPsta-NPlta+1:w*NPsta)));
        ltay = mean(abs(y(w*NPsta-NPlta+1:w*NPsta)));
        ltaz = mean(abs(z(w*NPsta-NPlta+1:w*NPsta)));
    end
    if stax/ltax > smin && stax/ltax < smax && stay/ltay > smin &&...
            stay/ltay < smax && staz/ltaz > smin && staz/ltaz < smax
        R(w) = 1;
    else
        R(w) = 0;
    end
end

i = 1;
j = 0;
while i <= length(R)-(NPwl/NPsta)
    suma = sum(R(i:i+((NPwl/NPsta)-1)));
    if suma == NPwl/NPsta
        j = j+1;
        if i == 1
            xm(:,j) = x(1:((i+((NPwl/NPsta)-1))*NPsta));
            ym(:,j) = y(1:((i+((NPwl/NPsta)-1))*NPsta));
            zm(:,j) = z(1:((i+((NPwl/NPsta)-1))*NPsta));
            i = i+NPwl/NPsta;
            in = i;
        else
            if j == 1
                xm(:,j) = x((i-1)*NPsta+1:((i+((NPwl/NPsta)-1))*NPsta));
                ym(:,j) = y((i-1)*NPsta+1:((i+((NPwl/NPsta)-1))*NPsta));
                zm(:,j) = z((i-1)*NPsta+1:((i+((NPwl/NPsta)-1))*NPsta));
                i = i+NPwl/NPsta;
                in = i;
            else
                if in == i
                    xm(:,j) = x((i-NPow/NPsta-1)*NPsta+1:(i-NPow/NPsta-1+NPwl/NPsta)*NPsta);
                    ym(:,j) = y((i-NPow/NPsta-1)*NPsta+1:(i-NPow/NPsta-1+NPwl/NPsta)*NPsta);
                    zm(:,j) = z((i-NPow/NPsta-1)*NPsta+1:(i-NPow/NPsta-1+NPwl/NPsta)*NPsta);
                    i = i-NPow/NPsta+NPwl/NPsta;
                    in = i;
                else
                    xm(:,j) = x((i-1)*NPsta+1:((i+((NPwl/NPsta)-1))*NPsta));
                    ym(:,j) = y((i-1)*NPsta+1:((i+((NPwl/NPsta)-1))*NPsta));
                    zm(:,j) = z((i-1)*NPsta+1:((i+((NPwl/NPsta)-1))*NPsta));
                    i = i+NPwl/NPsta;
                    in = i;
```

```
                end
            end
        end
    else
        i = i+1;
    end
end

SS = input('Do you want avoid signal saturation?(yes/no): ','s');
SS = strcmp('yes',SS);

if SS == 1
    acmax = max([max(abs(x)) max(abs(y)) max(abs(z))]);
    for c = 1:size(xm,2)
        if max(abs(xm(:,c))) <= 0.995*acmax && max(abs(ym(:,c))) <= 0.995*acmax &&...
                max(abs(zm(:,c))) <= 0.995*acmax
            xmn(:,c) = xm(:,c);
            ymn(:,c) = ym(:,c);
            zmn(:,c) = zm(:,c);
            ce(c) = 0;
        else
            ce(c) = c;
        end
    end
    for c = 1:length(ce)
        if ce(c) ~= 0
            xmn(:,ce(c)) = [];
            ymn(:,ce(c)) = [];
            zmn(:,ce(c)) = [];
        else
        end
    end
    x=xmn;
    y=ymn;
    z=zmn;
else
    x = xm;
    y = ym;
    z = zm;
end


archiout=strcat(archi,'.mat');
save (archiout,'x','y','z','dt');
%-------------------------------------------------------------------------

archiout1 = strcat(archi,'corr.002');
save(archiout1, '-ascii', 'ycorr')
archiout2 = strcat(archi,'corr.001');
save(archiout2, '-ascii', 'xcorr')
archiout3 = strcat(archi,'corr.003');
save(archiout3, '-ascii', 'zcorr')
%-------------------------------------------------------------------------

['The Extraction Procedure has been finished sucesfully']
['Number of data recorded: ' num2str(length(xrec))]
['Sampling rate: ' num2str(sr)]
['Record Duration (sec): ' num2str(length(xrec)*dt)]
['One file has been created: ' archiout]
%=========================================================================
```

```
archi1=archi;
x0=x;
y0=y;
z0=z;

nit= input('==> Number of iteration for smoothing process (<5): ');

['Processing the Nakamuras Spectral Ratios.....Please Wait...']
%% FFT for each window (including overlaping)

NP = twl*sr;
nw=size(x0,2);
Np=NP;
w=hann(NP);

for i=1:3
    if(i==1) x2=x0;
        elseif (i==2)
                x2=y0;
        else x2=z0;
    end;
    for j=1:nw
      X2(:,j)=abs(fft(detrend(x2(:,j).*w)));
%==========================================================================

%% FFT Smooth  (Thanks to Dr. L. Suarez)
        Xg=zeros(NP,1);
        Xg(:,1) = X2(:,j);
        for k = 1 : nit
            Sw(1) = Xg(1);
            Sw(2) = ( Xg(1)+Xg(2)+Xg(3) )/3;
            Sw(Np-1) = ( Xg(Np-2)+Xg(Np-1)+Xg(Np) )/3;
            Sw(Np) = Xg(Np);
            Sw(3:Np-2)= ( Xg(1:Np-4)+Xg(2:Np-3)+ Xg(3:Np-2)+Xg(4:Np-1)+Xg(5:Np) )/5;
            Xg= Sw;
        end;
        if (nit>=1)
            X2(:,j)=Sw;
        end;
    end;
    if(i==1) X0=X2;
      elseif (i==2)
        Y0=X2;
      else Z0=X2;
    end;
end;
%=========================================================================

%% Evaluation of Nakamura's spectra (HVR)

f=0:(1/dt)/length(X0):(1/dt)-(1/dt)/length(X0);
Xm = mean(X0,2);
Ym = mean(Y0,2);
Zm = mean(Z0,2);
HVX=mean(X0(2:length(X0),:)./Z0(2:length(Z0),:),2);
HVY=mean(Y0(2:length(Y0),:)./Z0(2:length(Z0),:),2);

%% H/V spetral ratio of the merged horizontal components

M = input('==> How merge the horizontal components? (Arithmetic: A, Cuadratic: C):','s');
M = strcmp('A',M);
```

```
if M == 1
    Hm = 0.5*(Xm+Ym);
    HVm = Hm(2:length(Hm))./(Zm(2:length(Zm)));
else
    Hm = 0.5*(Xm.^2 + Ym.^2);
    HVm = (Hm(2:length(Hm))./(Zm(2:length(Zm))).^2).^0.5;
end

%% Ploting the obtained results

figure;
plot(f(2:length(f)),HVX,'k','LineWidth',2);
legend(': Mean HVSR East-West')
hold on
plot(f(2:length(f)),X0(2:length(X0),:)./Z0(2:length(Z0),:),':');
plot(f(2:length(f)),HVX,'k','LineWidth',2);
hold off
grid off;
axis ([0 (0.5/dt) 0 25]); title(['Horizontal to Vertical Ratio for ',archi1])
xlabel('Frequency (Hz)'); ylabel('HVSR')

figure;
plot(f(2:length(f)),HVY,'k','LineWidth',2);
legend(': Mean HVSR North-South')
hold on
plot(f(2:length(f)),Y0(2:length(Y0),:)./Z0(2:length(Z0),:),':');
plot(f(2:length(f)),HVY,'k','LineWidth',2);
hold off
grid off;
axis ([0 (0.5/dt) 0 25]); title(['Horizontal to Vertical Ratio for ',archi1])
xlabel('Frequency (Hz)'); ylabel('HVSR')

figure;
plot(f(2:length(f)),HVX,'--k',f(2:length(f)),HVY,'-k');
legend(': Mean HVSR East-West',': Mean HVSR North-South')
grid off;
axis ([0 (0.5/dt) 0 25]); title(['Horizontal to Vertical Ratio for ',archi1])
xlabel('Frequency (Hz)'); ylabel('HVSR')


figure;
semilogx(f(2:length(f)),HVX,'--k',f(2:length(f)),HVY,'-
k',f(2:length(f)),HVm,':k','LineWidth',2);
legend(': Mean HVSR East-West',': Mean HVSR North-South',': Merged HVSR' )
grid off;
axis ([1/twl (0.5/dt) 0 max([max(HVX) max(HVY) max(HVm)])]); title(['Horizontal to Vertical
Ratio for ',archi1])
xlabel('Frequency (Hz)'); ylabel('HVSR')

figure;
plot(f,Xm,'--k',f,Ym,'-k',f,Zm,':k','LineWidth',2);
legend(': Mean East-West Fourier Spectrum',': Mean North-South Fourier Spectrum',': Mean
Vertical Fourier Spectrum')
grid off;
axis ([0 (0.5/dt) 0 max([max(Xm) max(Ym) max(Zm)])]); title(['Mean FFT X,Y,Z for ',archi1])
xlabel('Frequency (Hz)'); ylabel('Amplitude')

f=f';
archiout1=strcat(archi,'_',num2str(twl),'sec_f.txt');
save(archiout1,'f','-ASCII');
```

```
archiout2=strcat(archi,'_',num2str(twl),'sec_HVX.txt');
save(archiout2,'HVX','-ASCII');
archiout3=strcat(archi,'_',num2str(twl),'sec_HVY.txt');
save(archiout3,'HVY','-ASCII');
archiout4=strcat(archi,'_',num2str(twl),'sec_HVm.txt');
save(archiout4,'HVm','-ASCII');

['The Nakamuras Spectra Ration has been calculated']
['File Processed : ' archi1]
['Time Windows (seconds): ' num2str(twl)]
['Overlap Window (seconds):' num2str((ow/100)*twl)]
['Number of Windows processed: ' num2str(size(xm,2))]
['Three files has been created: ' archiout1 ' , ' archiout2 ' , ' archiout3]
[' HVSRAVv2 by: Raul J. Ritta - Puerto Rico Strong Motion Program -2009']

%% END
```

Program for processing seismic accelerograms

```
% ---------------------- Programa HVSREA.m -------------------------------%
% Programa para calcular y graficar la Transformada discreta de Fourier de  %
% un acelerograma sísmico usando la FFT. El espectro de Fourier se suaviza  %
% promediando los valores vecinos de cada punto ("running average").        %
% Tambien se calcula el cociente espectral H/V.                             %
% --------------- Revisado en: 27-Abril.-2009 - Raul Jose Ritta ----------%
%Canales:
%- Canal #1 = Transversal = E-O
%- Canal #2 = Longitudinal = N-S
%- Canal #3 = Vertical
clc; clear all; close all; addpath('C:\Users\RAUL\Material uprm\THESIS\Mediciones\Mediciones
Raul\10, 21-04-2009 (Sismos)\Mayo2007\')

g    = 981;                           % aceleración de la gravedad: cm/s^2
dt   = 0.005;                         % intervalo de tiempo de acelerog.: seg
fac  = 0.3*g;                         % máxima aceleración del suelo: cm/s^2
nit  = 3;                             % nro. de iteraciones para suavizar
ngr  = 0.4;                           % porciento del total de ptos. para graficar
nombre = 'ETNABF004';
for comp= 1:3
if comp == 1
    nom = strcat(nombre,'long')
elseif comp == 2
    nom = strcat(nombre,'trans')
else
    nom = strcat(nombre,'vert')
end
terr    = (detrend(load ([nom,...
    '.txt']))).*(g/1.25);           % lectura del archivo con el registro y correccion del
mismo
[nr,nc] = size(terr);                 % filas y columnas del archivo
xg = 0;
xg(1:nr*nc)= terr';                   % vector con los datos del archivo
xg = xg(201:12400);                 % recorte del sismo
xm = max( abs(xg) );                  % máximo valor del acelerograma original
xg = [fac/xm*xg, zeros(1,10)];        % agrega 0's al final del acelerograma
N  = length(xg);                      % nro. de puntos del nuevo acelerograma
```

```
if N ~= 2*fix(N/2)                      % verifica is N es un nro. impar
   N     = N + 1                        % si es impar se incrementa N en 1
   xg(N) = 0;                           % agrega una dato al acelerograma
end
T   = N*dt;                             % intervalo de muestreo final
t   = 0: dt: (N-1)*dt;                  % vector con tiempos discretos

figure; plot( t,xg/g, t,zeros(1,N) ); grid on;
axis tight; title(['Acelerograma del terremoto de ',nom,' escalado']);
xlabel('Tiempo [seg]'); ylabel('Aceleración [en fracciones de g]');

disp('==> Datos del acelerograma registrado :')
disp(['    Maxima aceleracion registrada : ',num2str(xm),' cm/s^2']); disp(' ')

% --------- Cálculo de la transformada discreta del acelerograma --------%

wny = pi/dt;                              % frecuencia de Nyquist: rad/seg
dw  = 2*pi/T;                             % intervalo de frecuencia: rad/seg
Np  = round(ngr*wny/dw);                  % nro. de frecs. para graficar
w=0;
w   = 0 : dw : N/2*dw;                    % vector con frecuencias en rad/s
f   = w/(2*pi);                           % vector con frecuencias en ciclos/s
Amp = 0;
Amp = dt * abs(fft(xg));                % magnitud de la TD discreta

% ------- Suavizado y gráfico de la amplitud de la TF del registro  ------%

Xg   = Amp;
Xgm(:,comp) = Xg(1:Np)';
for k = 1 : nit
   Sw(1)      = Xg(1);
   Sw(2)      = ( Xg(1)+Xg(2)+Xg(3) )/3;
   Sw(Np-1)   = ( Xg(Np-2)+Xg(Np-1)+Xg(Np) )/3;
   Sw(Np)     = Xg(Np);
   Sw(3:Np-2) = ( Xg(1:Np-4)+Xg(2:Np-3)+ Xg(3:Np-2)+Xg(4:Np-1)+Xg(5:Np) )/5;
   Xg         = Sw;
end

figure; plot( f(1:Np),Amp(1:Np),':', f(1:Np),Sw(1:Np),'LineWidth',2); grid on;
axis tight; title(['Espectro de Fourier del registro de ',nom])
xlabel('Frecuencia f [ciclos/seg]'); ylabel('Amplitud')
legend(': original',': suavizado')



% ---------- Cálculo del pico del espectro de Fourier del registro -------%

[Xm,id] = max( abs(Amp) );
fm = f(id);
wm = w(id);
Tm = 1/fm;
disp('==> Datos del espectro de Fourier :')
disp(['    Frecuencia de Nyquist : ',num2str(wny),' rad/s'])
disp(['    Frecuencia de Nyquist : ',num2str(wny/(2*pi)),' Hz'])
disp(['    Intervalo de frecuencias : ',num2str(dw),' rad/s'])
disp(['    Intervalo de frecuencias : ',num2str(dw/(2*pi)),' Hz']); disp(' ')
disp('==> El pico del espectro de Fourier ocurre en :')
disp(['    Frecuencia en Hertz : ',num2str(fm)])
disp(['    Frecuencia en rad/s : ',num2str(wm)])
disp(['    Periodo en segundos : ',num2str(Tm)])
```

```
end

% ------------- Grabado de ls espectro de Fourier de cada componente -----%

M = [Xgm f(1:Np)'];
archiout=strcat(nombre,'_','FFT.txt');
save(strcat('C:\Users\RAUL\Material uprm\THESIS\Mediciones\Mediciones Raul\10, 21-04-2009
(Sismos)\Mayo2007\',archiout),'M','-ASCII');

% ------------ Calculo y graficado de los cocientes espectrales H/V ------%

HVX = M(:,2)./M(:,3);
HVY = M(:,1)./M(:,3);
HVM = ((M(:,2).^2 + M(:,1).^2)./(2*M(:,3).^2)).^(0.5);

for c = 1:3
    if c == 1
        Xg = HVX;
    elseif c == 2
        Xg = HVY;
    else
        Xg = HVM;
    end
    for k = 1 : nit
        Sw(1)      = Xg(1);
        Sw(2)      = ( Xg(1)+Xg(2)+Xg(3) )/3;
        Sw(Np-1)   = ( Xg(Np-2)+Xg(Np-1)+Xg(Np) )/3;
        Sw(Np)     = Xg(Np);
        Sw(3:Np-2) = ( Xg(1:Np-4)+Xg(2:Np-3)+ Xg(3:Np-2)+Xg(4:Np-1)+Xg(5:Np) )/5;
        Xg         = Sw;
    end
    if c == 1
        HVXs = Xg;
    elseif c == 2
        HVYs = Xg;
    else
        HVM = Xg;
    end
end

figure
semilogx(M(:,4),HVYs,'k',M(:,4),HVXs,':K',M(:,4),HVM,'--K','linewidth',2 )
legend(': Norte-Sur HVSR',': Este-Oeste HVSR',': Merged HVSR')
xlabel('frecuencia [Hz]')
ylabel('HVSR')
title(['Cociente Espectral Horizontal/Vertical de ',nombre])
axis ([0 f(Np) 0 max([max(HVXs) max(HVYs)])]);
```

Program to determine the spectral ratio with respect to a reference site

```
% ---------------------- Programa SRRS.m --------------------------------%
% Programa para calcular y graficar el cociente espectral Hs/Hr, es decir,
% el cociente entre el espectro de Fourier en un sitio y el correspondiente
% a un sitio de referencia en roca, respecto a un mismo evento sismico.
% Luego los cocientes espectrales son suavizados promediando los valores
% vecinos de cada punto ("running average").        %
% ----------- Revisado en: 27-Abril-2009 - Raul Jose Ritta --------------%
```

```
%Canales:
%- Columna #1 = Longitudinal = N-S
%- Columna #2 = Transversal = E-O
%- Columna #3 = Vertical
%- Columna #4 = frecuencias discretas

clc; clear all; close all; addpath('C:\Users\RAUL\Material uprm\THESIS\Mediciones\Mediciones
Raul\10, 21-04-2009 (Sismos)\Mayo2007\')

nit  = 3;                               % nro. de iteraciones para suavizar
nombre1 = 'ETNABF004';                  % estacion de referencia
nombre2 = 'ETNAAZ004';                  % sitio # 1
nombre3 = 'ETNAAO003';                  % sitio # 2
for comp= 1:3
if comp == 1
    nom = strcat(nombre1,'_FFT');
    Mr = load([nom,'.txt']);            % lectura de la matriz con los espectros y las frec.
disc.
elseif comp == 2
    nom = strcat(nombre2,'_FFT');
    M1 = load([nom,'.txt']);            % lectura de la matriz con los espectros y las frec.
disc.
else
    nom = strcat(nombre3,'_FFT');
    M2 = load([nom,'.txt']);             % lectura de la matriz con los espectros y las frec.
disc.
end
end

% -- Calculo, suavizado y graficado de los cocientes espectrales Hs/Vr --%

HH_NS_25 = M1(:,1)./Mr(:,1);
HH_EO_25 = M1(:,2)./Mr(:,2);
HH_NS_95 = M2(:,1)./Mr(:,1);
HH_EO_95 = M2(:,2)./Mr(:,2);
HHM_25 = (HH_NS_25+HH_EO_25)/2;
HHM_95 = (HH_NS_95+HH_EO_95)/2;
Np = length(HH_EO_95);

for c = 1:6
    if c == 1
        Xg = HH_NS_25;
    elseif c == 2
        Xg = HH_EO_25;
    elseif c == 3
        Xg = HH_NS_95;
    elseif c == 4
        Xg = HH_EO_95;
    elseif c == 5
        Xg = HHM_25;
    else
        Xg = HHM_95;
    end
    for k = 1 : nit
        Sw(1)      = Xg(1);
        Sw(2)      = ( Xg(1)+Xg(2)+Xg(3) )/3;
        Sw(Np-1)   = ( Xg(Np-2)+Xg(Np-1)+Xg(Np) )/3;
        Sw(Np)     = Xg(Np);
        Sw(3:Np-2) = ( Xg(1:Np-4)+Xg(2:Np-3)+Xg(3:Np-2)+Xg(4:Np-1)+Xg(5:Np) )/5;
        Xg         = Sw;
    end
```

```
    if c == 1
        HH_NS_25s = Xg;
    elseif c == 2
        HH_EO_25s = Xg;
    elseif c == 3
        HH_NS_95s = Xg;
    elseif c == 4
        HH_EO_95s = Xg;
    elseif c == 5
        HHM_25s = Xg;
    else
        HHM_95s = Xg;
    end
    X = 0;
end

figure
plot(Mr(:,4),HH_NS_25s,'k',Mr(:,4),HH_EO_25s,'--K',Mr(:,4),HHM_25s,':k','linewidth',2 )
legend(': Norte-Sur Hs/Hr',': Este-Oeste Hs/Hr',': Merged Hs/Hr')
xlabel('frecuencia [Hz]')
ylabel('Hs/Hr')
title(['Cociente Espectral Hor_sitio/Hor_roca de ',nombre2])
axis ([0 max(Mr(:,4)) 0 max([max(HH_NS_25s) max(HH_EO_25s) max(HHM_25s)])]);

figure
plot(Mr(:,4),HH_NS_95s,'k',Mr(:,4),HH_EO_95s,'--K',Mr(:,4),HHM_95s,':k','linewidth',2 )
legend(': Norte-Sur Hs/Hr',': Este-Oeste Hs/Hr',': Merged Hs/Hr')
xlabel('frecuencia [Hz]')
ylabel('Hs/Hr')
title(['Cociente Espectral Hor_sitio/Hor_roca de ',nombre3])
axis ([0 max(Mr(:,4)) 0 max([max(HH_NS_95s) max(HH_EO_95s) max(HHM_95s)])]);
```

Program for determination of the theoretical transfer functions of a soil deposit

```
% ---------------------- Programa FTransf.m ------------------------------%
% Programa para calcular y graficar las Funciones de Transferencia
% para un depósito de suelo formado por N capas y que termina en
% una "roca" elástica de profundidad infinita. Se consideran dos casos:
% 1) F. de T. entre el afloramiento rocoso y la superficie del depósito,    % 2) F. de T.
entre la interfase suelo-roca y la superficie del depósito.
% ------------ Modificado en: 23-Febrero- 2009 - por Raul J. Ritta -------%
% ---------------------- Autor: Luis E. Suarez --------------------------%
clc; clear all; close all

g  = 32.2;                                    % acel. de la gravedad: ft/s^2
sw = [125 120 125 100 110 115 100 140]';      % pesos unitarios: lb/ft^3
c  = [770 1061 511 646 953 1725 2555 10000]'; % velocidad de ondas S: ft/s
N  = length(c);                               % nro. de capas de suelo
h  = [3.94 6.23 18 21 13.78 13.12 22.31 200]; % profundidad de las capas: ft
G0 = c.^2.*sw/g;                              % módulos de corte baja def.: psf
zi = 0.03*ones(N,1);                          % razones de amortiguamiento
wm = 50*2*pi;                                 % máx. frecs. p/graficar: rad/s
dw = 0.01;                                    % incremento en frec. p/graficar
om = 1e-4: 0.1: wm;                           % vector con frecuencias: rad/s
nw = length(om);                              % nro.de frecuencias discretas

Gc = G0.*(1 + i*2*zi);                        % módulos de corte complejos
```

```
cc = c .* sqrt(1+i*2*zi);                       % velocidad de ondas S complejas
k  =  1./cc * om;                               % números de onda complejos

kh  = diag(h)* k;                                % variables auxiliares para ...
eip = exp(+i*kh);                                % calcular las funciones ...
ein = exp(-i*kh);                                % ar(omega) y br(omega)

a  = zeros(N,nw);                                % matrices con funciones ...
b  = zeros(N,nw);                                % ar(omega) y br(omega)
a(1,:) = ones(1,nw);                             % funciones iniciales  ...
b(1,:) = ones(1,nw);                             % a1(omega) y b1(omega)
for r = 2 : N
    dr     = Gc(r-1)*cc(r) / ( Gc(r)*cc(r-1) );
    a(r,:) = (1+dr)/2.*eip(r-1,:).*a(r-1,:) + (1-dr)/2.*ein(r-1,:).*b(r-1,:);
    b(r,:) = (1-dr)/2.*eip(r-1,:).*a(r-1,:) + (1+dr)/2.*ein(r-1,:).*b(r-1,:);
end

F1N = ( a(1,:) + b(1,:) ) ./ ( a(N,:) + b(N,:) );   % FT afloram. a superf.
F1r = 1 ./ a(N,:);                                  % FT roca basal a superf.

Fd1 = diff(abs(F1N),1) / dw;                        % 1ra derivada de |FT|
Fd2 = diff(abs(F1N),2) / dw^2;                      % 2da derivada de |FT|
Z   = Fd1(1:nw-2).*Fd1(2:nw-1);
I   = find(Z < 0 & Fd2 < 0);                        % índices de frecs. nat.
wn  = om(I);                                        % frecs. naturales
nf  = length(wn);                                   % nro. de frecs. naturales
Fm  = abs(F1N(I));                                  % magnitud de la FT
[Fm1,iw] = max(abs(F1N));                           % pico de la FT para w1
wn(1) = om((iw));                                   % primera frec. natural
Fm(1) = Fm1;

disp('*** Frecuencias naturales del depósito [rad/s]:'); disp(' '); disp(wn)
disp('*** Frecuencias naturales del depósito [Hertz]:'); disp(' '); disp(wn/(2*pi))

figure; plot( om,abs(F1r), om,abs(F1N),'-+','Markersize',1.5 ); grid on;
axis tight;; xlabel('Frecuencia \omega [rad/seg]'); ylabel('|F_1_j(\omega)|')
title('Funciones de Transferencia entre roca y superficie libre');
legend(': roca superf.-superficie',': roca basal-superficie'); hold on;
for j = 1 : nf
    plot( [wn(j),wn(j)],[0,Fm(j)],'r-.')
end
hold off

f = om/(2*pi);
figure; plot( f,abs(F1r), f,abs(F1N),'-+','Markersize',1.5 ); grid on;
axis tight;; xlabel('Frecuencia f [Hertz]'); ylabel('|F_1_j(f)|')
title('Funciones de Transferencia entre roca y superficie libre');
legend(': roca superf.-superficie',': roca basal-superficie'); hold on;
for j = 1 : nf
    plot( [wn(j),wn(j)]/(2*pi),[0,Fm(j)],'r-.')
end
hold off
```